# NEW SUPRAMOLECULAR ASSEMBLIES OF TOXIC METAL COORDINATION COMPLEXES

by

TIMOTHY GLEN CARTER

A DISSERTATION

Presented to the Department of Chemistry
and the Graduate School of the University of Oregon
in partial fulfillment of the requirements
for the degree of
Doctor of Philosophy

March 2010

**University of Oregon Graduate School**

**Confirmation of Approval and Acceptance of Dissertation prepared by:**

Timothy Carter

Title:

"New Supramolecular Assemblies of Toxic Metal Coordination Complexes"

This dissertation has been accepted and approved in partial fulfillment of the requirements for the Doctor of Philosophy degree in the Department of Chemistry by:

Michael Haley, Chairperson, Chemistry
Darren Johnson, Member, Chemistry
Shih-Yuan Liu, Member, Chemistry
James Hutchison, Member, Chemistry
Eric Johnson, Outside Member, Biology

and Richard Linton, Vice President for Research and Graduate Studies/Dean of the Graduate School for the University of Oregon.

March 20, 2010

Original approval signatures are on file with the Graduate School and the University of Oregon Libraries.

An Abstract of the Dissertation of

Timothy Glen Carter for the degree of Doctor of Philosophy

in the Department of Chemistry to be taken March 2010

Title: NEW SUPRAMOLECULAR ASSEMBLIES OF TOXIC METAL COORDINATION COMPLEXES

Approved: _____
Professor Darren W. Johnson

Supramolecular chemistry is a relatively new and exciting field offering chemists simplistic approaches to generating complex assemblies through strategically designed ligands. Much like the many spectacular examples of supramolecular assemblies in nature, so too are chemists able to construct large, elegant assemblies with carefully designed ligands which bind preferentially to target metal ions of choice. An important concept of supramolecular chemistry, often subtle and overlooked, is secondary bonding interactions (SBIs) which in some cases, act as the glue to hold supramolecular assemblies together. This dissertation examines SBIs in a number of systems involving the pnictogen elements of arsenic and antimony as well as aromatic interactions in self-assembled monolayers. The first half of this dissertation is an introduction to the concepts of supramolecular chemistry and secondary bonding interactions and how they are used in the self-assembly process in the Darren Johnson

laboratory. Chapter I describes how secondary bonding interactions between arsenic and aryl ring systems and antimony and aryl ring systems assist with the assembly process. Chapter II is a continuation of the discussion of SBIs but focuses on the interactions between arsenic and heteroatoms. The second half of this dissertation will describe work performed in collaboration with Pacific Northwest National Laboratory (PNNL) in Richland, WA. This work was performed under the guidance of Dr. R. Shane Addleman in conjunction with Professor Darren W. Johnson of the University of Oregon. This portion describes novel systems for use in heavy metal ion remediation from natural and unnatural water sources. Chapters III-V describe functionalized mesoporous silica for use in heavy metal uptake from contaminated water sources. Chapter V describes a new technology invented during this internship at PNNL which utilizes weak bonding interactions between aryl ring systems to produce *regenerable* green materials for toxic metal binding. This work is ongoing in the Darren Johnson lab.

This dissertation includes my previously published and co-authored material.

# CURRICULUM VITAE

NAME OF AUTHOR: Timothy Glen Carter

PLACE OF BIRTH: Beloit WI

DATE OF BIRTH: January 13th, 1976

GRADUATE AND UNDERGRADUATE SCHOOLS ATTENDED:

University of Oregon
San Francisco State University
University of Wisconsin Stevens Point

DEGREES AWARDED:

Doctor of Philosophy in Chemistry, 2010, University of Oregon
Bachelor of Science in Chemistry, 1998, University of Wisconsin Stevens Point

AREAS OF SPECIAL INTEREST:

Supramolecular Self-assemblies with Toxic Metal Ions
Fluorescent Labeling of Amino Acids and Small Peptides
Monomer and Polymer Synthesis

PROFESSIONAL EXPERIENCE:

Graduate Research Assistant, Department of Chemistry, University of Oregon, Eugene Oregon, 2005-2010.

Graduate Teaching Assistant, Department of Chemistry, University of Oregon, Eugene, OR, 2004-2005.

Chemist, Biosearch Technologies, Inc., Novato, CA, 1999-2004.

Chemist, Axys Pharmaceuticals, South San Francisco, CA, 1999.

GRANTS, AWARDS AND HONORS:

National Science Foundation IGERT Fellowship, 2006-2009

PUBLICATIONS:

Lindquist, N. R.; Carter, T. G.; Cangelosi, V. M.; Zakharov, L. N.; Johnson, D. W. Accepted, **2010**.

Cangelosi, V. M.; Carter, T. G.; Zakharov, L. N.; Johnson, D. W. *Chem. Commun.* **2009**, 5606-5608.

Addleman, R. S.; Bayes, J. T.; Carter, T. G.; Fontenot, S. A.; Fryxell, G. E.; Johnson, D. W. **2009** U.S. Pat. Appl. # 61/120,321.

Fontenot, S.A.; Carter, T.G.; Johnson, D.W.; Fryxell, G.; Addleman, R.S.; Warner, M.C.; Yantasee, W. In *Trace analysis with Nanomaterials*; Pierce, D.T, Zhao, J.X., Eds.; Wiley-VCH: 2010.

Carter, T.G.; Yantasee, W.; Sangvanich, T.; Fryxell, G.E.; Johnson, D.W.; Addleman, R.S. *Chem. Commun.* **2008**, *43*, 5583-5585.

Yantasee, W.; Warner, C. L.; Sangvanich, T.; Addleman, R. S.; Carter, T. G.; Wiacek, R. J.; Fryxell, G. E.; Timchalk, C.; Warner, M. G. *Environ. Sci. Technol.* **2007**, *41*, 5114-5119.

Carter, T. G.; Vickaryous, W. J.; Cangelosi, V. M.; Johnson, D. W. *Comments Inorg. Chem.* **2007**, *28*, 97-122..

Carter, T. G.; Healey, E. R.; Pitt, M. A.; Johnson, D. W. *Inorg. Chem.* **2005**, *44*, 9634-9636.

Carter, T.; Reddington, M. **2005** U.S. Pat. Appl. #2005-51666.

Lyttle, M.H., Walton, T.A., Dick, D.J., Carter, T.G., Beckman J.H. and Cook, R.M. *Bioconjugate Chem.*, **2002** *13*(5), 1146-1154.

Lyttle, M. H.; Carter, T. G.; Cook, R. M. *Org. Proc. Res. & Dev.*, **2001**, *5*, 45-49.

Lyttle, M. H.; Carter, T. G.; Dick, D. J.; Cook, R. M. *J. Org. Chem.* **2000** *65*, 9033-9038.

# ACKNOWLEDGMENTS

I would like to sincerely thank my research advisor, Professor Darren W. Johnson, for continued support and thought provoking conversation throughout my graduate career. I would also like to thank my committee chair, Professor Michael M. Haley, and the other members, Professor James E. Hutchison, Professor Shih-Yuan Liu and Professor Eric A. Johnson for practical advice and valuable input toward my research. I would like to acknowledge Dr. R. Shane Addleman of Pacific Northwest National Laboratory for providing me the internship opportunity in his research group and Dr. Wassana Yantasee of Oregon Health and Science University for her advice and guidance during my internship at PNNL. Dr. Rather and Dr. Zakharov for their crystallographic expertise. Ginny Cangelosi and Zack Mensinger for providing valuable feedback and editorial assistance for this dissertation. Monica Thilges for her editorial suggestions on nearly all my published and unpublished material. My fellow 2004 classmates, Adam Marwitz, Justin Crossland, Matt Carillo and Pat Blower for their late night stress relieving sessions. Ginger Shultz for her frequent and necessary lunch meetings. I would also like to thank every person that has assisted me with my studies by providing advice or lending ideas to help my research move forward. Finally, I would like to thank the National Science Foundation (NSF) IGERT for three years of funding.

This dissertation is dedicated to my father, Orland Doak Carter, who instilled the necessary skill set to succeed.

TABLE OF CONTENTS

Chapter Page

Chapter Page

# LIST OF FIGURES

Figure Page

Figure Page

Figure Page



Chapter V

# LIST OF SCHEMES

Scheme Page

Chapter II



Chapter III

# LIST OF TABLES

Tables Page

# LIST OF EQUATIONS

# CHAPTER I

## SUPRAMOLECULAR ARSENIC COORDINATION CHEMISTRY

Some of this work has been previously published and is reproduced with permission from: Carter, T. G.; Vickaryous, W. J.; Cangelosi, V. M.; Johnson, D. W. *Comments Inorg. Chem.* **2007**, *28*, 97-122.

### General Overview

This dissertation describes the investigation of weak molecular interactions in the generation of supramolecular assemblies for binding toxic metal ions. This work can be separated into two categories: solution phase organothiolate arsenic self-assemblies and solid supported 'regenerable' sorbent materials for heavy metal uptake. Although seemingly different with respect to the type of chemistry from a cursory inspection (organic metal-ligand versus inorganic materials chemistries), the use of weak forces to achieve efficient binding and the mechanism of binding for both categories is very similar and will be discussed in detail. The concepts of supramolecular chemistry will be introduced first, followed by my research relating to the use of organothiolate ligands to bind arsenic with a discussion of Secondary. Bonding Interactions (SBIs) and their relevance in the self-assembly process. The remainder of this dissertation will cover work relating to silica-based sorbent materials for use in toxic metal ion capture from

native water sources, including the novel material developed during a collaboration with scientists at Pacific Northwest National Laboratory (PNNL) in Richland, WA.

Chapter I surveys our approach to developing design strategies to prepare self-assembled nanoscale supramolecular complexes containing main group ions, with a particular emphasis on supramolecular arsenic(III) coordination chemistry. The majority of material the originated in a publication in *Comments on Inorganic Chemistry* (**2007**, 28, 97-122, © Taylor & Francis Group, LLC). This article was coauthored with W. Jake Vickaryous and Virginia M. Cangelosi who provided content, including experimental data, results and conclusions from their research for this manuscript. Professor Darren W. Johnson, also listed as a coauthor, provided intellectual and editorial contributions to this publication.

## Introduction to Supramolecular Metal-ligand Self-assembly

Supramolecular chemistry has been described in 1969 by Jean-Marie Lehn—Nobel Prize recipient for chemistry in 1987 for his pioneering work in the field—as the "the chemistry of the intermolecular bond" or simply put, the linking of molecules by intermolecular interactions much like atoms are linked covalently in traditional synthesis.[1] This can be demonstrated graphically by the simplified representation presented in **Figure 1** where *n* number of difunctional ligands (double arrow lines) cooperatively interact with *m* number of metal ions (spheres) to form a discrete complex, or in some examples, complexes held together by non-covalent contacts.

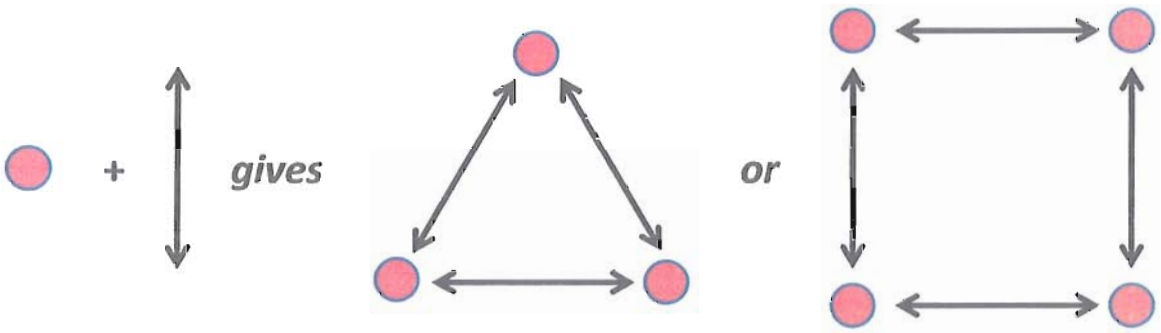


**Figure 1** Cartoon representation of bisfunctional ligands (arrows) and metal ions (spheres) undergoing self-assembly to form discrete supramolecular complexes of various shapes.

The supramolecular self assembly process for metal-ligand systems is often high yielding and can be influenced by numerous factors including solvent interactions, the presence of guest molecules or by varying concentrations of either component. Traditionally, self-assembled supramolecular complexes utilize either classic *d*-block transition metal centers with tetrahedral, octahedral or square planar coordination geometries, *f*-block metal-centers with expanded coordination geometry, or in some cases, a combination of the two[2,3] (**figure 2**).

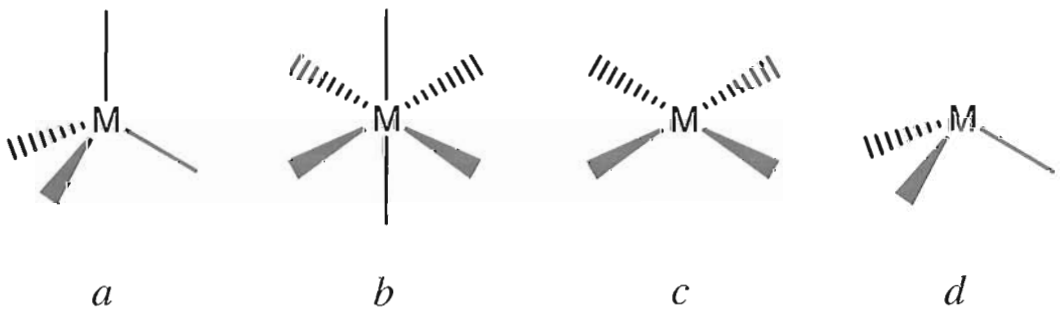


**Figure 2** Typical transition metal coordination geometries (*a*) tetrahedral, (*b*) octahedral and (*c*) square planar. Main-group elements, specifically pnictoges with an oxidation state of +3, prefer (*d*) trigonal pyramidal coordination geometries.

The result is typically a high symmetry coordination complex containing metal centers with predictable coordination geometries which utilize directing ligands to assist in the self-assembly process.[4-6] By targeting a metal ion's preferred bonding geometry with a well designed rigid ligand, supramolecular chemists have generated spectacular examples of self-assemblies such as Höpfl's tin triangle[7] and Kieltyka's platinum square[8] **(Figure 3)**.

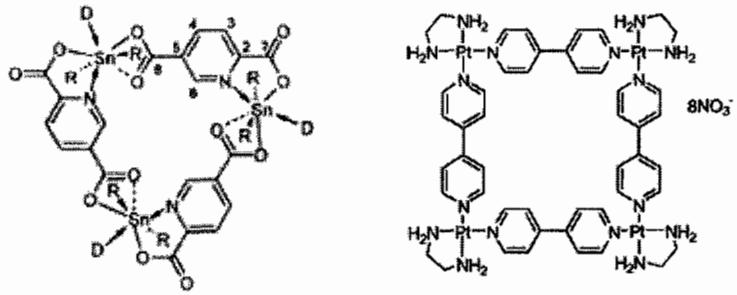


**Figure 3** Examples of self-assembled supramolecular complexes. Höpfl and coworkers coordinated three tin centers with three pyridinedicarboxylate ligands to form a triangle (left) and Kieltyka and coworkers demonstrated platinum's ability to form a square-like structure with four dipyridyl ligands.

Supramolecular chemistry also provides an alternative approach to generating structures with high metal to ligand ratio which are often unattainable or if attainable, are doomed by a much more inefficient pathway using traditional synthetic approaches. For example, Raymond's group has synthesized tetrahedral structures by the self-assembly process starting from a simple naphthyl precursor and adding dicatechol functionality via amide linkages **(Figure 4)**.

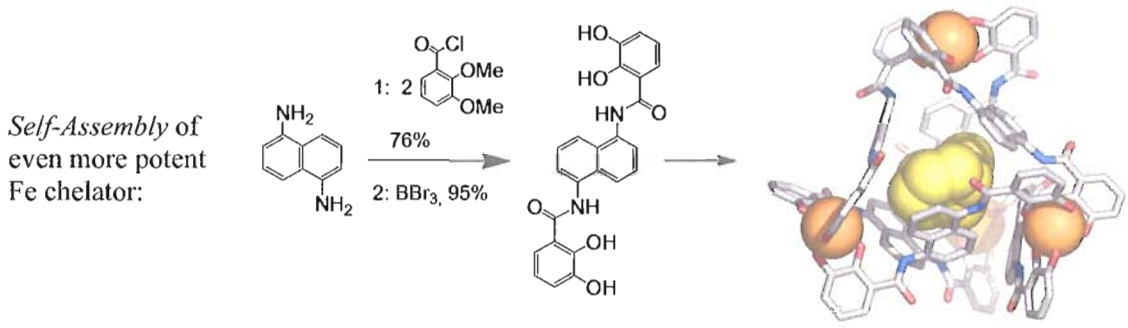


**Figure 4** High yielding two step synthesis generates dicatechol ligand capable of binding two metal centers. When combined with six ligands and four metals, a self-assembled tetrahedron is formed.

The high yielding, two-step synthesis combined with the self-assembly process often makes the supramolecular chemistry approach to metal chelation a *greener* alternative to traditional metal chelators. Supramolecular chemistry provides a powerful pathway to achieve high order, often symmetrical structures through the careful design of organic ligands to target a whole host of metal ions based on their preferred coordination geometries.

## Overview of Research

A flurry of research activity has emerged in recent years resulting in reliable strategies for the formation of spectacular self-assembled metal-ligand clusters and capsules. Main group ions have not shared in this burst of activity. In fact, ions in this part of the periodic table have largely been overlooked for use as directing elements in self-assembly reactions, despite the need for improved chelators for main group ions for a variety of applications. Over the last two decades, there has been increasing interest in

self-assembled nanoscale coordination complexes for use in a variety of applications including nanofabrication, molecular switches, host-guest chemistry and nanoscale chemical reactors.[9-15] The incorporation of toxic metals and main group metalloid ions such as lead and arsenic, respectively, into self-assembled supramolecular complexes has received less scrutiny. Only a few examples can be found in the literature of complexes that incorporate main group elements in the self-assembly process, and of those,[16-19] only a few contain the highly toxic metalloid arsenic.[20-27] The overlying focus of this chapter is the discussion of design, synthesis and analysis of interactions between organothiol-based ligands and arsenic(III), antimony(III), bismuth and other main group metals and metalloids as a means to improve the understanding of their coordination chemistry, specifically, and main group supramolecular chemistry as a whole.

Our supramolecular approach to metal chelation stems from the hypothesis that enhanced metal-ion specificity can be achieved by targeting the unusual coordination geometries of main group ions. Furthermore, the thermodynamic driving force provided by metal-ligand self-assembly reactions results in robust products. Typically, the self-assembly process of discrete supramolecular molecules leads to high and even quantitative yields as a result of this stabilization. Additionally, other weak forces such as secondary bonding interactions further amplify the thermodynamic stability of these self-assembled nanoscale complexes.[28]

Our approach to arsenic chelation focuses on the use of rigid, multidentate organothiol ligands which target the unusual, but predictable, trigonal pyramidal coordination geometry of arsenic(III). The reversibility of As-thiolate bond formation

allows for the self-assembly of discrete compounds to occur. We have successfully used this approach to synthesize dinuclear $As_2L_3$ assemblies as well as a tetranuclear $As_4L_2$[29] assembly and a variety of $As_2L_2Cl_2$ macrocycles and $As_2LCl_2$ complexes. This chapter also reviews the diastereoselectivity in the self-assembly of these macrocycles and discusses the use of secondary bonding interactions as a means to bolster complex formation. For a recent review of the broader area of main group supramolecular chemistry see Pitt, et al.[30]

## Motivation of Arsenic Research

We have selected arsenic as the primary target for nanoscale coordination complex formation for three main reasons: 1) there are few chelators optimized for the preferred coordination geometry of arsenic, specifically, and the Group 15 ions in general 2) the coordination geometry of arsenic with thiolate ligands is predictable (trigonal pyramidal) and 3) As-S bonds are sufficiently labile to allow for self-assembly to occur.[31,32] Arsenic, a semi-metal element, is best known for its toxicity toward humans, with the (+3) and (+5) oxidation states the most prevalent species found in the environment.[33] Arsenic occurs naturally, and is found in ores of both common and coinage metals resulting in an environmental hazard associated with mining and metal smelting.[34,35] Naturally contaminated well water has reached catastrophic proportions in Bangladesh, exposing tens of millions of people to arsenic resulting in numerous types of cancers and skin afflictions.[36-38] Locally, a survey conducted of the Willamette Basin in western Oregon, USA concluded that more than 20 percent of wells tested have levels

above the current EPA limit of 10μg/L.[39] With the ever-expanding population growth in the Willamette Basin (and the world as a whole), the likelihood of human exposure increases greatly, thus making research geared toward the study of arsenic and other toxic ions essential.

## Ligand Design Strategy for Supramolecular Arsenic Complexes

Although the (+5) oxidation state of arsenic is the most prevalent form found in surface water,[40] it is the (+3) state that is more toxic to humans as well as a more challenging target for remediation.[41] Arsenic(III) species have a high affinity for thiol containing biological structures such as cysteine residues in proteins and enzymes.[42,43] When coordinated with organothiolate ligands, As(III) typically prefers a trigonal-pyramidal geometry with a stereochemically active lone pair.[44-46] In rare instances, arsenic(III) can adopt a distorted octahedral[47] or even tetrahedral geometry, typically the result of weakly coordinating sulfur, oxygen or nitrogen atoms located in close proximity to the arsenic thiolate center (**Figure 5**).[19,48,49]

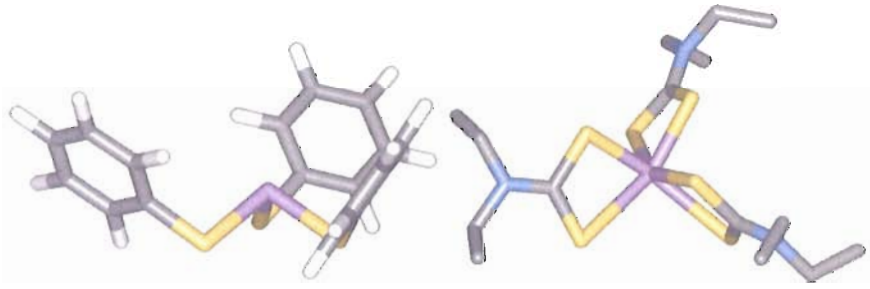

**Figure 5** Stereo chemically active lone pair (left) and distorted octahedral (right) crystal structure examples of As(III).

The Johnson group has utilized this strategy to synthesize numerous examples of As(III), as well as other pnictogens-based, self-assembled supramolecular structures using rigid mono- and dithiolate ligands.

## Secondary Bonding Interactions Stabilize Supramolecular Structures

Secondary bonding interactions (SBI's) have the potential to assist in the formation of self-assembled complexes containing organothiol-based ligands and main group elements. SBI's can occur between main group metals and aromatic systems, heteroatoms such as O, N, S and the halogens.[41,42,50-54] Numerous studies have been published in which supramolecular chemists are utilizing SBIs as a design criterion to aid in the self-assembly process. In doing so, supramolecular chemists are expanding the forces that drive self-assembly reactions.[9,55]

The most comprehensive study to date of secondary bonding interactions with arsenic describes the interactions between As(III) and either thiocarboxylic or dithiocarboxylic acid ligands.[56] Utilizing crystallographic and computational data, Tani and coworkers successfully measured close-contact distances with a number of substituted arsenic complexes and neighboring thiocarboxylato or dithiocarboxylato ligands. They then compared their findings to compounds devoid of secondary bonding interactions and discovered that often, in the solid state, ligands were twisted out of plane to maximize close-contact interactions between the arsenic metal center and either the oxygen or sulfur of the carboxylate group. Additionally, bond elongation was observed suggesting that the interaction occurs between the nonbonding lone pairs of either the

ligand oxygen or sulfur atom and the $\sigma^*$ orbital of an As-S bond (**Figure 6**). In some instances, As-S bond lengthening of as much as 0.19 Å was observed, consistent with the population of an As-S $\sigma^*$ orbital caused by a charge transfer from the heteroatom lone pair to the antibonding orbital of arsenic. UV/Vis spectroscopy provided confirmation of this charge transfer interaction by the observation of hypsochromic, or higher energy, peak migrations.

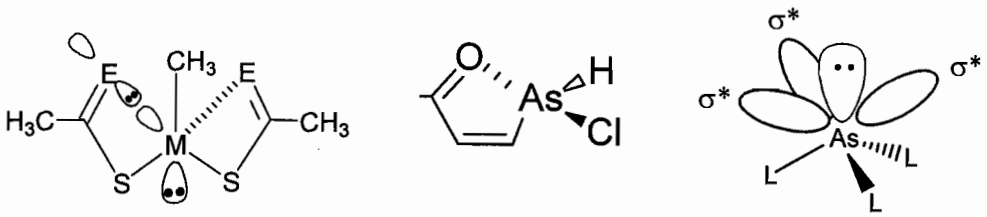


**Figure 6** Secondary bonding interactions between the lone pair of E (E = O or S) and an adjacent σ* orbital of a metal center (M=As) resulting in bond elongation (left). Model system for computational determination of As···O SBI strength (center). Qualitative diagram depicting the approximate positions of the As-**L** σ* orbitals. Each σ* orbital is located diametrically opposite an As-L bond.

Despite this extensive experimental work, quantification of the strength of the interaction between arsenic and the adjacent heteroatoms remains elusive. However, computational calculations by Tani and coworkers of stabilization energies based on phosphorous-oxygen and phosphorous-sulfur model interactions concluded that arsenic has a higher SBI stabilization energy than phosphorous. This was demonstrated experimentally by a increase in the measured SBI's between arsenic and the heteroatoms compared to phosphorus despite the larger atomic radius of arsenic.

## Self-assembly of Discrete Dinuclear Assemblies ($M_2L_3$ Complexes)

1,4-bis(mercaptomethyl)benzene ($H_2$**1**, **Figure 7**) has the appropriate functionality and geometry to act as a bridging ligand between multiple arsenic ions. In the presence of KOH in methanol and tetrahydrofuran, 1,4-bis(mercaptomethyl)benzene ($H_2$**1**) and $AsCl_3$ assemble into a dinuclear $As_2$**1**$_3$ complex.[20] Slow diffusion of pentane into a solution of $As_2$**1**$_3$ in chloroform yields crystals suitable for X-ray diffraction. The solid state structure is shown in **Figure 7**.

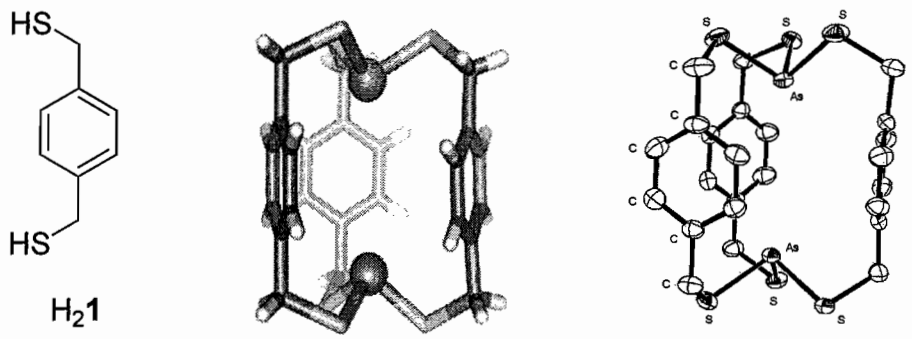


**Figure 7** 1,4-Bis(mercaptomethyl)benzene $H_2$**1** (left), $As_2$**1**$_3$ self-assembled complex with both arsenic lone pairs pointing into the cavity of the complex due to lone pair-$\pi$ interactions (center) and ORTEP diagram of the $As_2$**1**$_3$ crystal structure (left). The cocrystallized $CHCl_3$ solvent is omitted for clarity.

In this assembly, there are several close contacts between the arsenic ions and the aromatic rings. Each arsenic ion makes close contacts with two carbons of each aromatic ring—in effect each arsenic ion is involved in a $\eta^2$-secondary bonding interaction with each of three aromatic rings. Off-center arsenic-arene interactions such as these have previously been observed in the packing of separate discrete molecules. For example, Schmidbaur and coworkers crystallized a cyclophane adduct of arsenic trichloride with $\eta^1$ and $\eta^2$-secondary arsenic-arene interactions.[20,57] The $As_2$**1**$_3$ assembly (**Figure 7**) exhibits

multiple low-hapticity arsenic-arene interactions in an intramolecular and multinuclear fashion.

The exact nature of the arsenic-arene interaction warrants examination in the context of the direction of electron flow between the As(III) center and the arene. The π-system of an aromatic ring may act as either an electron donor or acceptor. For example, the cation-π[58] and anion-π[59] interactions are well-known examples of arenes acting as Lewis bases or Lewis acids, respectively. Similarly, arsenic(III) may act as either a Lewis base or a Lewis acid. Arsenic(III), particularly in arsines, is easily recognized as a Lewis donor because it is in the same group as nitrogen and phosphorus and similarly often exhibits a stereochemically active lone pair which, in some cases, may participate in coordinative bonding. Trialkyl arsine complexes are well known to coordinate metal ions through the lone pair on arsenic. Therefore, this lone pair cannot entirely be considered to be inert. As a representative example, triphenylarsines participate in dative bonding to platinum(II) in the complexes $PtI_3(AsPh_3)$ and $PtI_2(AsPh_3)$pyr as described by Kuznik and coworkers.[49] Proceeding down the Group 15 elements, from nitrogen to bismuth, the Lewis basicity decreases due to increasing localization of the lone-pair electrons in an s-orbital. Contrarily, the Lewis acidity of the elements increases on going down the group. The acceptor orbitals responsible for the Lewis acidity may be regarded as three σ* orbitals oriented 180° opposite the three full bonds of arsenic in a trigonal pyramidal coordination geometry (**Figure 6**).[60] Arsenic occupies an intermediate position in that neither its Lewis basicity nor its Lewis acidity dominates, and either reactivity pattern may occur.

Two lines of evidence suggest that the arsenic-arene interaction involves electron donation from the π-system of the aromatic ring to the arsenic(III) ion. First, the interaction is primarily observed between arsenic and electron-rich arenes.[61] There is also a corresponding dearth of examples of arsenic interacting with electron-poor arenes. Second, the aromatic ring is often significantly tilted with respect to the three-fold axis of trigonal pyramidal arsenic(III) so that one of the σ* orbitals is perpendicular to the plane of the aromatic ring.[62] This may be regarded as an orientation that maximizes orbital overlap between the arene-π system and one of the σ* orbitals.

The directionality of the arsenic-arene interaction with respect to the σ* orbitals is exemplified in the structure of the $As_2\mathbf{1}_3$ assembly. Looking down the As-As axis, each aromatic ring is turned inward so that one side of the aromatic ring is closer to each arsenic ion (**Figure 8**). The shorter arsenic-arene distances are oriented nearly opposite of each As-S bond, in the expected position of the As-S σ* orbitals.

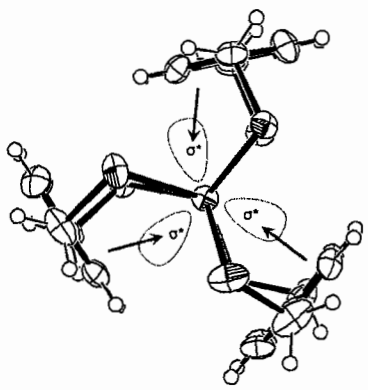


**Figure 8** The crystal structure of the $As_2\mathbf{1}_3$ assembly looking down the As-As axis. Superimposed on this structure are arrows representing electron flow into the estimated positions of the σ* orbitals.

The crystallization of the $As_2\mathbf{1}_3$ assembly is diastereoselective. There is a chiral axis that runs through each arsenic ion: the three As-S-C bonds around each arsenic ion are bent and tilted like the blades of a propeller. Because each of the arsenic ions has its own chiral axis, the overall chirality of the assembly could in theory be Δ,Δ; Δ,Λ; or Λ,Λ (where Δ denotes a clockwise and Λ designates a counterclockwise twist along the As-As axis). In the crystalline state, only the *meso*-Δ,Λ diasteromer—which has a plane of symmetry perpendicular to the arsenic-arsenic axis—is observed.

In solution the complex is fluxional. The $^1$H NMR spectrum of the $As_2\mathbf{1}_3$ assembly shows only one singlet in the aromatic region and one singlet in the methylene region. There are significantly fewer signals than expected for the solid state structure; all of the methylene protons in the static solid state structure are diastereotopic. A dynamic process must be interconverting the diastereomeric protons in solution: the axial chirality at each arsenic ion is rapidly switching. Given the high barrier to pyramidal inversion of arsines, the most likely mechanism of interconversion involves reversing the twist of each arsenic-sulfur-carbon bond. This interconversion process presumably involves a transition state structure where the C-S-As angle is intermediate between a clockwise and a counterclockwise twist. This process is illustrated in **Figure 9**.

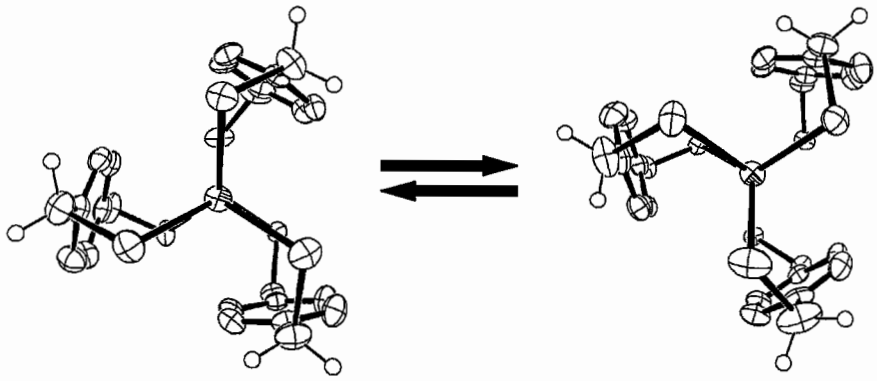

**Figure 9** Interconversion between the two conformations of the "meso" $As_2\mathbf{1}_3$ complex likely proceeds via a torsional twist about the As-S-C angle.

Although this dynamic process involves reversing the axial chirality at each arsenic center, there is no observed formation of the homoconfigurational Δ,Δ and Λ,Λ diastereomers. The stereochemical inversion at one arsenic ion exhibits mechanical coupling to the stereochemical inversion at the other arsenic ion. The transition state geometry for the interconversion process, therefore, may require all the sulfur and methylene carbons to be in the same plane as the arsenic-arsenic axis. Alternatively, the interconversion may proceed in two steps with each individual metal center inverting separately, albeit with the concentration of the transient intermediate too low to measure.[63]

Examples from the Johnson research group do exist as chiral assemblies in the solid state and are believed to be the result of As-arene interactions.[64] In each example, the proximity of the aryl group to the arsenic centers results in a stabilized twisted structure (**Figure 10**). However, in solution, these complexes interconvert as indicated by the sharp singlet in the $^1$H NMR for the methylene portons.

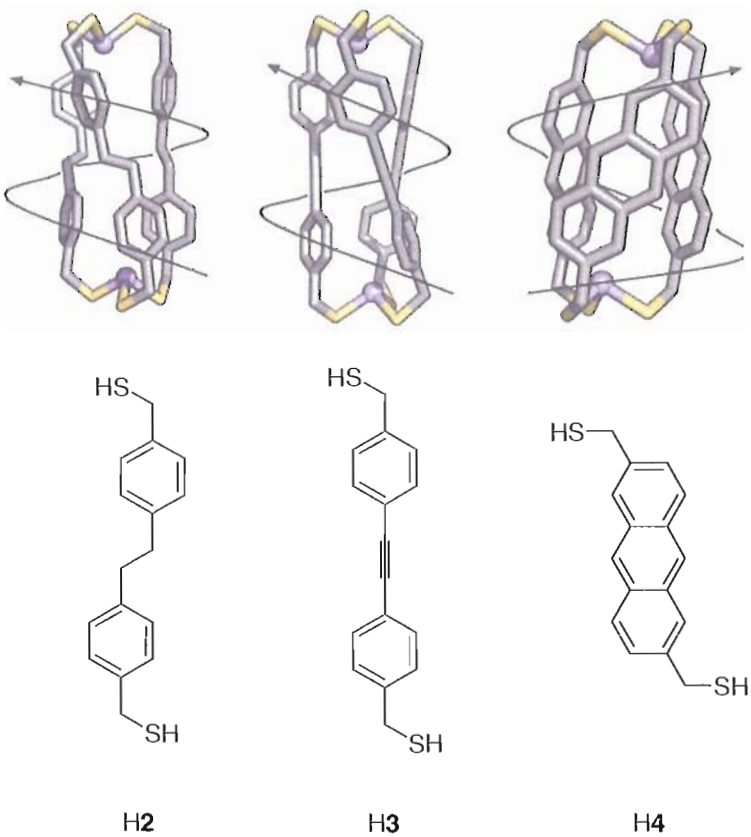


**Figure 10** Examples of twisted assemblies in the solid state (top) from the corresponding ligands below. $As_2L_3$ assemblies exits as Δ,Δ along the metal centers with ligand pitch indicated by the directing of the spiraled arrow.

## *Syn-* and *Anti-* $As_2\mathbf{1}_2Cl_2$ Macrocyles

In the absence of base, 1,4-bis(mercaptomethyl)benzene ($H_2\mathbf{1}$) and $AsCl_3$ assemble into a mixture of *anti-* and *syn-*$As_2\mathbf{1}_2Cl_2$ macrocycles (**Figure 11 and 13**). The macrocycles exist as an equilibrium mixture of *syn-* and *anti-*diastereomers in solution, although the individual isomers can be crystallized selectively. Pentane diffusion into a $CHCl_3$ solution of $AsCl_3$ and $H_2\mathbf{1}$ under different conditions of concentration and stoichiometry allowed selective crystallization of the individual isomers.[21] In the

presence of excess $AsCl_3$, the *anti*-macrocycle selectively crystallizes as an $AsCl_3$ solvate. A mixture of $H_2$**1** and $AsCl_3$ at higher concentrations produces crystals containing exclusively the *syn*-diastereomer.

In the crystal structures of the *anti*- and *syn*-macrocycles (**Figures 11 and 13**, respectively), the arsenic-$\pi$ attraction is again evident in these dinuclear As(III) complexes. Arsenic-arene distances are as short as 3.165 Å, which is less than the sum of the van der Waals radii of arsenic and carbon. Therefore, each arsenic ion is participating in arsenic-arene secondary bonding interactions with two aromatic rings.

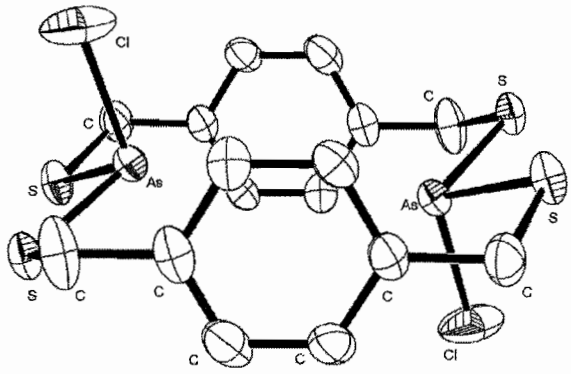


**Figure 11** ORTEP representation of the crystal structure of the *anti*-$As_2$**1**$_2Cl_2$ macrocycle. Cocrystallized $AsCl_3$ is omitted from the diagram.

However, given the approximations inherent in van der Waals and ionic radii, definite assignment of a secondary interaction is strengthened by additional lines of evidence. That is, a short interatom distance, less than the sum of the van der Waals radii, does not necessarily mean the two atoms are participating in a secondary bonding interaction. The values given in tables of van der Waals radii involve several assumptions and are averaged for elements in many different compounds. The authors of

commonly cited tables of van der Waals radii themselves caution in the very papers so cited that their values are averages involving many approximations (see Bondi[65] and Shannon[66]). For example, tables of van der Waals radii begin with the assumption that the atoms are spherical. Furthermore, the radius of a given atom is assumed to be invariant regardless of factors including: different substituents, different numbers of bonds, different oxidation states, different phases and different orientations. An atom is assigned the same radius regardless of these factors, even though this is inaccurate. An example famously given to illustrate the variation of van der Waals radius with orientation involves carbon tetrachloride. The chlorine atoms in carbon tetrachloride are 2.87 Å apart, significantly shorter than the sum of their van der Waals radii (3.6 Å), yet Pauling observed that $CCl_4$ does not show any of the properties that would be associated with the great strain resulting from the repulsion between such close chlorine atoms.[67] The van der Waals radius in directions close to the bond (C-Cl bond) is less in this case.

Possibly, the strongest additional evidence for a given secondary interaction is spectroscopic observation of association in solution. The well-known infrared spectroscopic signature of hydrogen bonding is an archetypal example. In the case of the arsenic-π interaction, there is some solution NMR evidence and some limited solid-state infrared spectroscopy supporting the existence of the arsenic-π interaction. In many cases, however, it is necessary and convenient to assign secondary bonding interactions solely on atomic coordinates derived from the material in the solid state—both to understand the forces influencing crystal packing and in cases where competitive solvation makes measurement in solution difficult.

In addition to short contact distances between atoms, secondary bonding interactions are corroborated in the solid state by considering the orientations of reactive orbitals on the interacting species (**Figure 6**). The strongest arguments for secondary interactions in the solid state involve species in orientations such that their orbitals are clearly aligned to allow for an interaction. The case is considerably bolstered when it can be shown that the participating atoms are distorted out of place in order to maximize the interaction. The orientation of reactive orbitals should be appropriate and, depending on the proposed strength of the interaction, there should be structural distortion consistent with that interaction.

The crystal structure of *anti*-$As_2\mathbf{1}_2Cl_2$ is shown in **Figures 11 and 12** with an arsenic-arsenic distance of 5.02 Å and each arsenic ion makes close contact with two carbons of each aromatic ring of the ligand. Considering the nature of the arene-arsenic donor-acceptor interaction, one might expect each aromatic ring to be tilted slightly inward to make better contact with the presumed acceptor $\sigma^*$ orbitals on each arsenic ion. Unfortunately, considerable disorder of the positions of the arene carbons makes it difficult to draw conclusions regarding whether the interaction is influencing the lay of the aromatic rings (**Figure 11**). Regardless, the nearly parallel orientation of the two arene rings and their proximity to the As(III) ions suggest that the necessary orbitals are in an appropriate geometry for an $\eta^2$-secondary interaction.

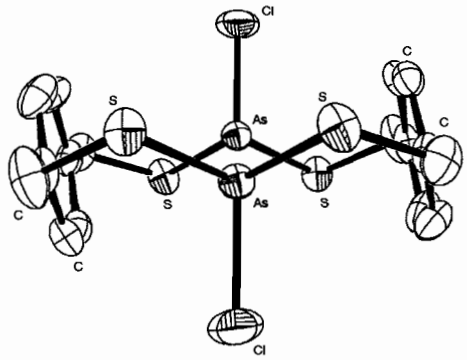


**Figure 12** ORTEP representation of the crystal structure of anti-$As_2\mathbf{1}_2Cl_2$ macrocycle looking down the As-As axis. Cocrystallized $AsCl_3$ is omitted from the diagram.

The crystal structure of the *syn*-macrocycle shown in **Figure 13** has an arsenic-arsenic distance considerably shorter than the *anti* diastereomer (4.65 Å). Each arsenic ion makes close contact with two carbon atoms of each aromatic ring of the ligand. The two aromatic rings of the macrocycle are again nearly parallel. Presumably, any movement of one aromatic ring to make better contact with one σ* orbital would weaken contact with another σ* orbital on the other arsenic ion. Still, the closest As(III)-$C_{ortho}$ distances do occur opposite an As-S bond, in the expected vicinity of an acceptor As-S σ* orbital. Despite the lack of dramatic structural distortions, the necessary orbitals are again in an orientation appropriate for $\eta^2$-secondary bonding interactions.

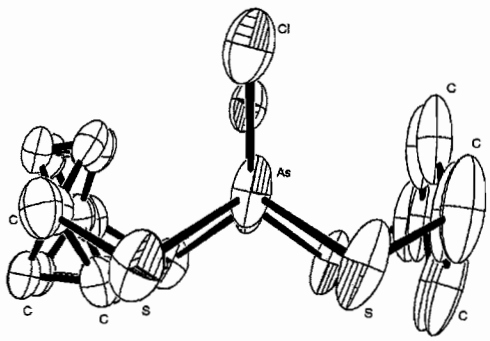


**Figure 13** ORTEP representation of the crystal structure of the syn-$As_2\mathbf{1}_2Cl_2$ macrocycle looking down the As-As axis. Rotational disorder of the left phenyl ring has been modeled as partial occupancy in two different orientations.

The presence of multiple arsenic-arene interactions enforces unexpectedly short arsenic-arsenic distances in each macrocycle. CAChe molecular mechanics minimizations (MM2, MM3)—which do not take arsenic-arene secondary interactions into account—suggest that the arsenic-arsenic distance would be no less than ca. 6 Å. The crystal structure shows the influence of the arsenic-arene interactions: the arsenic atoms are significantly drawn into the center of the macrocyclic cavity with an arsenic-arsenic distance of only 5.02 Å in the *syn*-macrocycle and only 4.65 Å in the *anti*-isomer.

## Controlling Diastereomeric Excess in $As_2L_2Cl_2$ Macrocyles

Another aspect of our laboratory's research is the careful control of solid state structures by either varying crystallization conditions (e.g. solvent choice, rate and crystallization techniques) or through ligand modification. Similar to the 1,4-bis(mercaptomethyl)benzene system described above, three isomeric naphthalene-based ligands, 2,6-bis(mercaptomethyl)naphthalene ($H_2$**2**), 1,5-bis(mercaptomethyl)naphthalene ($H_2$**3**), and 1,4-bis(mercaptomethyl)naphthalene ($H_2$**4**) (**Figure 14**), were each reacted

with $AsCl_3$ to form self-assembled equilibrium mixtures of *syn*- and *anti*-macrocycles. By using these ligands which differ only by the ring positions of the mercaptomethyl groups, we were able to access different ratios of the two macrocyclic isomers including mostly *syn*, mostly *anti*, and an almost statistical mixture of the two.[26]

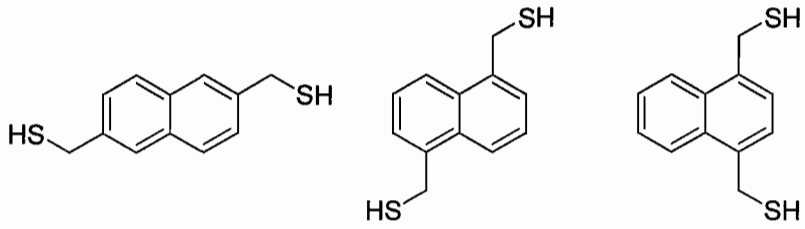


$H_2$**5** $H_2$**6** $H_2$**7**

**Figure 14** Isomeric naphthalene-based dithiol ligands.

Within these macrocycles, the arsenic-$\pi$ interaction causes the arsenic atom and its coordination sphere to be pulled toward the ligand backbone. Some steric congestion is present around the chlorine and sulfur atoms (**Figure 15**) and the diastereomer with the least amount of unfavorable steric strain forms in excess (giving rise to a diastereomeric excess, (de)).

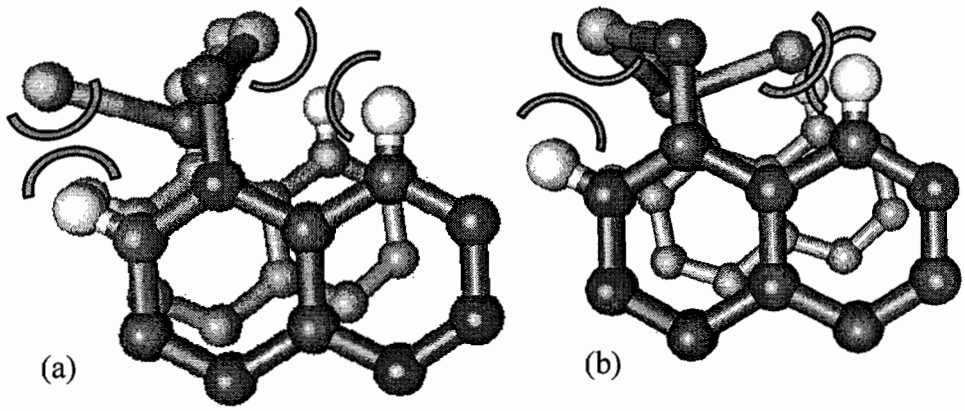


**Figure 15** Partial ball and stick models of $As_2\mathbf{5}_2Cl_2$ showing the steric repulsions between chlorine and sulfur atoms when the chlorine atom is pointing away from (a) and toward (b) the hydrocarbon backbone of the ligand.

The de of these macrocycles in solution has been measured using $^1$H NMR spectroscopy and found to be only 9% for $As_2\mathbf{5}_2Cl_2$ (it is not known which isomer is in excess). Neither the crystal structure nor the computer models indicate any steric strain in either isomer, so the small de is not surprising. Crystals were obtained of *anti*-$As_2\mathbf{5}_2Cl_2$ (**Figure 15a**) and the structure reveals a clear arsenic-$\pi$ interaction within a cavity that is too small to accommodate any guests screened to date (metal cations, $H^+$ or small organic molecules).

*Anti*-$As_2\mathbf{6}_2Cl_2$ exists in 85% de in solution as determined by $^1$H NMR spectroscopy. The observed excess seen for this macrocycle can be attributed to the large difference in steric interactions between the chlorine atom and the naphthalene backbone of the ligand when the Cl is pointing into the cavity (toward C-H) or pointing out (toward H). Again, crystals were obtained and found to be 100% *anti* (**Figure 15b**).

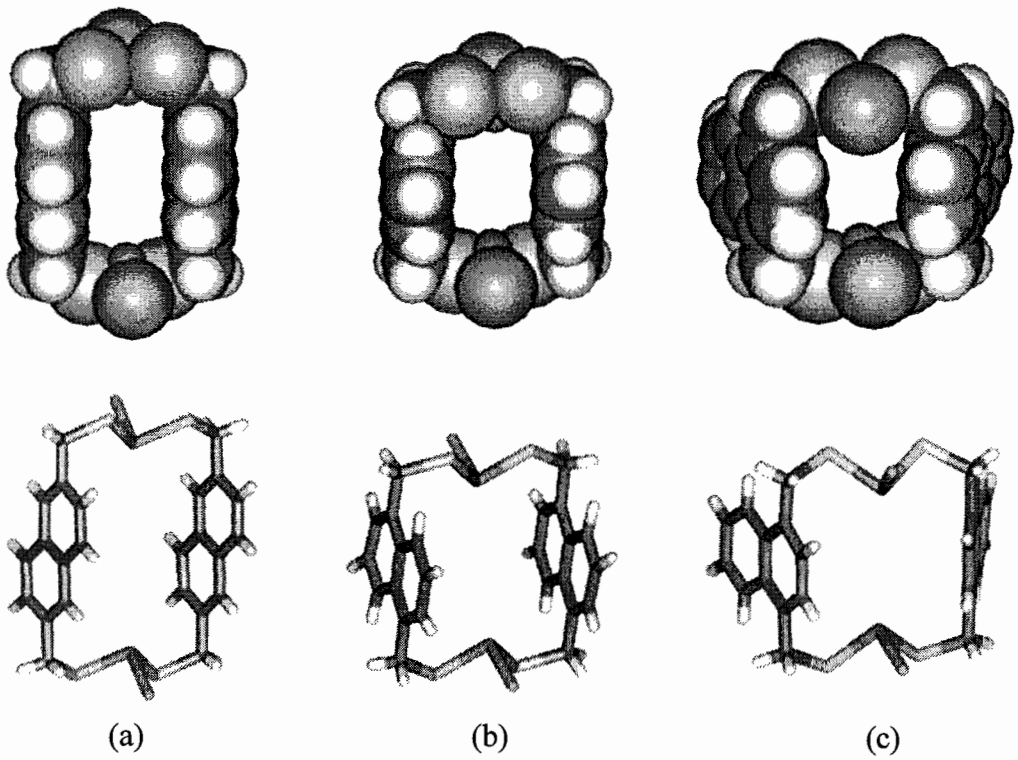


**Figure 16** Representations of single-crystal X-ray structures of $As_2\mathbf{L}_2Cl_2$ macrocycles derived from napthalene-based ligands. Space filling and wireframe representations of (a) *anti*-$As_2\mathbf{5}_2Cl_2$, (b) *anti*-$As_2\mathbf{6}_2Cl_2$ (c) *syn*-$As_2\mathbf{7}_2Cl_2$ macrocycles.

In the case of $As_2\mathbf{7}_2Cl_2$ macrocycles a 90% de of the *syn* macrocycles exists in solution. In the solid state, however, the *syn* isomer crystallizes exclusively (**Figure 15c**). Diastereocontrol is important in our design scheme to utilize macrocycles as synthons for larger assemblies. For instance, *syn*-macrocycles are preorganized to form larger discrete assemblies allowing us to study host-guest chemistry, while *anti*-macrocycles can be functionalized to provide extended structures. We are currently pursuing this goal, as well as trying to design ligands that will form arsenic-containing macrocycles with improved diastereocontrol.[26]

## Supramolecular $Sb_2L_2Cl_2$ Assemblies

Antimony is also able to participate in self-assembly with dithiol ligands. In the absence of base, 1,4-bis(mercaptomethyl)benzene ($H_2$**1**) and antimony(III) form a dinuclear $Sb_2$**1**$_2Cl_2$ complex (Figure 11). This macrocycle also exhibits pnictogen-arene interactions: each antimony(III) ion participates in an $\eta^2$-secondary interaction with one aromatic ring of the macrocycle and an $\eta^3$-secondary interaction with the opposite ring.[68] The shortest Sb-C interactions are again opposite an antimony-sulfur bond consistent with the view that the $\pi$-cloud of the arene ring is donating into the Sb-S $\sigma^*$ orbital (**Figure 16b**). For example, the Sb-$C_{ortho}$ distance opposite the Sb-S bond is 3.50Å versus 3.61Å for the other *ortho*-carbon atom. Since the antimony-chlorine bonds point away from, and bisect the two As-S bonds, regardless of the way the two arene rings are canted, there will always be two *ortho*-carbon atoms positioned closer to the antimony ions than the other two.

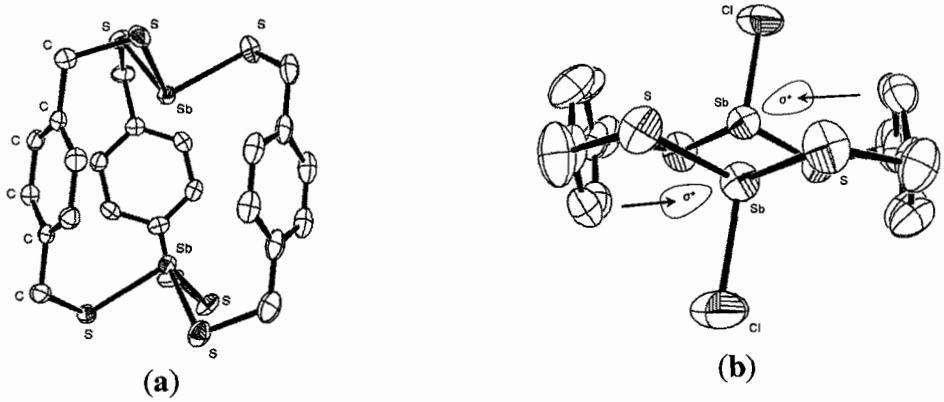


**Figure 17** ORTEP representation of the single crystal X-ray structure of (a) $Sb_2$**1**$_3$ and (b) $Sb_2$**1**$_2Cl_2$.

Similarly to the case for arsenic, the deprotonated thiolate ligands assemble with $SbCl_3$ to form an $Sb_2\mathbf{1}_3$ complex. Interestingly, this assembly is chiral and posesses a helical twist, crystallizing as a racemic mixture of enantiomers (**Figure 17a**). The Sb-Sb distance in this complex is only 4.30 Å, due to stronger antimony-$\pi$ interactions. To achieve this proximity between antimony atoms, the ligand must adopt a helical twist to "compress" the complex. As in the case for $As_2\mathbf{1}_3$, a dynamic torsional rotation inverts the helical and *meso* conformations in solution.

The crystal structure of $Sb_2\mathbf{1}_3$ readily demonstrates the presence of many intramolecular Sb-arene secondary interactions. Each Sb(III) ion makes close contacts with two carbons of each of the three aromatic rings. The orientations of these close contacts are consistent with the expected positions of available reactive orbitals. Furthermore, the assembly bears further structural evidence consistent with electronic donation from the $\pi$-system into the Sb-S $\sigma^*$ orbital. Each aromatic ring is twisted inward in a manner that maximizes contact between the ring carbons and the expected positions of the Sb-S $\sigma^*$ orbitals

## Conclusion

Our work continues to focus on the design and synthesis of organothiol ligands for use in supramolecular coordination chemistry of arsenic and other main group elements. The lack of efficient chelators for toxic ions such as arsenic drives this work forward and the use of supramolecular chemistry provides for a different approach to arsenic sequestering. Metal binding specificity and interesting emergent spectral

properties comprise two encouraging results we have observed thus far in this line of research. We are optimistic that rich host-guest chemistry and new structures types are soon to follow on the basic science end of this research. Applications in sensing stemming from a supramolecular approach to metal chelation will be investigated, and we are currently exploring the use of these ligands to provide nanostructured materials for use as sorbents for water purification.[69,70]

## Bridge to Chapter II

Chapter II extends the discussion of secondary bonding interactions to include two mononuclear arsenic complexes and is based in part on published and unpublished results. In the first half of Chapter II, SBIs between arsenic and the β-mercapto imido oxygen of a naphthalimide ligand are investigated by NMR, UV-Vis and X-ray chrystallography. In the second half of Chapter II, 1-mercapto-2-phenyl stilbene was reacted with dimethylarsenic iodide and investigated by variable temperature NMR and computational analysis. Chapter III contains unpublished results pertaining to toxic metal ion uptake from natural water sources. Chapter IV contains unpublished results and focus on the use of cationic sorbent material to bind oxyanions from natural water sources. Chapter V contains published and unpublished material and describes a recent collaboration between myself and scientists at Pacific Northwest National Laboratory.

# CHAPTER II

## MONONUCLEAR ARSENIC COMPLEXES: PROBING SECONDARY BONDING INTERACTIONS (SBIS) IN ARSINE COMPLEXES

Some of this work has been previously published and is reproduced with permission from: Carter, T.G.; Healey, E.R; Pitt, M.A.; Johnson, D.W. *Inorg. Chem.* **2005**, *44*, 9634-9636

### General Overview

This chapter discusses the concept of secondary bonding interactions (SBIs) at both a theoretical and experimental level. A number of systems were explored in an attempt to further elucidate the nature of SBIs with respect to both arene and heteroatom arsenic containing molecules. The diimide work outlined early in this chapter stems partially from the publication 'Secondary Bonding Interactions Observed in Two Arsenic Thiolate Complexes' in *Inorganic Chemistry* (2005, 44 (26), 9634-9636, © American Chemical Society).[1] This article was co-authored with Elisabeth Rather Healey who performed X-ray crystallographic analysis, Melanie A. Pitt who performed experimental and editorial

assistance and Professor Darren W. Johnson who provided intellectual input and editorial assistance. Additionally, computational studies will be included along with the published results as well as a brief literature review on the topic of SBIs, unpublished spectroscopic studies and an unpublished structure with three-fold symmetry imparted by secondary bonding interactions between arsenic and intramolecular imido oxygens. The remaining content of this chapter covers the design and synthesis of arene-containing molecules for use in both UV-Vis and NMR spectroscopic studies and includes conclusions based off of experimental and computational studies. A more detailed description of SBIs can be found in chapter I of this dissertation.

## Introduction

Supramolecular approaches to arsenic(III) chelation represent a relatively emerging field,[2-7] due in part to the peculiar coordination geometry of this highly toxic ion. Our research group has produced many spectacular examples of self-assembled supramolecular complexes by concomitant utilization of computational modeling and synthetic approaches. The unusual trigonal-pyramidal coordination geometry of As(III) features a stereochemically active lone pair when coordinated by sulfur-based ligands[A] and is predictable enough to be exploited as a target for specific ligand design.[8-10]

The characteristic coordination of As(III) by sulfur-containing biological molecules such as glutathione or cysteine has recently been reported in the context of developing a better understanding of arsenic toxicity.[9,11] However, there are relatively few known

[A] See Chapter I Figure 6 for examples of the preferred binding geometry for arsenic(III)-thiolate and stereo chemically active lone pair.

structures of arsenic thiolate complexes: a search of the Cambridge Structure Database (CSD)[12] reveals only 83 examples of an As(III) ion coordinated by one or more organothiolate ligands.[B] The use of thiolate ligands optimized for the specific coordination geometry of As(III) that also possess additional functional groups capable of exhibiting secondary bonding interactions is relevant toward designing specific chelators and sensors for this toxic main group element.

We incorporate weak attractive forces known as secondary bonding interactions (SBIs) into our design strategy for forming self-assembled complexes containing organothiolate-based ligands and main group elements. SBIs can occur between main group metals and an aromatic system, heteroatoms such as O, N, S and the halogens.[13,14] SBIs can be predictable, occurring within the sum of the van der Waals radii of two or more atoms,[15,C] and can offer a potentially powerful method for ligand design to optimize chelation of main-group metals.[16] More and more examples are appearing in the literature where supramolecular chemists are utilizing SBIs as design criteria to aid in the self-assembly process. In doing so, supramolecular chemists are expanding beyond traditional self-assembly forces such as metal coordination or hydrogen bonding.[17,18]

As mentioned in Chapter 1 of this dissertation, the most comprehensive study of secondary bonding interactions for arsenic is limited to As(III) and either thiocarboxylic or dithiocarboxylic acid derivatives.[19] The authors utilized both crystallographic and computational data to successfully measure close contact distances with a number of

---

[B] A CSD (Conquest Version 1.10, 2008 Release) search of compounds that possessed at least one As-S bond (with S also bonded to a C) revealed 83 structures of which only 63 contained an As ion not also bonded to a carbon or transition metal atom.

[C] The mean van der Waals radii as calculated by Bondi are: As-1.85 Å, O-1.52 Å, N-1.52 Å and S-1.80 Å.

substituted arsenic complexes and neighboring thiocarboxylato or dithiocarboxylato ligands **Figure 1**.

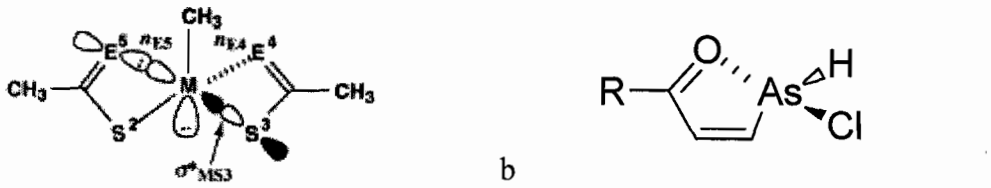


**Figure 1** Secondary bonding interactions (dashed line and overlapping white filled orbital depictions) between the lone pair of electrons on E (oxygen or sulfur) and an adjacent σ* orbital of a metal center (M = As) resulting in bond elongation (solid line and overlapping black and white filled orbital depictions) (a) and model system for computational determination of As···O SBI strength (b).

As-S bond elongation was also observed suggesting that the interaction involves the participation of the electron density of the nonbonding lone pairs of either oxygen or sulfur with the $\sigma^*$ orbitals of adjacent As-S bonded ligands (**Figure 1a**). UV-Vis spectroscopy provided confirmation of charge transfer interaction by the observation of hypsochromic, or higher energy, peak migrations. Tani and coworkers have suggested that the strength of SBIs between heteroatoms and main group elements are similar to that of a weak hydrogen bond.[20] Computational studies of the pnictogens forming vinylic five-member ring systems with SBIs to oxygen have an assigned value around 2 kcal/mol for arsenic, depending on the substituents off the arsenic center (**Figure 1b**).[21]

Despite the extensive experimental work performed by the authors, they were unsuccessful in quantifying the strength of the interaction between arsenic and the adjacent heteroatoms. The use of SBIs[13,14] between As(III) and heteroatoms of

appropriate ligands offers an additional and complementary tool for designing ligands specific for this ion.

## Results and Discussion

This section of Chapter II reports the synthesis and crystal structure of a new first-generation sulfur-based ligand *N*-(2-mercaptoethyl)-1,8-naphthalimide, H**1**–capable of binding As(III) *via* a thiolate group with a complementary SBI between the imido oxygen and arsenic. The naphthalimide core was chosen as a model for future supramolecular chelators due to the proximity of its imido oxygens atoms to the thiol and for its well known electronic absorption and emission properties.

The complexes [As**1**$_2$Cl] and [As**1**$_3$] form by treatment of H**1** with $AsCl_3$. Thiol ligand H**1** was synthesized (**Scheme 1**) in *ca.* 85% yield[22] and formed light brown single crystals suitable for diffraction analysis from diffusion of acetonitrile into a $CHCl_3$ solution of H**1**.

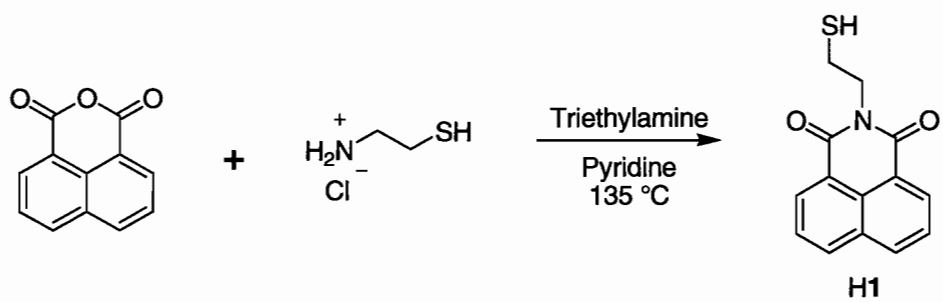


**Scheme 1** H1 synthesis by combining cysteamine HCl with triethylamine in pyridine and stirred for 20 minutes under a nitrogen atmosphere. 1,8-naphthalic anhydride was added and the solution heated to 135°C overnight.

The single crystal X-ray structure of H1 consisted of two sets of layers of ligands interacting *via* aromatic face-to-face π-π stacking with an intermolecular distance between adjacent layers of 3.45 Å (**Figure 2**, also see **Appendix A** for crystallographic values).

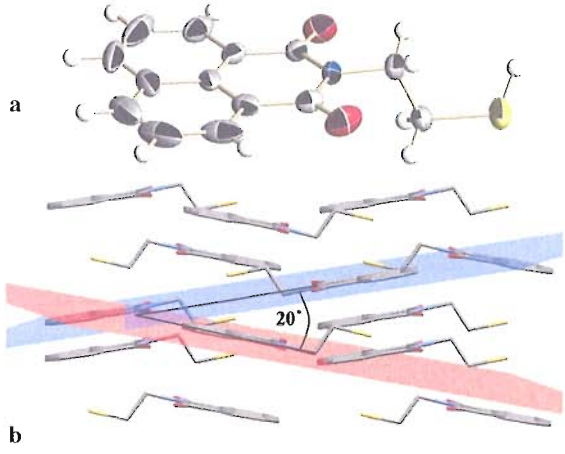


**Figure 2** Crystal structure of the ligand H**1**. (a) ORTEP representation with 50% thermal ellipsoids and (b) view of the crystal packing down [101] showing the non-parallel arrangement between the planes of aromatic stacking formed by H**1**.

The planes formed by these two sets of layers are twisted at an angle of *ca.* 20°. This non-parallel arrangement is sustained by weak interactions between aromatic CH and oxygen atoms of the imide with d(C···O) = 3.21 Å. Furthermore, in the crystalline state the mercapto ethylene moiety adopts the expected *anti* conformation with a dihedral angle between the sulfur atom and the nitrogen atom of the imide of 177°.

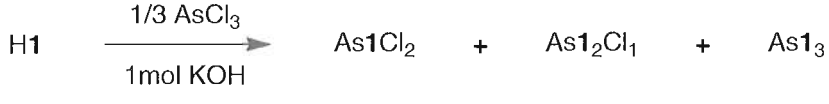


**Scheme 2** Addition of arsenic trichloride to H**1** in a 1:3 ratio in the presence of base formed As$\mathbf{1}_m$Cl$_n$ where m=1-3 and n=0-2 as verified by NMR spectroscopy.

Treatment of **H1** with $AsCl_3$ and a stoichiometric amount of KOH yields a mixture of [As**1**$Cl_2$], [As$\mathbf{1}_2$Cl] and [As$\mathbf{1}_3$] complexes according to $^1$H NMR spectroscopy (**Scheme 2**). Pale yellow crystals suitable for X-ray analysis were obtained for both the [As$\mathbf{1}_2$Cl] and [As$\mathbf{1}_3$] complexes (**Figure 3**, see also **Appendix A**).

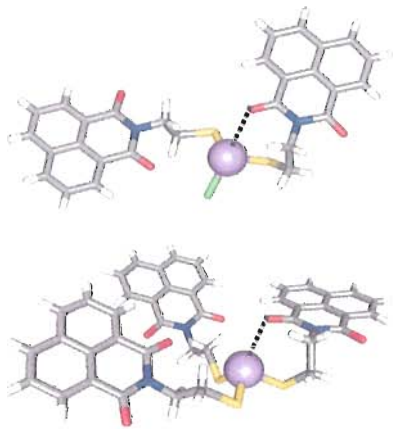

**Figure 3** X-ray crystal structures of the two complexes [As$\mathbf{1}_2$Cl] (top) and [As$\mathbf{1}_3$] (bottom) showing the *gauche* conformation adopted by the mercapo-ethylene moieties allowing for the secondary As•••O bonding interactions (dashed lines) within the complexes.

The structure of [As$\mathbf{1}_2$Cl]·$CHCl_3$ reveals that the complex is stabilized by As···O secondary bonding interactions (d(As···O) = 2.91 Å) resulting from one ligand adopting a higher energy *gauche* conformation about the mercapto-ethylene moiety with a dihedral angle between the sulfur and nitrogen atoms of ca. 51° (**Figure 4**). This secondary bonding interaction is within the range of previously observed As···O secondary interactions,[D,19] and it suggests that in the crystalline state crystal packing forces and/or the As···O secondary interaction is at least strong enough to compensate for one unfavorable *gauche* interaction. The other ligand exists in the expected *anti* conformation with a corresponding dihedral

[D] A CSD search revealed that the few As···O secondary bonding interactions previously observed are in the range of 2.71-2.94Å. For a representative example see K. Tani et al.

angle of ca. 170°. Presumably, the rate of crystallization of the complex prevents additional As···O interactions from forming. The crystal packing of [As**1**$_2$Cl]·CHCl$_3$ is sustained by aromatic stacking similar to that observed for H**1** (**Figure 2b**), with distances between the centroids of naphthalimide moieties of adjacent arsenic complexes ranging from 3.40 to 3.65 Å.

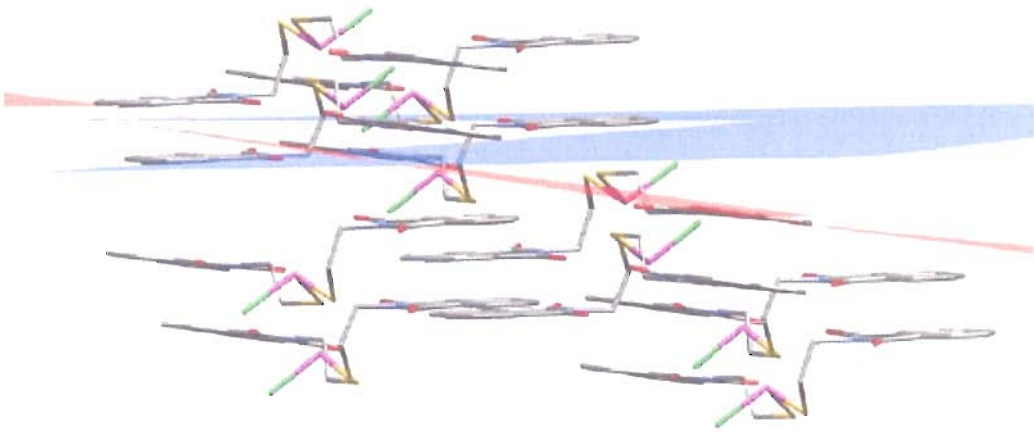

**Figure 4** Packing diagram of As**1**$_2$Cl in the crystalline state generated using the program Mercury. All non-hydrogen atoms are shown in wireframe with arsenic purple, oxygen red, sulfur yellow, chlorine green, nitrogen light blue and carbon gray.

Measured bond lengths of 2.25 Å for the As-Cl opposite of the weakly bound oxygen in As**1**$_2$Cl (**Figure 3 top**) are within calculated values of 2.2 Å.[15] However, a search of the CSD for structures containing AsCl$_x$ with observed secondary bonding interactions produced a wider range of bond elongations. The measured value of As**1**$_2$Cl falls between reported lengths for As-Cl bonds that do not experience weak SBIs (2.19 Å) and for As-Cl bonds opposite of a weakly bound heteroatom (2.38 Å).

The crystal structure of [As**1**$_3$] reveals that two of the ligands adopt the expected *anti* conformation ((S-C-C-N) = 180° and 170°), while the third thiolate again adopts a *gauche* conformation to allow for one weak As···O interaction (d = 3.21 Å) with a corresponding dihedral angle of ca. 60° (**Figure 3**). Crystal packing is similar to that of H1 (**Figure 2b**) and [As**1**$_2$Cl] (**Figure 4**) with the two sets of planes sustained by aromatic stacking (d(centroid-centroid) = 3.50 to 3.56 Å) and twisted at an angle of ca. 37° (**Figure 5**).

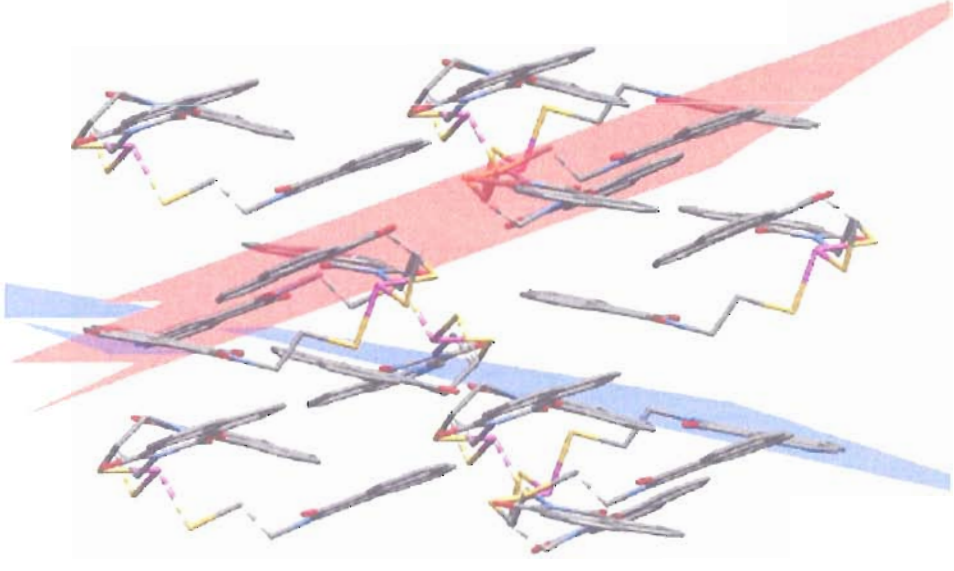

**Figure 5** Packing diagram of As**1**$_3$ in the crystalline state generated using the program Mercury. All non-hydrogen atoms are shown in wireframe with arsenic purple, oxygen red, sulfur yellow, chlorine green, nitrogen light blue and carbon gray.

A different polymorph of the original [As**1**$_3$] complex was obtained by slow diffusion of $AsCl_3$ into a solution containing deprotonated ligand **1** (**Figure 6**).

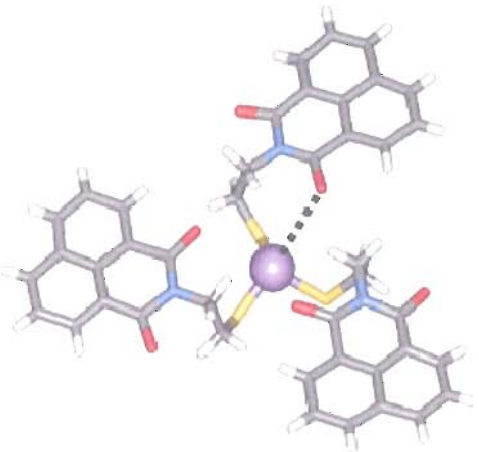

**Figure 6** Crystal structure of $C_3$ symmetric arsenic complex [As**1**$_3$]. Representative secondary bonding interactions are denoted by dashed line. As···O distance of 3.16 Å for the $C_3$ symmetric polymorph versus an As···O distance of 3.21 Å for the non-symmetric structure.

The resulting complex was found to be $C_3$-symmetric down the arsenic center with one imido oxygen from each ligand involved in an SBI with an As···O distance of 3.16 Å which is less than that of [As**1**$_2$Cl] and the non $C_3$ symmetric [As**1**$_3$] complex of 3.21 Å. As mentioned above, the alkyl linkage of each ligand is forced into the higher energy *gauche* conformation, accounting for a 2-3 kcal/mol increase in energy as well as nonparallel π-stacking crystal planes. A slight bond elongation was observed in the $C_3$ symmetric complex with As-S bonds measuring 2.25 Å versus 2.22 Å for the non-SBI As-S bond in the unsymmetrical [As**1**$_3$].

## Variable Temperature NMR Studies

Based on the new $C_3$-symmetric complex and the potential for such a structure to be *locked* in conformation in solution due to the SBIs, attempts to quantify the As···O secondary bonding interactions were performed by solution-phase variable temperature

NMR (VT-NMR) studies. Crystals, of the new $C_3$-symmetric polymorph were grown as described in the experimental section. To assure the proper polymorph of the crystalline material, the space group was verified by X-ray analysis and compared to the known $C_3$ symmetric structure for preliminary studies. The crystals were then dissolved in $CDCl_3$ with no further purification, yielding promising initial room temperature NMR data. The appearance of a complex spectrum consisting of splitting patterns consistent with a chiral $C_3$-symetric complex containing diastereotopic protons was observed both in the aromatic and aliphatic regions.

It was rationalized that if the complex was indeed locked in conformation at room temperature in solution on the NMR time scale, then heating the sample by VT-NMR should impart enough energy to cause a departure from the locked conformation. A freely rotating structure should cause the diastereotopic protons to become equivalent and the split peaks, particularly Hd and Hd', to coalesce into an averaged triplet from the coupling with He,e'. Crystals were once again obtained as described above and the unit cell verified to match the known $C_3$ symmetric complex. The crystals were washed with chloroform, methanol, 4:1 methanol/water mixture and again with methanol before being dried under high vacuum. The As**1**$_3$ complex is only sparingly soluble in chloroform and methanol, therefore, the above washes assure pure product by removing unreacted starting material and KCl byproduct. The washed and dried crystals were dissolved in deuterated 1,1,2,2-tetrachloroethane and heated to 100 °C from room temperature by 10 °C intervals with a fifteen-minute equilibration time between runs. The result of this

experiment did not provide any peak migration; mainly due to the absence of the complex splitting patterns with this solvent system.

It would appear that the strength of the As···O SBI is solvent dependent due to the observation of splitting in $CDCl_3$ but not in $C_2D_2Cl_4$. An alternative approach involved cooling the sample and checking for the appearance of a new peak as a result of limiting the available energy for rotation of the ligands. The $C_2D_2Cl_4$ sample was chilled to -60 °C from room temperature again at 10 °C intervals and a fifteen-minute equilibration time. The NMR spectra of the prepared crystals in tetrachloroethane were devoid of any secondary structure observed in the preliminary experiment using chloroform as the solvent. In an attempt to recreate the preliminary NMR studies, crystals from the above purification were dissolved in $CDCl_3$ and the sample was slowly cooled to -40 °C from room temperature as described above. Initially, a well-defined spectrum was obtained at room temperature with no indication of complex splitting. However, at temperatures as low as 0 °C, peaks observed in the preliminary study appeared to grow from the baseline. As the temperature was decreased, this time at 5 °C intervals, the peaks appeared to grow in intensity, suggesting that the structure was indeed becoming locked in conformation in solution as the temperature decreased **Figure 7**.

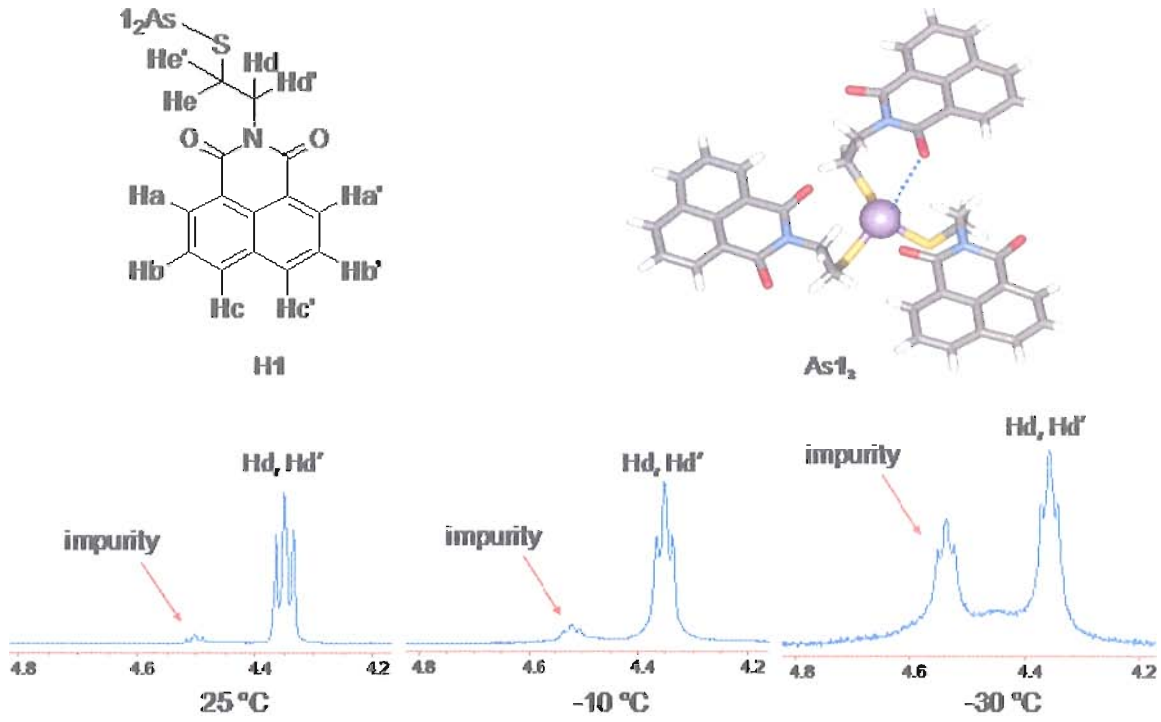


**Figure 7** Variable temperature NMR spectrum of $C_3$-symmetric crystals in chloroform. [As**1**$_3$] with protons labeled (Top left). $^1$H spectra of at Hd at 25 °C (bottom left), -10 °C (bottom center) and -30 °C (bottom right). The growth of the downfield peak is due to the decrease solubility of [As**1**$_3$] in $CDCl_3$.

However, this interpretation of the data was incorrect. The appearance of new peaks was not due to the complex being locked in the higher energy $C_3$ symmetric conformation in solution, but instead was due to the decreased solubility of the complex in low temperature chloroform. The peaks observed that increased in intensity were merely an impurity, perhaps As**1**$_2$Cl, confined to baseline noise and masked by the much larger peaks of the complex in solution when at room temperature. The appearance of the new peaks was due to the decrease in concentration of As**1**$_3$ as the temperature decreased. This was verified by comparing the relative height of the aromatic peaks of the complex with the residual solvent peak for chloroform and trimethylsilane (TMS) reference. As

the sample was heated back to room temperature in the manner described above, the peaks associated with the complex grew in intensity and the impurity peaks retreated back to mere baseline noise. A simple bench-top experiment was carried out by chilling the NMR tube containing the complex by means of a dry ice/acetone bath. This experiment produced colorless crystals along the glass wall of the tube which disappeared upon warming. Similar crystals were observed when the NMR tube was removed from the magnet while still chilled. Again, the crystals disappeared as the sample tube warmed to room temperature.

Although the variable temperature NMR studies did not yield any quantifiable secondary bonding interaction data, it did provide a qualitative range—lying above that to overcome three *gauche* interactions and below that of approximately 5 kcal/mol. This is in good agreement with previous studies assigning a value close to a weak hydrogen bond as well as work performed by Minkin and coworkers suggesting a value of 2 kcal/mol.[20,21] As an alternative approach, UV-Visible spectroscopy was performed in an attempt to measure SBIs by observing perturbations in the spectra of the bound and unbound ligand H1.

## UV-Visible Spectroscopy of As-H1 Complexes

Previous work by Vickaryous[23,24] and Schmidbaur[25] demonstrated the ability of arsenic to have through-space interactions with an electron rich aromatic π-system. Based off of low-level molecular mechanics calculations it was hypothesized that the naphthalene core would interact with arsenic by an arsenic-π secondary bonding

interaction due to the close proximity of the ligand to the metal center. It was therefore believed that the interaction should impart a change in the spectral properties of the naphthalimide core, resulting in either a red or blue shift in the ultraviolet (UV) absorption spectrum. The basis of such an observation can be explained by a charge transfer between the lone pair of the arsenic metal center and $\pi^*$-orbitals of the aromatic ring system. Rao reported changes in the absorption spectrum of the aromatic system due to interactions between a phenyl ring and the lone pair of a nearby oxygen moiety.[26] The expected spectral shifts are dependent on the direction of flow of electron density. A bathochromic (lower energy) shift will result from a metal to ligand interaction caused by a decrease in the energy gap between ground and excited states of the ligand resulting from increased electron density of the aromatic chromophore.[27] A hypsochromic (higher energy) shift will be observed due to a ligand-to-metal interaction as seen between arsenic and a dithiocarboxylate ligand studied by Tani and coworkers[19].

Upon addition of arsenic trichloride to a 2:1 dichloromethane/methanol solution containing deprotonated ligand (**1**), no such shift in wavelength was observed in the two prominent peaks at $\lambda_{238}$ and $\lambda_{335}$ nm. However, an increase in peak height at $\lambda_{335}$ was observed to give a peak ratio of 0.81 (relative height of $P_{335}/P_{238}$) after deprotonation of **1** with solid KOH. This is considerably larger than the peak ratio of 0.67 for the protonated ligand H**1**. The addition of base causes the nearly colorless solution of H**1** to appear bright yellow. Upon addition of $AsCl_3$, the yellow solution becomes colorless once again as the As**1**$_3$ complex forms. The UV-Visible spectrum of As**1**$_3$ has a peak ratio of 0.49, slightly smaller than the native ligand (**Figure 8**).

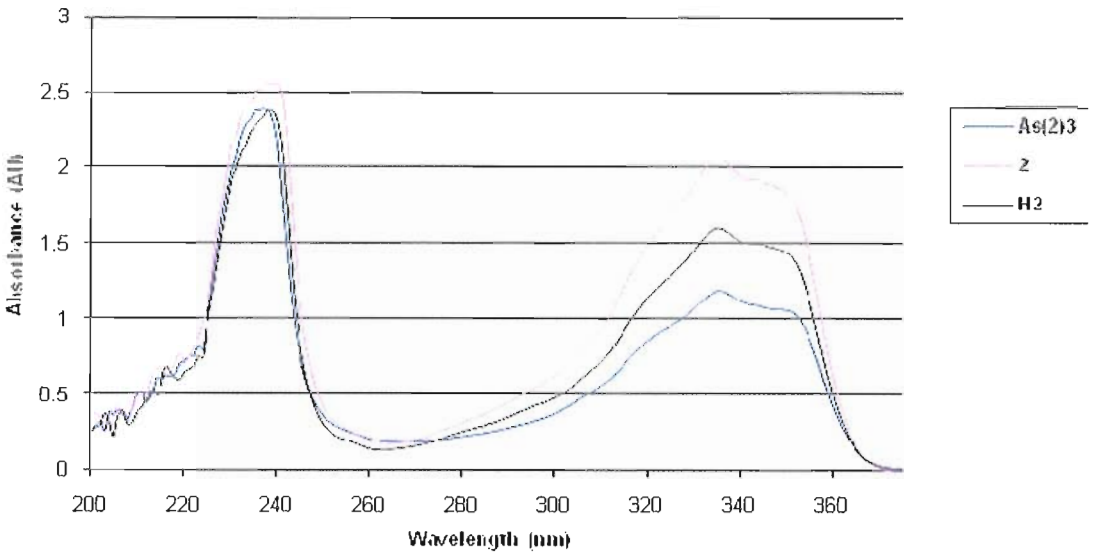


**Figure 8** Qualitative UV spectra of protonated ligand H**1** (black), deprotonated **1** (pink) and [As**1**$_3$] (blue) in a 2:1 dichloromethane methanol solution. Relative peak height ratios were determined by P335/P238 to give 0.67, 0.81 and 0.49, respectively.

Using the peak at $\lambda_{238}$ as an indicator to qualitatively assume similar concentrations between solutions, by Beer's law ($A = \varepsilon bc$ where A = absorption, $\varepsilon$ = molar extinction coefficient, b = path length and c = concentration), a change in absorption must be due in part to a change in the molar extinction coefficient ($\varepsilon$) at $\lambda_{238}$. This is in good agreement with respect to similar systems reported in the literature pertaining to perylene diimide systems (**Figure 9**).[28]

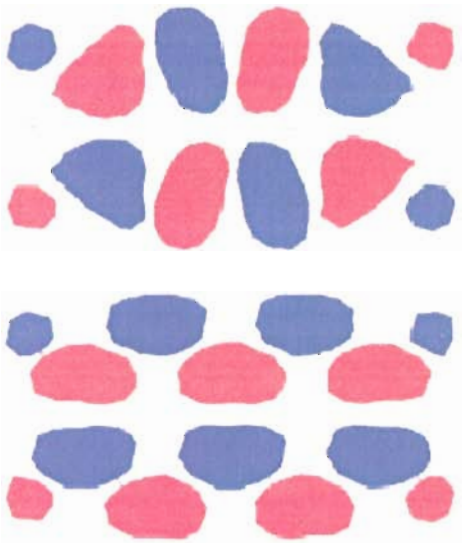

**Figure 9** HOMO (top) and LUMO (bottom) of perylene bisimides as reported by Würthner. Nodes exist for both frontier orbitals at the imide nitrogens inhibiting the mixing of orbitals between atoms appended to the imide nitrogen.

The authors of the aforementioned work attribute the observed trend to nodes in the HOMO and LUMO at the imide nitrogen. The result is a reduction in orbital mixing between the imide and the substituents of the imide (**Figure 10**); therefore no peak shift is observed.

The likely change in extinction coefficient has been attributed to changes in vibronic motions, dubbed the "loose bolt effect."[29] Essentially, bulkier groups off the imide nitrogen cause a decrease in vibronic motion thus a decrease in the extinction coefficient. Upon complex formation, the addition of the heavier arsenic results in a decreased extinction coefficient as observed.

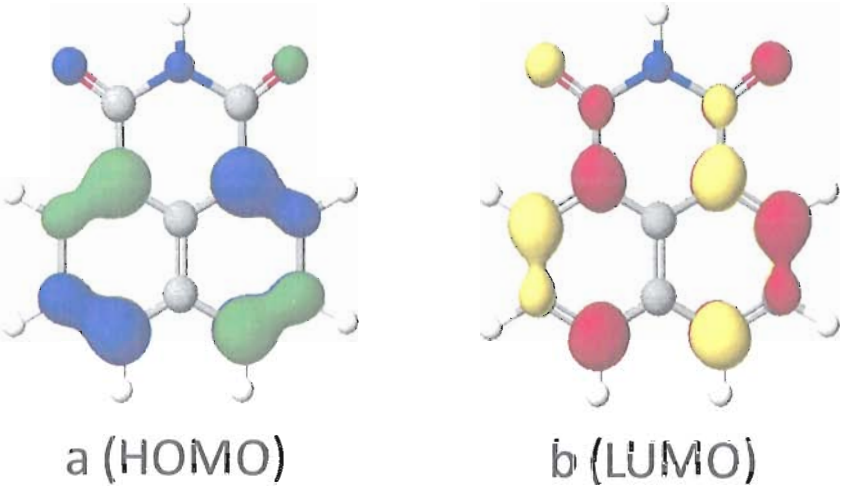


**Figure 10** CAChe computational calculations of the HOMO (a) and LUMO (b) of 1,8-naphthalimide. A node is present at the imide nitrogen for both models. This limits the orbital mixing between the conjugated imide and the nitrogen substituents.

The observed increase in extinction coefficient with the deprotonated ligand might be explained by the loss of hydrogen bonding between the thiol proton and imide oxygen. The effect of the hydrogen bond would cause an overall stabilization of the imide substituent, thus affecting the vibronic motion. Changes in the peak height are most likely not the result of an inductive effect on the imide nitrogen as a result of the changing environment of the thiol moiety. The change in molar extinction coefficient can also explain the observed color change between solutions; as ε increases, the underlying yellow color of the deprotonated ligand became more apparent. Likewise, as ε decreased, the faint yellow color is no longer observable in the case of As**1**$_3$ (Figure 11)

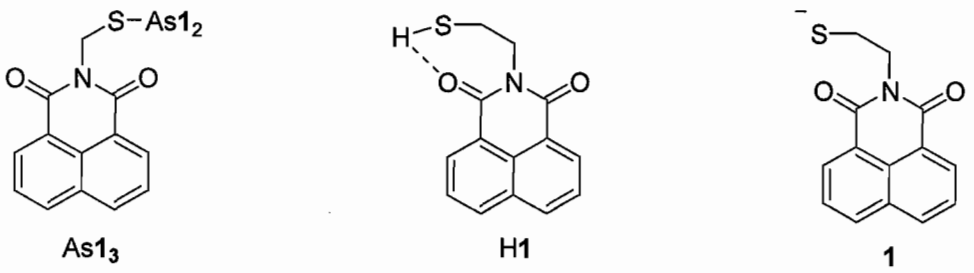


**Figure 11** Proposed structures corresponding to observed UV-Vis data in Figure 8.

Regardless of the nature of the observed changes in peak heights, peak migration did not occur. This suggests that arsenic is not perturbing the spectral properties of the naphthalimide ligand as expected. The lack of electronic interaction might be explained by the ability of the ligands to freely rotate in space, which is not conducive to promoting As···$\pi$ interactions. This also suggest that the imido oxygen atoms are not interacting with the $\sigma^*$ orbitals of arsenic as seen in the solid state structures.

Density Functional Theory (DFT) calculations with Spartan '08 indicate that in the gas phase, As···O interactions are likely to occur (**Figure 12**). Such an interaction should also perturb the absorption spectra by a charge transfer process from the oxygen lone pairs to the arsenic center (**Figure 10**). Tani and coworkers noted a hypsochromic shift in a similar system due to the increased HOMO-LUMO gap resulting from such an interaction.[19] Perhaps low temperature UV-Vis analysis could provide a decrease in kinetic energy to hinder bond rotation to the point at which SBIs would dominate and induce spectral changes. Of course this introduces new variables such as viscosity change and solubility issues which require experimental challenges to be overcome to assure proper data collection and analysis.

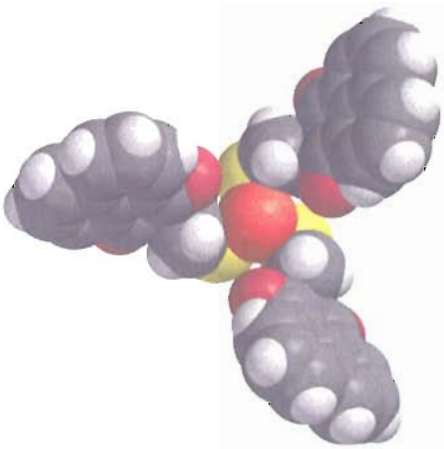

**Figure 12** DFT model using Spartan B3LYP predicts As···O secondary bonding interactions in the gas phase. Such interactions were not observed by UV-Vis as indicated by the lack of either a higher or lower energy absorbance shift.

## Substituted Triphenylethylene Systems for SBI Quantification

In addition to studying arsenic-heteroatom secondary bonding interactions, my work also focused on arsenic-arene interactions in an attempt to assign a quantitative value and better understand the role this interaction plays during the self-assembly process of $[As_2\mathbf{L}_2Cl_2]$ and $[As_2\mathbf{L}_3]$ complexes. As described in detail in Chapter 1, all $M_2\mathbf{L}_3$ self-assembled complexes (where M = P, As, Sb, Bi or a mixture of any two, **L** = aryl containing ligand) studied in our research laboratory to date show a conserved interaction where the aryl rings twist in a manner to maximize overlap with the antibonding orbitals of the metal centers (**Figure 13**)

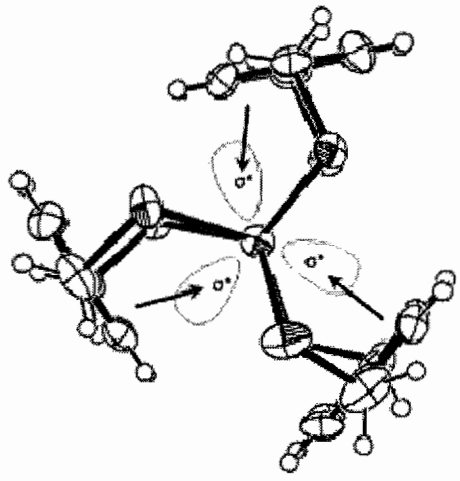

**Figure 13** Crystal structure of the [$As_2\mathbf{2}_3$] assembly where **2** is 1,2-bis(mercaptomethyl) benzene viewed down the As-As axis. Superimposed on this structure are arrows representing electron flow into the estimated positions of the σ* orbitals resulting in an inward tilt of the benzene rings of **2**.

We believe that this SBI is essential for the self-assembly process to take place due to the lack of complex formation with ligands devoid of this interaction. We have seen examples of self-assembled complexes in our laboratory where the ligands twist to fill the inner void space of the cavity thus limiting the actual number of As-arene interactions.[30] Nonetheless, these interactions are still present and believed to be an important driving force for self-assembly to occur.

To probe the As-arene SBI, a simplified system was devised which utilized a mercapto triphenylethylene ligand which, when bound to arsenic(III), the σ* orbitals of the arsenic would lie over the π system of either the geminal or vicinal arene (**Figure 14**).

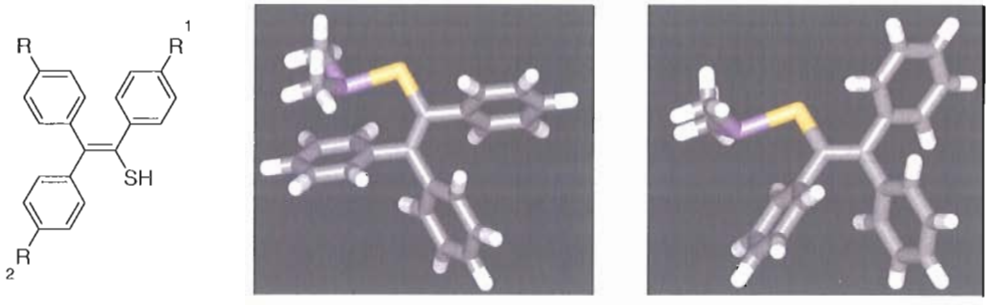


**Figure 14** Mercaptophenylstilbene ligand (left) CACHe model of dimethyl arsenic sitting over the vicinal phenyl ring (middle) CACHe model of dimethyl arsenic sitting over geminal phenyl ring. Electron withdrawing and donating substituents in the *para* positions will be used to favor one ring attraction over the other.

Low level molecular mechanics (MM) calculations by CACHe suggest a mere 3 kcal/mol difference in energy between the two conformations in **Figure 14** with the dimethyl arsenic resting over the geminal arene exhibiting a slightly lower energy. By utilizing electron withdrawing (EW) or electron donating groups (EDG), it is postulated that the location of the arsenic can be manipulated to favor the ring with greater electron density. DFT calculations using Spartan supported this hypothesis however the difference between electron rich versus electron poor rings was less than 8 kcal/mol; a value requiring low temperature NMR to study.

Using traditional synthetic organic techniques, a number of substituents could be used to decorate the phenyl rings in virtually any position.[31] The most straightforward approach used Grignard chemistry of a benzyl chloride (substituted or not) and reacted with a benzophenone (di or monosubstitued typically in the *para* position) **Scheme 3**.

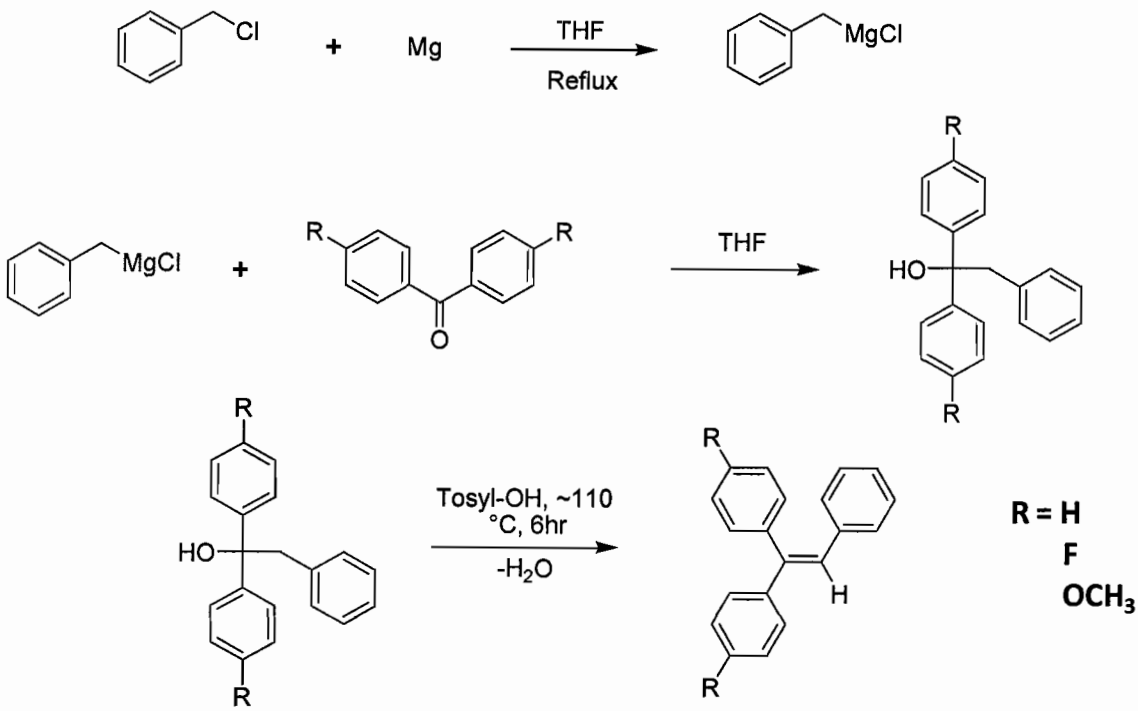


**Scheme 3** Synthesis of substituted phenyl stilbenes. Benzyl chloride is reacted with magnesium to form the Grignard reagent which is allowed to react with a substituted benzophenone. The resulting alcohol is dehydrated to form an alkene followed by bromination (not shown). The brominated alkene is reacted with magnesium to form a new Grignard which then reacts with elemental sulfur ($S_8$) to give the corresponding mercapto ligand.

To simplify the experiment so that only one mercaptostilbene bound to one arsenic center, masked organoarsenic species were synthesized (**Scheme 4**).[32,33]

****Caution must be used at all times when working with methyl or dimethyl haloarsines due to their reasonably high vapor pressure and extremely toxic nature. This material should only be handled in a hood with the sash lowered as far as possible and all gloves and equipment washed in a 10-20% bleach solution before being removed from the hood. Protective gear including a respirator must be worn along with lab coat and multiple layers of gloves.**


**Scheme 4** Synthesis of dimethylchloro arsenite. Dimethylarsenate is first dissolved in conc. HCl with a trace amount of NaI. $SO_2$ gas is bubbled into the solution for approximately 6 hr. The resulting yellow oil is syringed out of the flask and dried with $NaSO_4$. **Caution: dimethylchloro arsenite is extremely toxic and volatile. Care must be used at all times.

Dimethylchloro- and iodoarsine can be generated by the reduction of dimethyl arsenate (cacodylic acid) under strong acidic conditions with a catalytic amount of sodium iodide. Other substituted organoarsenite species can be synthesized by either Grignard type chemistry[34] or simple alkylation by organohalides.[35] Typically, alkalation results in a change in oxidation state from As(III) to As(V) requiring a reduction step using $SO_2$ gas and conc. HCl back to $AsR_2X$ where X = Cl or I.[32,33,36]

Addition of $AsMe_2I$ to the unsubstituted mercaptostilbene in the presence of *N,N*-diisopropylethylamine resulted in the formation of product as verified by $^1H$ and $^{13}C$ NMR. VT-NMR of the product produced peak migration as well as resolution of aryl peaks as they began to rotate freely at higher temperatures (**Figure 15**). The result of this experiment is inconclusive. It would appear that the arsenic was not positioned over one ring at any given time or that it sweeps over both rings causing an average of the $^1H$ resonance of the two methyl groups on the arsenic center. bCOSY and HMQC NMR experiments were performed both on the bound and unbound mercaptostilbene but provided little utility other than assisting in proton assignment.

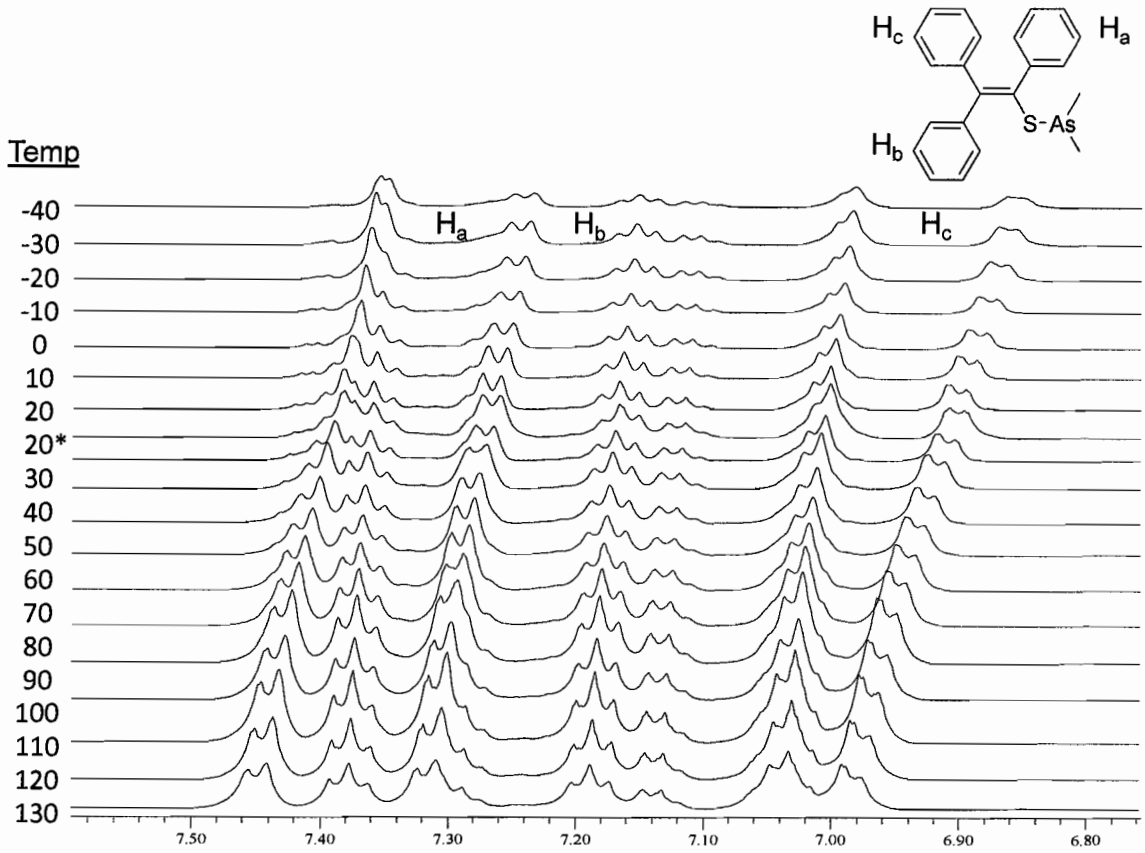


**Figure 15** VT-NMR of dimethylarsenic mercaptostilbene complex. Sample was run in 1,1,2,2-tetrachloroethylene and alowed to equilibrate for 15 minutes at each temperature change. The sample was first chilled then heated then returned back to 20°C. The * indicates the original spectrum to verify no degradation during the experiment.

This work is ongoing with both the 1,1-(4,4'-difluoro) and 1,1-(4,4'-dimethoxy)mercaptostilbenes awaiting testing. Additionally, *para* substituted diphenyl mercaptomethanes have been synthesized containing both an EWG and EDG and are awaiting testing.

## Conclusion

Despite widespread awareness of the hazards of arsenic contamination in living organisms and the environment, surprisingly few arsenic thiolate complexes are

structurally characterized. In fact, although it is well known that arsenic binds to cysteine sites in proteins[37] (which contain a similar β-mercapto*amido* structure), detailed structural studies of related arsenic thiolate complexes remain lacking. This work presents a β-mercapto*imido* ligand that binds to arsenic through its thiolate with supporting As···O secondary interactions. We continue to explore the importance of secondary As···O interactions and As-$\pi$ interactions in preparing specific chelators for arsenic. As demonstrated above by both NMR and UV-Vis studies, SBIs may not be of substantial strength in solution to the point of being measurable by these techniques. Nevertheless, SBIs have been observed in a number of self-assembled structures studied in the Johnson laboratory to date and continue to be studied due to their important role in the self-assembly process of arsenic-organothiolate complexes.

## Experimental

**General Procedures** $^{1}H$ and $^{13}C$ NMR spectra were recorded using a Varian Inova 300 ($^{1}H$ 299.95 MHz, $^{13}C$ 75.43 MHz) spectrometer at room temperature unless otherwise indicated. Chemical shifts (δ) are expressed in ppm downfield from either the residual non-deuterated solvent such as $CDCl_3$ ($^{1}H$ 7.26 ppm, $^{13}C$ 77.0 ppm) and $CD_2Cl_2$ ($^{1}H$ 5.32 ppm, $^{13}C$ 53.8 ppm) or by tetramethylsilane ($^{1}H$ 0.0 ppm, $^{13}C$ 0.0 ppm ). In some NMR experiments, MeOD ( $^{1}H$ 4.82 and 3.30 ppm, $^{13}C$ 49.0 ppm) was used to aid in solubility of the arsenic complexes but not used as a reference. Crystallographic data for H**1**, [As**1**$_2$Cl] and [As**1**$_3$] were collected at 153K on a Bruker SMART-APEX diffractometer using $Mo_{K\alpha}$ radiation (λ=0.7107 Å). Lorentz and polarization corrections

were applied and diffracted data were also corrected for absorption using the SADABS program. Structures were solved by direct methods and Fourier techniques. Structure solution and refinement were based on $|F|^2$. All non-hydrogen atoms were refined with anisotropic displacement parameters. The H atom of the S-H group were located and refined by riding coordinates and isotropic thermal parameters based upon the corresponding S-atom [U(S)=1.2Ueq (S)]. The water molecules of **1** was disordered over two positions and were refined with fixed site occupation factors (sof). All crystallographic calculations were conducted with the SHELXTL 6.10 program package and Mercury 1.2.1 © CCDC 2001-2004. IR spectra were recorded on a Nicolet Magan-FTIR 550 spectrometer using Omnic 6.0a. UV-Vis spectra were recorded on a Hewlett-Packard (Agilent) 8453 spectrophotometer using Chemstations A08.03. Mass Spectral data were collected on a Hewlett-Packard (Agilent) 1100 Series LC/MSD (1946D) spectrometer using Chemstations A08.03.

## Crystallographic Data

Intensity data for **1**H, [As**1**$_2$ Cl] and [As**1**$_3$] were collected at 153K on a Bruker SMART-APEX diffractometer using Mo$_{K\alpha}$ radiation ($\lambda$ = 0.7107 Å). Lorentz and polarization corrections were applied and diffracted data were also corrected for absorption using the SADABS program. Structures were solved by direct methods and Fourier techniques. Structure solution and refinement were based on $|F|_2$. All non-hydrogen atoms were refined with anisotropic displacement parameters. The H atom of the S-H group was located and refined by riding coordinates and isotropic thermal

parameters based upon the corresponding S-atom [U(S) = 1.2Ueq (S)]. The water molecules of **1** were disordered over two positions and were refined with fixed site occupation factors (sof). All crystallographic calculations were conducted with the SHELXTL 6.10 program package and Mercury 1.2.1 © CCDC 2001-2004.

*N-(2-mercaptoethyl)-1,8-naphthalimide* (H**1**) Combined cysteamine HCl (2.26g, 11.39mM), pyridine (40mL) and triethylamine (2.8mL, 20mM) and mixed for 10 minutes under $N_2$. 1,8-naphthalic anhydride (1.023g, 5.2mM) was added and the mixture heated to 135 °C for 12 hours while stirring under $N_2$. After heating, the mixture was cooled and filtered to remove excess cysteamine. The filtrate was rotary evaporated to yield crude product as a brown wax. Deionized water (100mL) was added and stirred followed by filtration and washes with DI water, 1:1 DI water/EtOH followed by EtOH to yield 1.14g pure product. (ca. 1.32g, 86%) $^1$H NMR (300 MHz, $CDCl_3$) δ=8.62 (dd 2 H J=7.5, 0.9Hz), 8.23 (dd 2 H J=8.4, 0.9Hz), 7.70 (t 2 H J=7.5Hz), 4.38 (t 2 H J=7.5Hz), 2.93-2.85 (m 2H), 1.53 (t 1H J=87Hz).

*As**1**Cl$_2$* Dissolved H**1** (0.05g, 195μM) in $CHCl_3$. Added $AsCl_3$ (0.216g, 119μg) to yield As**1**$Cl_2$ quantitatively by NMR. No crystalline product isolated to date. $^1$H NMR (300 MHz, $CDCl_3$) δ=8.62 (d 2 H J=7.2Hz), 8.26 (d 2 H J=8.1Hz), 7.79 (t 2 H J=8.1Hz), 4.57 (t 2 H J=7.2Hz), 3.52 (t 2H, 7.2Hz).

*As**1**$_2$Cl* Dissolved H**1** (0.05g, 195μM) in $CHCl_3$. Added $AsCl_3$ (0.108g, 60μM) followed by KOH in MeOH (5μL, 5nM). Approximately 50% yield by NMR. No increase in product with the addition of more base. $^1$H NMR (300 MHz, $CDCl_3$) δ =

8.59-8.54(m 4 H), 8.23-8.17 (m 4 H), 7.76-7.69 (m 4 H), 4.59-4.49 (m 4 H), 4.36 (t 2H, 7.5Hz), 3.37 (t 6 H, 7.2Hz) 2.9 (br. 2 H), 1.55 (br. 1H).

*As**1**$_3$* *N*-(2-mercaptoethyl)-1,8-naphthalimide (49 mg, 190μmol) was combined with 1 equivalent of solid KOH in a 2:1 mixture of $CH_2Cl_2$/MeOH (1050μL) and stirred until dissolved. $AsCl_3$ (5μL in 95μL of $CHCl_3$, 60μmol) was carefully layered onto this solution to yield single crystals of [As**1**$_3$] by slow diffusion. (These crystals diffract to provide a low-resolution data set that confirms the composition of [As**1**$_3$]. The crystals were washed sequentially with MeOH, 3:1 MeOH/$H_2O$, MeOH and then $CHCl_3$ (yield 56%). Single crystals were also obtained by slow evaporation from an NMR tube containing a mixture of [As**1**$Cl_2$], [As**1**$_2$Cl] and [As**1**$_3$] prepared with an excess of KOH. $^1$H NMR (300 MHz, $CDCl_3$) δ=8.58 (dd 3 H J=7.2, 1.2 Hz), 8.55 (dd 3 H J=7.2, 1.2 Hz), 8.22 (dd 3 H J=8.4, 1.2 Hz), 8.14 (dd 3 H J=8.4, 1.2 Hz), 7.75 (dt 6 H J=7.5, 0.9), 4.58 (m 3 H ), 4.44 (m 3 H), 3.17 (m 6 H).

*Benzylmagnesium chloride* To a flame dried 250 round bottom three neck flask with condenser and pressure equalizing addition funnel was added fresh magnesium turnings (0.663g, 27.3mmol), and an $I_2$ crystal. The glassware was flamed again under vacuum while stirring the turnings to activate the Mg surface and assure dryness. Once cooled and backfilled with $N_2$, still dried tetrahydrofuran (THF) was added to cover the turnings. Benzyl chloride was dissolved in THF (20mL) and transferred by cannula to the addition funnel and added drop wise while stirring vigorously. The reaction becomes self refluxing after half of the benzyl chloride is added. The reaction is refluxed an

additional 30 minutes after the addition of benzyl chloride with a heating mantle. The reaction mixture was cooled to room temperature and used as is with no characterization.

*1,1-(4,4'-difluoro-phenl)-2-phenylethanol* Benzyl magnesium chloride reagent was transferred via cannula into benzophenone (2.90g, 22.9mmol) in THF (20mL) while stirring. This was heated to reflux for 2hrs then cooled to room temperature. Saturated $NH_4Cl$ was added and stirred for 30 minutes. The organics were extracted with ethyl acetate (EtOAc) by partitioning the aqueous layer 3 times. The organic layer was washed once with brine and dried with $MgSO_4$ followed by filtration and removal of solvents in vacuo. *Yield:* 7.11g 95% yield.

*1,1-(4,4'-difluoro-phenl)-2-phenylethylene* Combined 1,1-(4,4'-difluoro-phenl)-2-phenylethanol (1.94g, 6.25mmol) with p-toluenesulfonic acid (Tosyl-OH, 0.499g, 2.63mmol) and toluene (20mL) in a round bottom flask with condenser under $N_2$ and heated to reflux for 4hrs. Added 10mL deionized water after cooling to room temperature and partitioned. EtOAc was added and the organics were washed 3 times discarding the aqueous layer. Washed the organic layer 2 times with brine and dried over $MgSO_4$ followed by filtration and evaporation of solvents under vacuo. *Yield:* 1.59g 87% after silica column chromatography (hexanes to 19:1 hex/EtOAc) TLC hexanes rf 0.25.

*1,1-(4,4'-difluoro-phenl)-2-bromo-2-phenylethylene* Dissolved 1,1-(4,4'-difluoro-phenl)-2-phenylethylene (8.2g, 28mmol) in carbontetrachloride (96mL) with $Br_2$ (5.1g, 31mmol) and heated to 35°C for 3hrs. Cooled to 0°C and added triethylamine (TEA, 10mL, 72mmol) while stirring. DI water was added and the reaction extracted

with EtOAc 3 times. Combined the organic layers and washed with brine, dried over $MgSO_4$ and filtered. Solvents were removed by vacuo. Purified by silica column with 5% EtOAc/Hex to give pure product TLC 10% EtOAc/Hex rf 0.8. *yield:* 7.89g 76%.

*2,2-Bis(4-fluorophenyl)-1-phenylethenethiol* Using flame 50mL rbf with condenser and stoppers Mg and $I_2$ where added under $N_2$ and re-flamed. Added 1,1-(4,4'-difluoro-phenl)-2-bromo-2-phenylethylene and still dried THF (20mL) and heated to reflux while stirring. Cooled after 1hr and added $S_8$ followed by 15hr reflux. Cooled, added 5mL dry THF and 10mL saturated $NH_4Cl$. Partitioned organics and washed aqueous layer 3 times with EtOAc. Combined organics and washed with brine followed by drying over $MgSO_4$, filtration and removal of solvents by vacuo. *Yield:*0.422g 93%. Flash column purification with silica and 1% EtOAc/Hex gave 0.121g 27% pure product as a yellow solid. TLC hexanes rf 0.15.

*2,2-Bis(4-methoxyphenyl)-1-phenylethenethiol* was made as outlined above from benzyl chloride.

*1,2,2-Triphenylethenethiol* was made by following the difluoro substituted stilebene procedure from commercially available 1-bromo-2-phenyl stilbene (10.0g, 29.8mmol), Mg (1.102g, 45mmol) $S_8$ (0.983g, 3.8mmol) and dry ethylether with an $I_2$ cyrstal. *Yield:* 8.604g 91% as pure product after silica plug with hexanes.

*Dimethyliodoarsine* **Caution must be taken when working with this material. This is highly volatile and very toxic. Protective gear including a respirator must be used even when working in a hood.** Cacadylic acid (8.332g, 60.4mmol) is dissolved in DI water (10mL) in a 50mL rbf. To this is added NaI (9.02g, 60.2mmol) drop wise while

bubbling $SO_2$ gas into the arsenate mixture. This is continued for 2hrs until a yellow oil forms at the bottom of the flask. The oil was removed by syringe and dried with $MgSO_4$ followed by distillation using micro-type glassware. The yield was not found due to the lack of desire to remove this material from the hood. NMR gave one singlet at 2.019 ppm from TMS.

*Dimethylarseno-2-phenylmercaptostilbene* 2-phenylmercapto (12.3mg, 0.426mmol) was combined with degassed $CCl_4D_2$ (600uL) in an NMR tube and mixed until dissolved while under $N_2$. Diisopropylethylamine (5.5mg, 0.426mmol) was added and the tube shaken briefly. To this, dimethyliodoarsine (9.9mg, 0.426mmol) was added and again shaken. All NMR experiments were performed by this preparation.

## Bridge to Chapter III

Chapter III introduces work performed while participating at an internship with Pacific Northwest National Laboratory (Richland, WA). This type of chemistry differs from the previous two chapters and focuses on the use of high surface area mesoporous silica substrates and iron(III) nanoparticles functionalized with reactive head groups arranged in monolayer for the capture of toxic ions. Studies include pH-dependent uptake observations as well as the effects water chemistry has on binding to target ions. Dimercaptosuccinic acid coated Fe(III) nanoparticles were also studied and the results given. The last section of Chapter III involves the attempt to develop and EPA standardized technique for pre-concentration of metal ions from remotely accessible water sources for use for in-field testing.

# CHAPTER III

# ION UPTAKE FROM NATURAL AQUEOUS MATRICES BY FUNCTIONALIZED SELF-ASSEMBLED MONOLAYERS ON MESOPOROUS SILICA (SAMMS)

Some of this work has been previously published and is reproduced with permission from: Yantasee, W.; Warner, C.L.; Sangvanich, T.; Addleman, R.S.; Carter, T.G.; Wiacek, R.J.; Fryxell, G.E.; Timchalk, C.; Warner, M.G. *Environ. Sci. Technol.* **2007**, *41*, 5114-5119.

## General Overview

Chapter III is the transition point between work exclusively performed at the University of Oregon (UO) and work performed during an ongoing collaboration with scientists at Pacific Northwest National Laboratory (PNNL). This work was part of an internship program offered at the UO in conjunction with PNNL which allows graduate students the additional opportunity to gain experience at a world class research facility. The work covered in this chapter was performed primarily at PNNL over a four month internship and will be submitted for publication to either the peer reviewed journal *Analytical Chemistry* or *Analysis*. Coauthors for this work include Dr. R. Shane Addleman (principal investigator), Wassana Yantasee and Professor Darren W. Johnson (co-principal investigator), Robert J. Wiacek who synthesized SAMMS materials, Thanapon Sangvanich who performed mass spectrometry analysis and Marvin Warner

who synthesized DMSA NP with me as lead author for performing uptake studies and SAMMS synthesis. This chapter also includes data from a coauthored paper by Wassana Yantasee *et al* titled 'Removal of Heavy Metals from Aqueous Systems with Thiol Functionalized Superparamagnetic Nanoparticles' for which I performed uptake studies with functionalized superparamagnetic iron nanoparticles. This chapter also includes additional work I performed pertaining to the use of a microwave reactor and hydrogen fluoride for the digestion of SAMMS materials and iron nanoparticles. This will not be submitted for publication outside of this dissertation.

## Introduction

It is well known that a number of metal ions pose a severe threat to the health and well-being of humans even at trace amounts by contaminating essential food and water stocks.[1,2] There is overwhelming evidence that increased consumption of toxic metal ions cause numerous diseases including cancers, renal failure and death.[3,4] Contaminated soils result in the uptake of these toxic metal ions by plants,[5] which ultimately end up in our food supply. Of these toxic ions, cadmium (Cd), lead (Pb), mercury (Hg) and arsenic (As) pose the greatest threat to human health and are ubiquitous throughout the World.[6] This is epitomized in the disastrous contamination of drinking water sources in Bangladesh through the process of tapping underwater aquifers contaminated with arsenic.[7] As a result, millions of people are exposed to arsenic at levels much higher than the World Health Organization's (WHO) guidelines of 10ppb.

There is great urgency for the development of inexpensive, effective sorbent materials capable of targeting specific ions to provide clean drinking water to the Earth's population.[8] Scientists at Pacific Northwest National Laboratory (PNNL) have successfully functionalized highly porous, high surface area silica-based materials with a variety of reactive head groups capable of binding target ions from natural and synthetic matrices.[9-12] Mobile crystalline material 41 (MCM-41) is one such material containing mesoporous structure (2-10 nm pore diameter) in a repeating hexagonal manner much like a honey comb.[13,14] With thin, amorphous walls and large porosity values of 60-80%, surface areas of up to 1000 $m^2/g$ have been measured by BET analysis.[15] MCM-41 pores can be 'tuned' by careful selection of the alkyl chain length of the cationic template (typically from 8-20 carbon atoms) making it a highly versatile material. This material is prepared by a sol-gel process using micelles as pore templates containing cationic head groups to bind to anionic silicate monomers.[16] The result is the formation of a soft body structure which is then calcined at elevated temperatures (400 to 600 °C) to remove water and organics resulting in the formation of a rigid silica framework capable of functionalization via silane chemistry after surface conditioning (**Figure 1**).

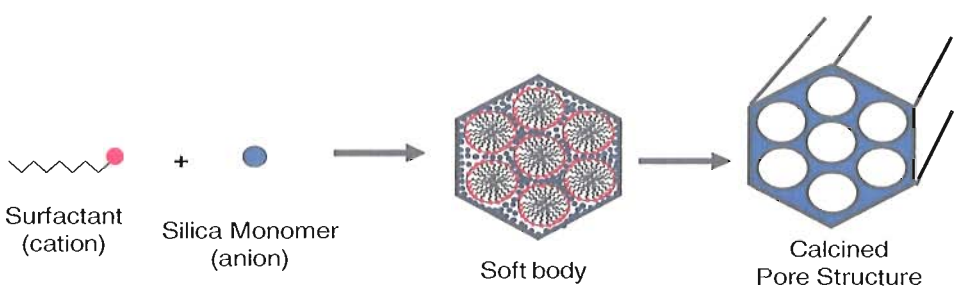


**Figure 1** Cationic ammonium templating groups are agitated with anionic silicate monomers to form soft body structures with uniform, repeating hexagonally arranged pores. The soft bodies are then calcined at elevated temperatures to remove water and organics to produce the final rigid structure.

After the calcination process, the amorphous silica pore surface is fairly devoid of free hydroxyl groups thus limiting its capacity to be modified by silane chemistry.[12,17] Before surface modification can take place, the calcined material is suspended in an organic solvent (typically toluene) and water is added to rehydrate the surface and generate additional reactive sites. Once hydrated, the surface can be modified with nearly any functional group stable to silane-type chemistry at a variety of density levels (**Figure 2**).

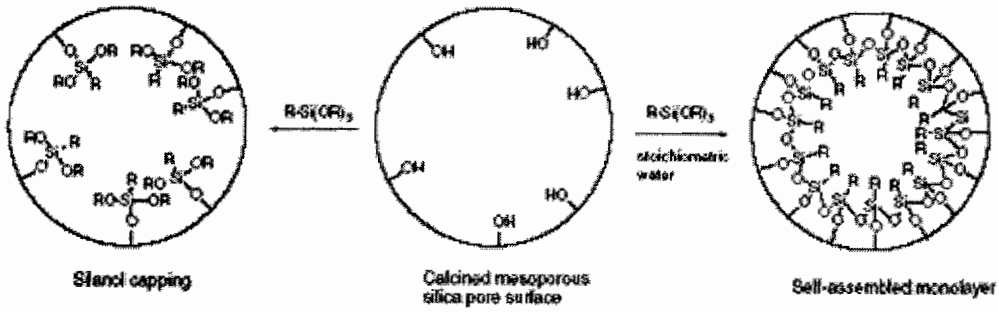


**Figure 2** Graphical representation of calcined pore mostly devoid of reactive hydroxyl groups (center). Modification by silane chemistry would result in capping of the limited hydroxyl groups and result in a low loaded material (left). The addition of water hydrates the surface, providing a much higher density of reactive hydroxyl groups.

In addition to water's role in hydrating the silica surface and increasing reaction sites, Whitesides and coworkers have shown that the water layer plays two important roles: 1) chlorosilanes are hydrolyzed into a reactive form when in contact with the water layer thus promoting bond formation with the surface hydroxyl groups[9] and 2) the functional silanes are able to 'float' atop the water layer and pack more efficiently to produce high density surface monolayers resulting in an increase in overall functional groups.[18] As a result of this increased mobility of the organosilane ligand, loadings as

high as 80% of theoretical maxima based off of surface area can be achieved. The result is a tightly formed self-assembled monolayer on mesoporous silica (SAMMS) which has demonstrated extremely high levels of uptake and capture of toxic ions from natural water sources.

## Thiol SAMMS

Thiol functionalized self-assembled monolayers on mesoporous supports (Thiol SAMMS$^{tm}$) is just one example of the multitude of functionalities available for target-specific ion capture. Thiol SAMMS is generated by the addition of 3-mercaptopropyltrimethoxy silane to MCM-41 as described above to yield a tightly packed monolayer with up to 5 organothiol functional head groups per square nanometer of surface—approximately 80% loading efficiency (**Scheme 1**). A final reflux and dehydration step induces cross linking of neighboring silanes to form a tightly bound monolayer network as verified by solid state $^{13}C$ and $^{29}Si$ NMR.[9,19]

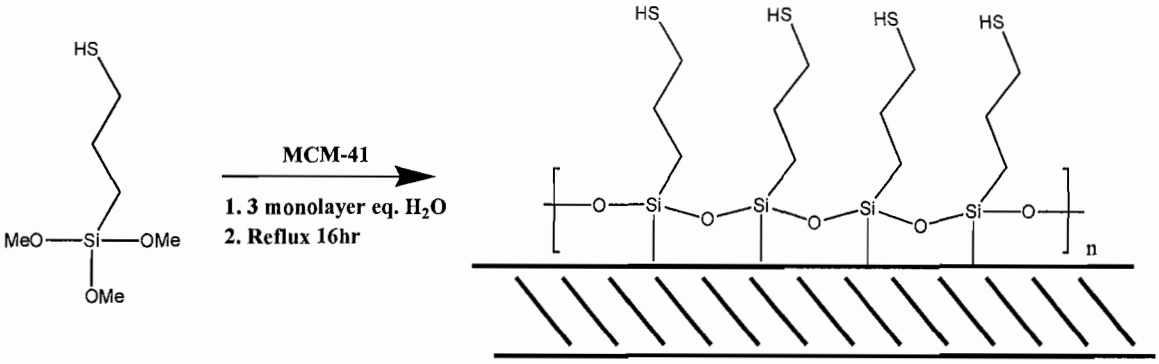


**Scheme 1** Mercaptopropylsilane binds to surface hydroxyls and cross-links with neighboring silanes to form a tightly bound 3-dimensional monolayer network.

Thiol SAMMS was found to be very efficient at binding mercury ($Hg^{2+}$) ion from laboratory prepared test samples containing various ions to simulate possible contamination sources or waste streams.[20] The work described in this section expands on the initial study to include uptake measurements in natural water matrices containing multiple metal ion targets over various pH ranges. At trace level metal concentration, data values are reported as the distribution coefficient ($K_d$) or the mass-weighted partition coefficient of the sorbent material and test solution unless otherwise stated as seen in **Equation 1**:

$$K_d=(C_o-C_f)V/C_fM$$

**Equation 1** Distribution coefficient $K_d$ is a mass-weighted partition coefficient between sorbent material and test solution and is more appropriate than reporting total uptake values (mg/g) when testing low metal concentration solutions.

where $C_o$ and $C_f$ are the initial and final concentration, respectively, of the target ions determined by ICP-MS, $V$ is volume in milliliters and $M$ is the mass in grams of the sorbent material.

From **Equation 1**, $K_d$ values for specific ions from multi-cation spiked test solutions can be determined and compared over various pH ranges. Because of the wide variation in $K_d$ values (typically ranging from $10^2$ to $10^7$) for different sorbent materials, data is often reported using a logarithmic scale for easier comparison and graphical interpretation. Typical uptake experiments use natural water matrices such as water from the Columbia River (Richland, WA) or ground water from a well-head located on the

Hanford site (Richland, WA) or sea water from the Pacific Ocean (Sequim, WA). Water samples are passed through a 0.45 μm filter before use to remove large solids and bioorganisms. This is to prevent spoilage of the water matrices over the course of the experiment. Thiol SAMMS are very hydrophobic and require a 'wetting' with methanol or ethanol before use in aqueous studies. This is done by the addition of 5-10 μL of alcohol before exposure to the aqueous test media. SAMMS are typically soaked for 2 hrs while being agitated slightly on a platform shaker set to 1Hz. After 2 hrs, a measured amount of sample is passed through a 0.2μm syringe filter and diluted to an appropriate volume for inductively coupled plasma mass spectrometry (ICP-MS). The ICP-MS data is then used in **Equation 1** to compare final metal concentration to original concentration and give the partition coefficient $K_d$.

In the first study of this chapter, Thiol SAMMS was compared to a commercially available thiol-based polystyrene resin GT73 (superseded by GT74) from Rohm and Haas. Three different water types were tested to determine the effects of natural ion concentrations and water chemistries. Metal cation stock solutions where made of each test matrix from commercially available standardized $Ag^{1+}$, $Cd^{2+}$, $Hg^{2+}$, $Pb^{2+}$ and $Tl^{1+}$ solutions. Test solutions were made fresh daily or used shortly after prepared and quantified by ICP-MS for each experiment. Samples were tested in triplicate from the same stock solution to assure accurate determination of $K_d$ with the average of the three runs reported.

Inspection of the log $K_d$ values reported in **Table 1** for the three test matrices and individual metal cations demonstrates the superior partition capacity Thiol SAMMS

possesses when compared to a common commercially available resin, GT73. In every test matrix and with every target ion, Thiol SAMMS outperforms GT73, sometimes by as much as three orders of magnitude in $K_d$. Surprisingly, both Thiol SAMMS and GT73 appear to be minimally affected by the makeup of the water sources tested. It was expected that sea water would hinder metal binding due to the high ion concentration, especially the sodium and chloride ion content. This does not appear to be the case, however.

| | Metals (Log $K_d$) | | | | |
|---|---|---|---|---|---|
| **Matrix (Neutral pH)** | **Ag** | **Cd** | **Hg** | **Pb** | **Tl** |
| Ground Water - Thiol SAMMS | 7.3 | 6.2 | 6.2 | 6.1 | 4.2 |
| Ground Water – GT73 Resin | 3.4 | 3.2 | 3.7 | 4.5 | 3.8 |
| River Water - Thiol SAMMS | 6.8 | 6.2 | 6.8 | 5.7 | 4.5 |
| River Water - GT73 Resin | na | 3.0 | 3.6 | 3.9 | 3.6 |
| Sea Water - Thiol SAMMS | 6.6 | 6.1 | 6.1 | 6.0 | 3.2 |
| Sea Water - GT73 Resin | 3.4 | 3.0 | 3.6 | 3.7 | 3.5 |

**Table 1** Comparison of Thiol SAMMS with commercially available thiol-based resin GT73 in three natural water samples spiked with metal cations at near neutral pH (as collected from the source with no adjustment). Values are reported as the log of $K_d$ due to the large variation in binding.

Similar tests were performed with the test matrices adjusted to pH 2 by the addition of $HNO_3$ to simulate acidified waste streams. Starting with the ground water samples, GT73 experienced a slight drop in $K_d$ values for the same metal ions while Thiol SAMMS experienced significant drops in $K_d$ values for $Ag^{1+}$, $Cd^{2+}$, $Pb^{2+}$ and $Tl^{1+}$ but not for $Hg^{2+}$. This trend was repeated with Columbia River water for GT73, being minimally affected while Thiol SAMMS experienced a slight drop of around one order of

magnitude for $Ag^{1+}$, $Hg^{2+}$, and $Tl^{1+}$ and a significant drop for $Cd^{2+}$and $Pb^{2+}$. In pH 2 sea water GT73 once again maintains similar $K_d$ values for all metal ions as in neutral water but Thiol SAMMS sees a large drop in $K_d$ for $Pb^{2+}$ and $Tl^{1+}$ (**Table 2**).

| | Metals (Log $K_d$) | | | | |
|---|---|---|---|---|---|
| **Matrix (pH 2)** | **Ag** | **Cd** | **Hg** | **Pb** | **Tl** |
| Ground Water - Thiol SAMMS | 0.7 | 2.8 | 6.2 | 3.2 | 3.2 |
| Ground Water – GT73 Resin | 2.8 | 2.5 | 3.4 | 3.3 | 3.3 |
| River Water - Thiol SAMMS | 5.9 | 2.4 | 5.6 | 3.0 | 3.1 |
| River Water - GT73 Resin | na | 2.5 | 3.4 | 3.2 | 3.3 |
| Sea Water - Thiol SAMMS | 7.0 | na | 5.8 | 2.7 | 2.7 |
| Sea Water - GT73 Resin | 3.2 | 2.4 | 3.4 | 3.0 | 3.3 |

**Table 2** Comparison of Thiol SAMMS with commercially available thiol-based resin GT73 in three natural water samples spiked with metal cations and pH adjusted to 2 with $HNO_3$. Values are reported as the log of $K_d$ due to the large variation in binding.

The likely explanation for Thiol SAMMS superior performance over GT73 under neutral conditions can be attributed to increased thiol headgroup density as a direct result of greater surface area versus GT73. Simply put, the high surface area of MCM-41 allows for an environment containing a densely packed monolayer rich in readily available binding sites. GT73 on the other hand is a cross-linked polystyrene-based polymer with free thiols appended to the phenyl substituents. Unfortunately, increased surface area does not explain the observed trends between GT73 and Thiol SAMMS in pH 2 test matrices. To further investigate this observation, $K_d$ measurements were taken over a wide pH range (0-8) in the three test matrices to track pH dependent uptake of

target ions (**Figure 3**). A newly developed chemisorbed thiol-based SAMMS material is described in Chapter 5 which experiences a similar trend to Thiol SAMMS.

## Results and Discussion of Thiol SAMMS

To be an effective sorbent material, it is necessary to maintain a high affinity for target ions over a wide range of conditions including natural variable ion abundance, the presence of competitively binding ligands and a range of pHs. This is a difficult task due to metal ion speciation changes and changes in binding to ligands in variable water chemistries. In addition to speciation changes, competitive metal hydrolysis reactions occur at pH extremes, thus inhibiting metal-ligand binding. pH dependent adsorption is an apparent characteristic of both Thiol SAMMS and other thiol-based sorbents such as GT73 and GT74 (albeit to a lesser extent) with metal cations—namely $Cd^{2+}$, $Pb^{2+}$ and $Cu^{+2}$—while $Ag^{+}$, $Tl^{+}$ and $Hg^{2+}$ are seemingly unaffected by a change in pH over a range of 0-7.[9,21,22] This concept is illustrated in **Figure 3** for the commercially available resin GT73. As pH decreases ($[H^{+}]$ increases) $Cd^{2+}$, $Pb^{2+}$ and $Cu^{+2}$ undergo what appears to be a titration curve around pH 2-2.5. However $Hg^{2+}$ and $Ag^{+}$ capacities appear unaffected by the change in pH.

Likewise, a plot of log $K_d$ values for the same metal ions with pH ranging from -1to 7 for Thiol SAMMS in $HNO_3$ spiked Nanopure water shows a similar trend with GT73 (**Figure 4**). As seen with GT73, $Cd^{2+}$ and $Pb^{2+}$ exhibit decreased binding as pH decreases.

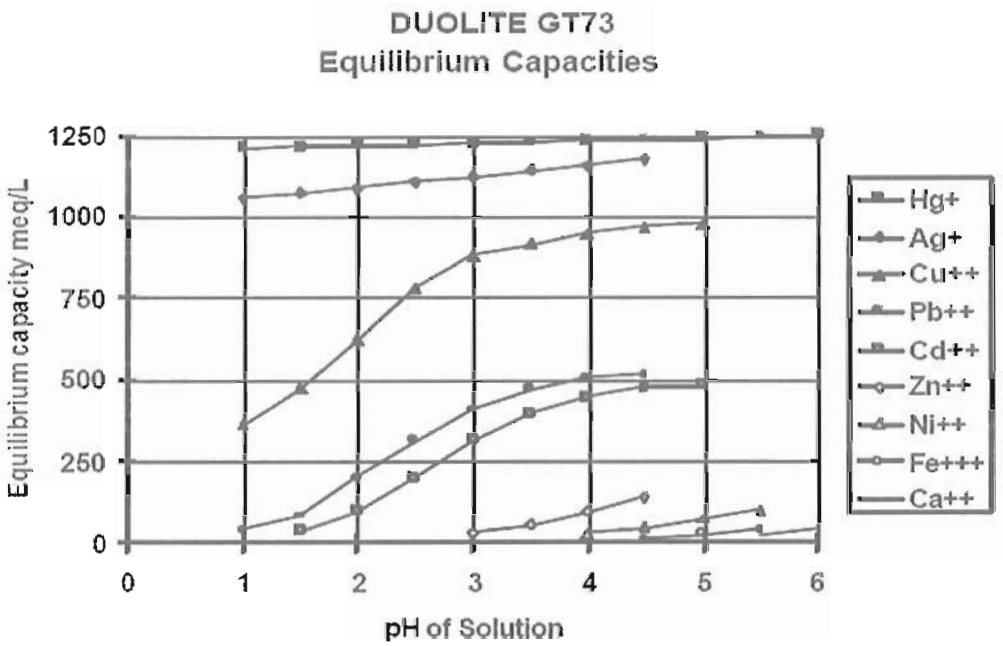


**Figure 3** pH dependent trends are observed with commercially available thiol-containing resin GT-73. Graph courtesy of Rohm and Hass document # PDS 0139A-Nov. 02. Note that $Hg^{+}$ should actually be $Hg^{2+}$.

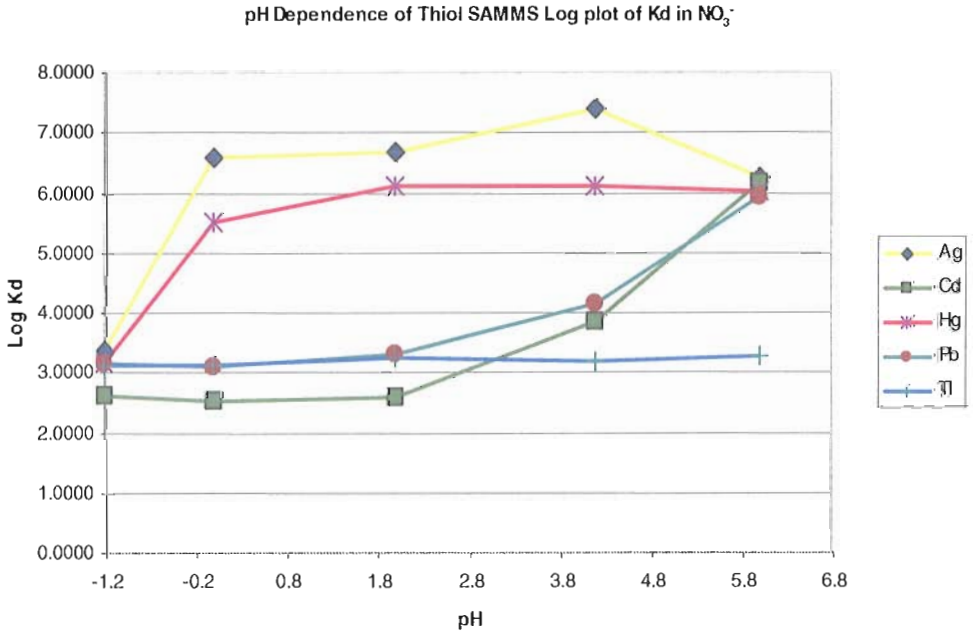


**Figure 4** Data illustrating pH dependent adsorption of $Ag^{+}$, $Cd^{2+}$, $Hg^{2+}$, $Pb^{2+}$ and $T^{l+}$ for Thiol SAMMS in $HNO_3$ spiked water solution. $Hg^{2+}$ is from $HgCl_2$ salt, $Pb^{2+}$ is from lead(II) acetate dissolved in Nanopure water. All others ions are from commercially available standardized nitrate solutions. Minimal uptake is observed at high acid concentrations.

With Thiol SAMMS, this decrease in binding occurs at pH 4 versus the much lower pH 2 for GT73. This can likely be attributed to the nature of the thiol functionality of Thiol SAMMS and GT73, specifically the difference in $pK_a$ for an alkyl thiol versus and aryl thiol, respectively. By pH 2, Thiol SAMMS may not be able to undergo binding due to a higher $pK_a$ than the aryl thiol of GT73. The following section explores the nature of the observed pH dependent binding of thiol sorbents. Chapter 5 also discusses this topic as it relates to a newly created chemisorb thiol-based SAMMS material which exhibits similar properties to Thiol SAMMS. Additional experiments were conducted to test the hypothesis of $pK_a$-dependent binding with alkyl versus aryl thiols with this material also found in Chapter 5.

## pH-Dependent Binding Mechanism of Thiol-Based Ligands

Initial literature investigations into the properties of the RS-H bond failed to yield any conclusive mechanism to describe the observed experimental relationship with regard to changing pH. To better understand the pH dependent experimental data, it is important to investigate two possible causes: 1) pH driven change in the nature of the metal aqua ion and 2) thiol group variation and how $pK_a$ affects metal binding.

The observed trends may be explained by a change in the nature of the aqua ion of the metal cations in question as exemplified in **Scheme 2**.[23]

$$M^{n+}(aq) + H_2O \rightleftharpoons M(OH)(aq)^{(n-1)+} + H_3O^+ \quad (pK_{hydrolysis} \text{ or } pK_{11})$$

**Scheme 2** pH-dependent metal hydrolysis under neutral conditions. The dissociation of a water molecule results in a metal aqua ion and a free proton.

Here, the equilibrium constant $pK_{11}$ is a measurement of the acidic nature of the metal ion and its ability to induce dissociation of a proton from a coordinated water molecule to free surrounding water molecules.[24] The hydrolysis equilibrium constant $pK_{11}$ can be considered to be analogues to the more familiar term $pK_a$ and is sometimes reported as such for $M(OH_2)_n$ aqueous systems[23]. **Scheme 2** is more representative of a neutral pH environment and changes slightly in acidic conditions to give **Scheme 3**.

$$M^{n+}(OH_2)(aq) + H_2O \rightleftharpoons M(OH)(aq)^{(n-1)+} + H_3O^+ \quad (pK_{hydrolysis} \text{ or } pK_{11*})$$

**Scheme 3** pH-dependent metal hydrolysis under acidic conditions. As pH decreases ([H+] increases), the equilibrium lies to the left hindering proton dissociation from the metal aqua ion.

The merit of such equilibrium is twofold: 1) the ease of hydrolysis of water can be directly related to proton dissociation of other similar ligands such as thiols, and, 2) this process is directly related to the water exchange rate which plays an active role in understanding the reactivity of metal aqua ions.[25]

The basic mechanism behind the deprotonation process can be explained in **Scheme 4**.

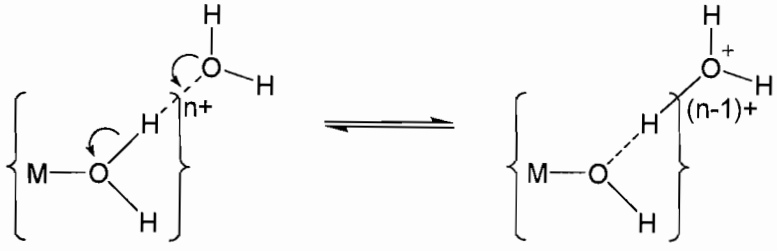


**Scheme 4** Hydrolysis mechanism of an aqua ligand. Acidic metals drive equilibrium further to the right and are thus less perturbed by an increase in proton concentration.

The analogous process for organothiol ligands would give **Scheme 5.**

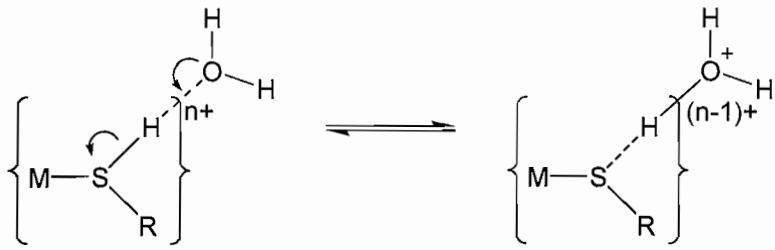


**Scheme 5** Likely mechanism for the deprotonation of thiolate ligand (labeled $pK_m$ in some cases).

A more simplistic approach would be the following reaction given in **Scheme 6.**[22]

$$M^{n+}(aq) + nRSH \rightleftharpoons (RS)_nM + nH^+$$

**Scheme 6** Simplified equations of proposed pH-dependent metal-thiolate equilibrium based off of Schemes 2 and 3 above.

In each scenario, the acidity of the metal center is responsible for proton dissociation of the organothiol ligand assuming the same ligand is studied. A more acidic metal ion center would drive the equilibrium to the right whereas the opposite would hold true for a less acidic center. Those metal centers with an equilibrium positioned farther to the right would be less perturbed or perturbed more slowly by an increase in $[H^+]$ (decrease in pH) versus those metals whose equilibrium lies to the right to a lesser degree. Such equilibrium would resemble a classic acid-base titration curve with changing $[H^+]$, which is in good agreement with the observed trends in the above data.

A table of $pK_{11}$ (or $pK_1$ as designated in Lange's Handbook of Chemistry) demonstrates the difference in acidities between metal ions investigated in the above systems (**Table 3**).[26]

| Substance | $pK_1$ | Hard/Soft |
|---|---|---|
| Iron(III) ion | 2.19 | H |
| →Mercury(II) ion | 3.7 | S |
| Copper(II) ion | 7.34 | S(B) |
| →Lead(II) ion | 7.8 | S(B) |
| Zinc(II) | 8.96 | B |
| →Cadmium(II) ion | 9.2 | S |
| Nickel(II) ion | 9.86 | B |
| →Silver(I) ion | >11.1 | S |
| →Thallium(I) | 13.36 | S |

**Table 3** $pK_{11}$ of common metal ions along with corresponding hardness/softness designations. Values obtained from Lange's Handbook of Chemistry. Blue arrows indicate $M^{2+}$ soft ions which follow the expected pH trend. Red arrows indicate $M^{1+}$ soft ions which deviate from the expected pH trend. H = hard, S = soft and B = both.

The observed experimental pH-dependent trend is apparent for the $M^{2+}$ ions of mercury, lead and cadmium (blue arrows in **Table 3**) as well as several other ions but deviates greatly for the $M^{1+}$ ions of silver and thallium (red arrows in **Table 3**). Both $Ag^{1+}$ and $Tl^{1+}$ have large $pK_1$ values yet are unaffected by pH, however silver binds approximately 3 orders of magnitude greater than thallium in our original study. This difference in the binding capacity of Thiol SAMMS is not in agreement with other thiol-based sorbents.[27] Unfortunately, only a few publications are available for thallium-thiol systems and Jacobson *et al* demonstrated near equal binding capacity for both $Ag^{1+}$ and $Tl^{1+}$ ions.[27] Both metals ions are considered to be 'soft' by Pearson's standards[28] and

both have relatively large ionic radii, with thallium having one of the largest of the elements.

A possible explanation for the high binding affinity for $Ag^{1+}$ to Thiol ligands is due to its relatively slow water exchange rate $k_{ex}$ of $10^6$ $s^{-1}$ versus $Pb^{2+}$ at $10^8$ $s^{-1}$ and $Hg^{2+}$ at $10^9$ $s^{-1}$.[23] Because there is a direct relationship between the rate at which water exchanges and complex formation with other ligands, the slow exchange rate of silver often leads to the formation of extremely stable complexes.[23] The formation of stable complexes plus the high affinity silver(I) has for thiol ligands is in good agreement with the observed trend and accounts for the high binding affinity with thiol SAMMS.

## Conclusion of pH-Dependency Study

It appears that the observed pH-dependent capture of metal ions can be primarily attributed to a metal ion's capacity to undergo hydrolysis and, secondarily, to an ion's water exchange rate or ease of forming a new, stable complex. Another factor of pH-dependent uptake may indeed be the difference in $pK_a$ between aryl thiols (GT73) and alkyl thiols (Thiol SAMMS). This would not explain why some metal ions are greatly affected by pH while others are not, but would explain why GT73 experienced very little change in $K_d$ values under acidic conditions while Thiol SAMMS did. The lower $pK_a$ of the aryl thiol may facilitate binding to metal ions even in high $[H^+]$ environments. It is the current belief that the combination of factors described above dictates the effectiveness of thiol-based sorbent materials toward soft metal cations.

## Dimercaptosuccinic Acid $Fe_3O_4$ Nanoparticles

In keeping with the theme of thiol-based sorbent materials for toxic metal cation remediation, dimercaptosuccinic acid coated iron oxide nanoparticles (DMSA NP) were investigated.[29] Iron oxide nanoparticles (Fe NP) possess many desirable properties making them an interesting material for use in aqueous systems. Fe NP can be treated with a number of ligands for use in metal ion remediation or even metal ion sensing from natural water sources and bodily fluids.[30] Typically, Fe NP are first synthesized by the stabilization of the nanoparticles with a lipophilic outer ligand shell. Exchange reactions of the outer shell can impart both functionality and in this case, water solubility. Examples of exchanged ligand shells include ethylenediaminetetraacetic acid (EDTA),[31] humic acids,[32] and, in this work, dimercaptosuccinic acid, all of which have good affinities toward toxic metal cations. Fe NP are superparamagnetic meaning they are attracted to a magnetic field and re-disperse when the field is removed. This is an attractive property due the potential of 'harvesting' the DMSA NP sorbent after achieving maximum uptake. These properties along with the ability of Fe NP to be easily dispersed in aqueous media make them ideal for heavy metal capture. Similar tests described above for Thiol SAMMS were also performed with DMSA NP to determine their feasibility as a sorbent material for toxic metal cation capture and are described below.

## DMSA NP Results and Discussion

DMSA NP were tested in either filtered natural water sources or in-house generated Nanopure water spiked with target metal cations. In some experiments, pH

was adjusted by the addition of $HNO_3$. DMSA NP were allowed to soak in metal ion spiked test solutions for two hours unless otherwise noted. After the two hour soak, a measured volume of test sample was removed, filtered with a 0.2 μm syringe filter and diluted appropriately for ICP-MS analysis. Values are reported in log $K_d$ unless otherwise noted.

In this study, Nanopure water was spiked with $Ag^{1+}$, $Cd^{2+}$, $Hg^{2+}$, $Pb^{2+}$ and $Tl^{1+}$ and the pH was adjusted with $HNO_3$. The initial and final ion concentrations were determined by ICP-MS with each sample run in duplicate. $K_d$ values were averaged and the log value graphed in **Figure 5**. From the data, it became apparent that the pH-dependent binding to $Pb^{2+}$ and $Cd^{2+}$ was not present with DMSA NP. The likely explanation for this observation is the added benefit of the chelation effect with $\alpha$-$\beta$ thiol head groups on the DMSA ligand. The chelation effect essentially states that when DMSA is bound to a cation, the thiols, ethyl backbone and metal center form a highly stable, five membered ring with optimized geometry, imparting favorable binding which is thus less perturbed by the effects of change in $[H^+]$.[33,34] Another explanation to the lack of observed pH-dependent behavior warranting mentioning is the catechol-salicylate mode of binding. Cohen and coworkers discovered that low pH, protonation of a catechol alcohol resulted in the metal center 'hopping' over to a carbonyl oxygen of 2,3-dihydroxybenzoyl amide ligand.[35] This too may occur with DMSA, where the protonation of one thiol may result in the metal center binding with the neighboring carbonyl oxygen thus no significant change in binding will occur as pH decreases.

In addition to being unaffected by pH due to the formation of a stable ring, DMSA NP experience very little leaching. Overall, DMSA NP perform quite well from fairly acidic to neutral pH. They do however suffer from lower $K_d$ values due to their decreased surface area, as compared to Thiol SAMMS.

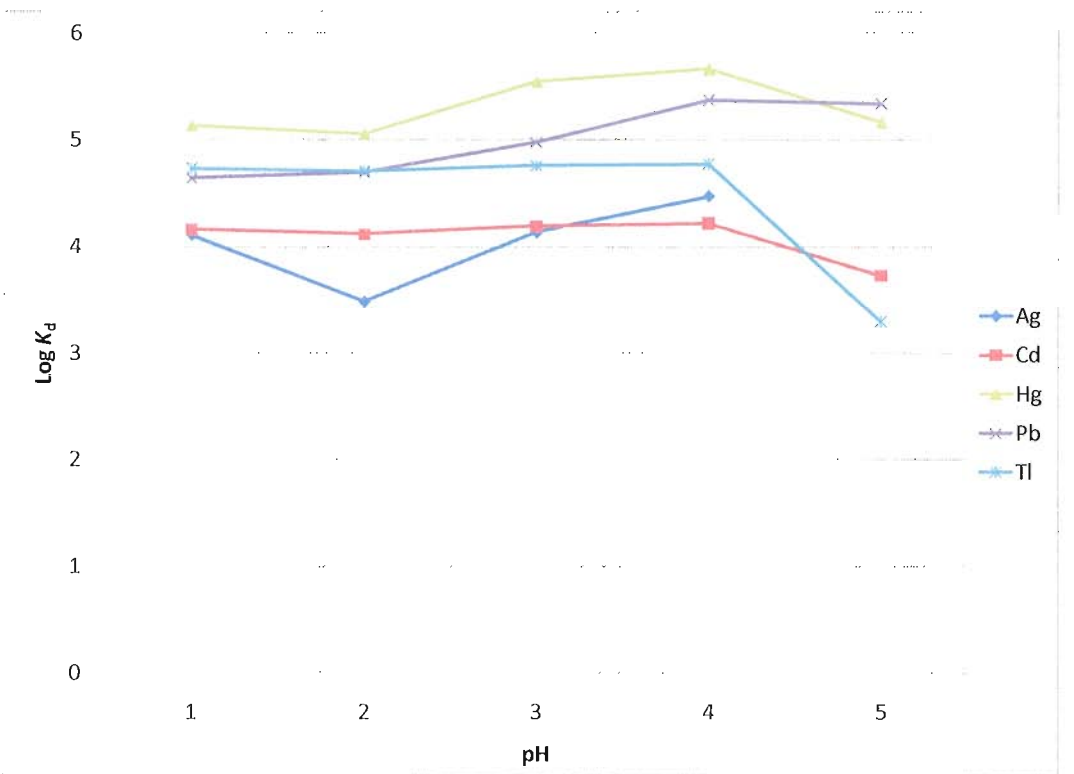


**Figure 5** DMSA NP uptake of $Ag^{1+}$, $Cd^{2+}$, $Hg^{2+}$, $Pb^{2+}$ and $Tl^{1+}$ in $HNO_3$ spiked Nanopure water at indicated pH values. Samples were soaked in the test solutions for two hrs and ion concentrations determined by ICP-MS.

DMSA NP were also tested for ion capture efficiency in metal cation spiked natural water sources to examine the effects that water chemistry played on ion uptake. As described above with Thiol SAMMS, natural water sources were first filtered then spiked with target ions. After a two hour soak, remaining ion concentrations were

quantified by ICP-MS. An additional test matrix (bovine serum albumin, BSA) was also examined to determine the feasibility of DMSA NP for use in *in vivo* metal ion capture therapy **Figure 6**.

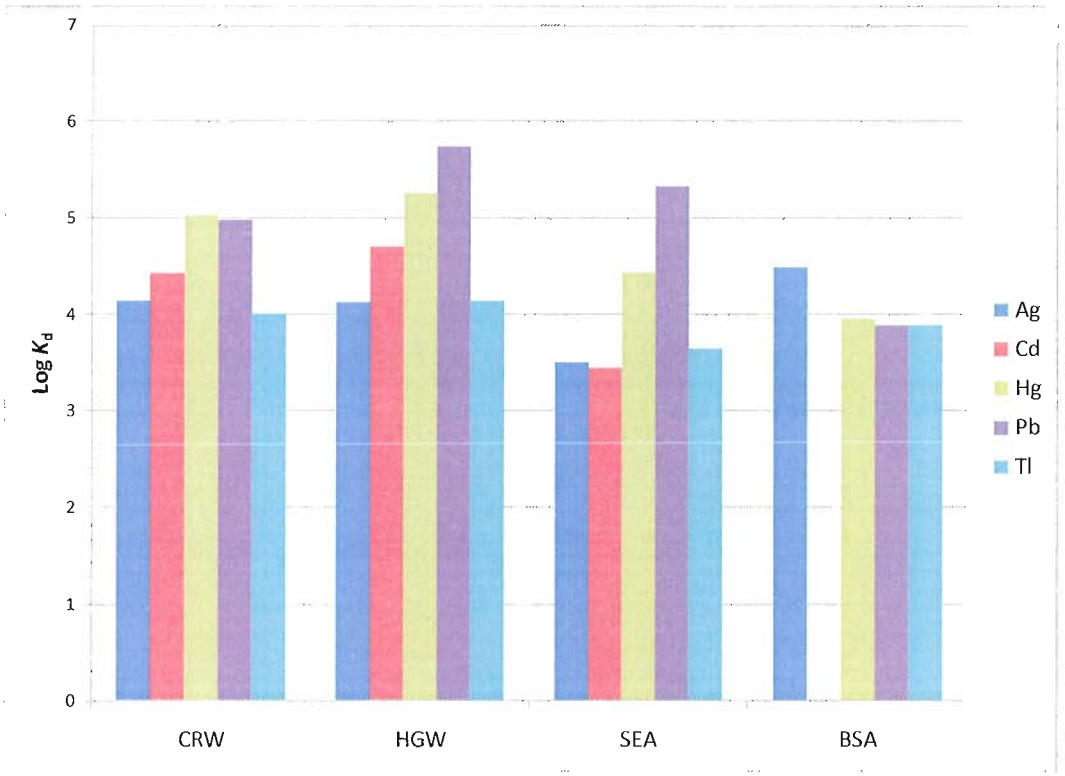


**Figure 6** Plot of log $K_d$ values for DMSA NP in Columbia River water (CRW), Hanford ground water (HGW), Pacific Ocean water (SEA) and bovine serum albumin (BSA).

DMSA NP performed fairly consistently in all four test matrices for all cations. $K_d$ values above $10^3$ are considered acceptable and values above $10^4$ exceptional with DMSA NP achieving values above $10^4$ for the fresh water sources.[36] DMSA NP performance is slightly lower than Thiol SAMMS under similar conditions, presumably due to the reduced number of binding sites as a result of decreased surface area.

However, this material does perform consistently better than the commercially available resin GT73 under most conditions. With the exception of $Cd^{2+}$ binding, DMSA NP also perform quite impressively in BSA, especially considering the complex nature and potential for competitive binding with metal ions in the mixture. A number of experiments have been performed by PNNL staff and others to demonstrate the ability of DMSA NP to work in a number of biological fluids for both uptake and detection of toxic ions.[29,30]

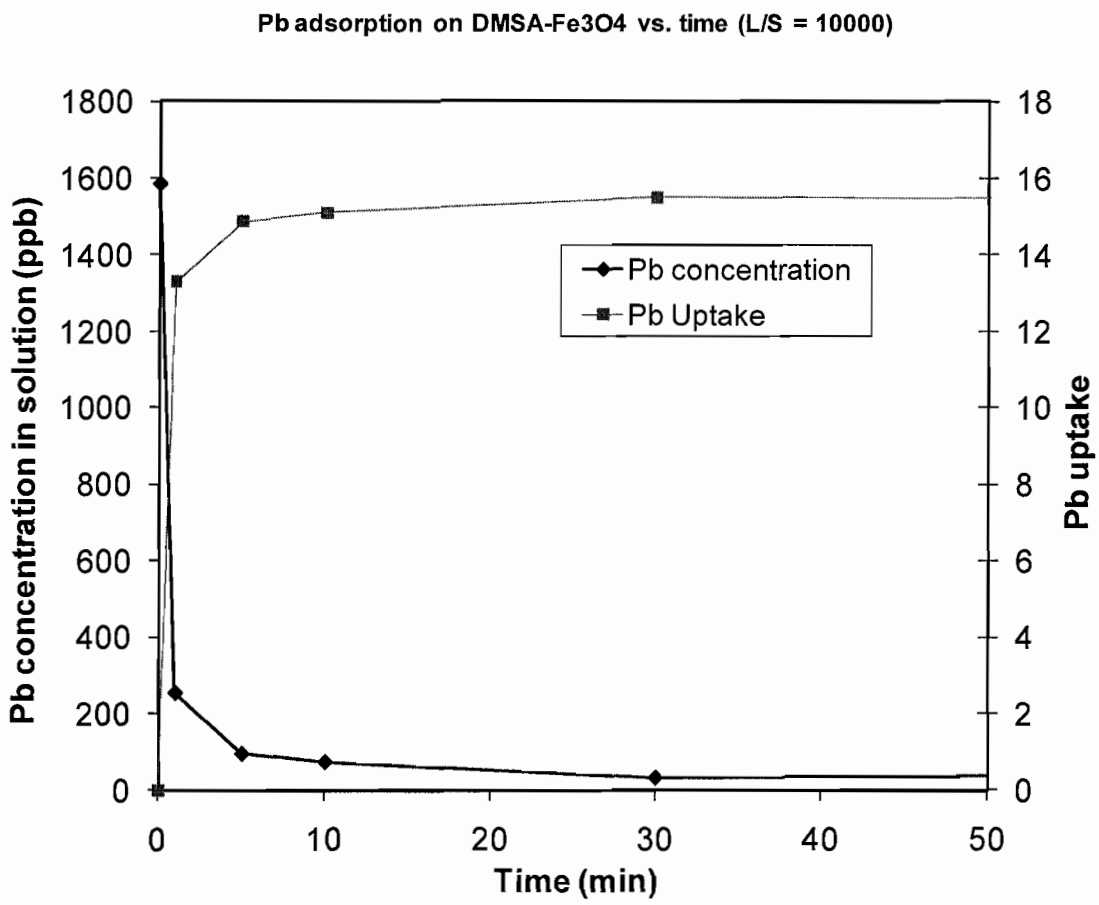


**Figure 7** DMSA kinetics study in Pb spiked 0.025M sodium acetate buffer. L/S of 10000 was used to minimize the effect of sampling during the experiment.

Lastly, kinetic studies were performed with DMSA NP in $Pb^{2+}$ spiked 0.025M sodium acetate buffer at pH 6.5. A 100 mL test solution spiked with $Pb^{2+}$ and a liquid-to-solid ratio (L/S) of 10000 (100mL/0.01g) was used so that the removal of test solution during the course of the experiment would have a minimal effect on ion capture. Test samples were taken at the following points: 0, 1, 5, 10, 30, 60, 120, 480 and 1440 minutes and the results were plotted in **Figure 7**. Inspection of the results from the first 50 minutes reveals near complete uptake by t = 30 min. No leaching was evident during the duration of the full test period of 1440 minutes, likely a result of the tight bonds between DMSA and the metal cation and DMSA and the Fe NP. To be an effective sorbent, especially for *in vivo* treatments, the material must be able to remain bound to the captured toxic ion.

## Microwave Digestion of Thiol SAMMS and Thiol Containing Fe Nanoparticles

There is currently no portable technology capable of sampling water sources in remote locations while providing accurate quantification of trace metals. Thiol SAMMS offers a unique opportunity to provide accurate analysis of minimally accessible water formations by pre-concentration of toxic ions followed by ICP-MS analysis in a certified laboratory. This can be achieved by passing a known amount of test sample over Thiol SAMMS, then taking the material back to a laboratory for acid digestion. The metal content of the test source can then be quantified by ICP-MS. This section explores the concept of utilizing microwave-based acid digestion of Thiol SAMMS and 2,3-dimercaptosuccinic acid coated iron nanoparticles (DMSA NP) following the

Environmental Protection Agency (EPA) guidelines from method 3052 in report # SW-846. This data demonstrates that Thiol SAMMS and DMSA NP materials can be loaded with a quantified amount of toxic metal cation, digested as outlined by the EPA as a certifiable laboratory technique and metal content of the resulting solution quantified by ICP-MS to give high returns of metal ions.

Thiol SAMMS were synthesized as described in this chapter and Feng *et al*[9] and DMSA NP as outlined by Sun *et al* and Yantasee *et al*.[29,37] Stock solutions were prepared by dilution of metal standards in either filtered (0.45 μm) Columbia River water (CRW) or filtered Hanford ground water (HGW) with a target concentration of 500 ppb for each metal. Final concentrations were determined by ICP-MS. Test solutions contained approximately 0.05 g of silica sorbent material or 0.01 g iron nanoparticles suspended in 50 or 10 mL metal stock solution, respectively. Solutions were mixed on a platform shaker for two hours, after which time, a small aliquot was removed from each test solution for metal uptake quantification. The remaining sorbent-containing solution was allowed to sit for 30 minutes followed by centrifugation for 30 minutes. The resulting pellet was rinsed 3 times with approximately 1 mL Nanopure water and stored hydrated until digestion. Microwave digestion was carried out as described by EPA method 3052 in report # SW-846. Briefly, the sorbent pellet was resuspended in its storage solution followed by addition of acid digestion solution (10 mL) and quickly transferred to the fluorinated polymer digester. A final temperature of 180 °C was reached over a five minute ramp followed by an isothermal period of 4.5 minutes. After this, the digesters and solutions contained therein were allowed to cool to 30 °C before

dilution. Digestion solutions were transferred separately to 50 mL volumetric flasks and water added to reach the final volume. Samples containing HF were first quenched with boric acid before dilution by the addition of 3 mL saturated boric acid. Solutions were stored until metal ion quantification by ICP-MS was performed.

The following acid solutions were used for the digestion process:

1. 10 mL, 95% $HNO_3$ / 5% HCl
2. 10 mL, 90% $HNO_3$ / 10% HCl
3. 10 mL, 75% $HNO_3$ / 25% HCl
4. 10 mL, 50% Nanopure water / 47.5% $HNO_3$ / 2.5% HCl
5. 10 mL, 95% $HNO_3$ / 5% HF
6. 10 mL, conc. $HNO_3$

Thiol SAMMS not loaded with metal was wetted with MeOH and digested with solution 1 as a control. DMSA NP were digested using 10 mL of concentrated $HNO_3$ (solution 6).

## EPA Standardized Digestion Results and Discussion

This study was performed to demonstrate that small filter-like cartridges containing Thiol SAMMS or DMSA NP can be used to pre-concentrate metal ions from remotely located test areas and accurately quantify toxic metal ion concentrations. By adhering to strict guidelines established by the EPA for infield water sampling, acid

digestion of test samples and metal ion quantification by ICP-MS, this technique can be implemented as a validated testing protocol.

**Table 4** is a compilation of data from the microwave digestion of Thiol SAMMS sorbent material loaded with select metal ions. Two test matrices were used, Columbia River water and Hanford site well water. Metal uptake was nearly 100% for each ion and matrix tested, which is in good agreement with previously acquired data.

| Sorbent | Matrix | Digest Solution (from above list) | % Uptake | | | |
|---|---|---|---|---|---|---|
| | | | $Ag^{1+}$ | $Cd^{2+}$ | $Hg^{2+}$ | $Pb^{2+}$ |
| Thiol SAMMS | Filtered Well Water | 1 | 100 | 100 | 100 | 100 |
| | | 2 | 100 | 100 | 100 | 100 |
| | | 3 | 100 | 100 | 100 | 100 |
| | Filtered River Water | 4 | 100 | 99.9 | 99.9 | 99.9 |
| | | 5 | 100 | 100 | 99.6 | 100 |
| | | 6 | 100 | 100 | 99.7 | 100 |
| | | | % Recovery | | | |
| | Filtered Well Water | 1 | 23 | 87 | >100 | 95.5 |
| | | 2 | 77.8 | 93 | >100 | >100 |
| | | 3 | 75 | 82.6 | >100 | 90.9 |
| | Filtered River Water | 4 | 53.3 | 86.7 | 78.9 | 86.7 |
| | | 5 | 8.9 | 86.4 | 81.6 | 86.4 |
| | | 6 | 35.6 | 80 | 74.4 | 84.4 |

**Table 4** Percent uptake and recovery for select metal cation for Thiol SAMMS in filtered Hanford site well water and Columbia River water in Richland, WA. Recovery percentages exceeded 100% in some runs most likely due to calibration error of the ICP-MS resulting in drift.

Recovery percentages after digestion, however, seemed to vary greatly between metal ions and acid solutions in this experiment. Recovery rates greater than 100% indicate two possible errors in the analysis technique: 1) introduction of metals from external sources such as test containers, SAMMS materials or acid sources or 2) improperly calibrated ICP-MS resulting in drift during the analysis of the digest solutions. Scenario 2 is most likely the cause of error due to the lack of any obvious anomalous trends in metal concentration between samples.

Similar digestion experiments were carried out with DMSA NP. As previously demonstrated, DMSA NP were found to achieve high uptake percentages from metal ion spiked solutions as measured by ICP-MS (**Table 5**).

| Sorbent | Matrix | % Uptake | | | |
|---|---|---|---|---|---|
| | | $Ag^{1+}$ | $Cd^{2+}$ | $Hg^{2+}$ | $Pb^{2+}$ |
| DMSA NP | Filtered Ground Water | 99.9 | 97 | 97.5 | 99.9 |
| | | % Recovery | | | |
| | | >100 | >100 | >100 | >100 |

**Table 5** Percent uptake and recovery for selected metal cations for DMSA NP in filtered ground water from a well located on the Hanford site (Richland, WA). Recovery percentages exceeded 100%. Runs were performed in duplicate.

The DMSA NP digest solutions were analyzed by ICP-MS at the same time as the above Thiol SAMMS thus resulting in the same introduced error. Both experiments are worth revisiting in the future based on the promising data given above. In some digest test solutions, both Thiol SAMMS and DMSA NP solids were completely dissolved. This

was verified both visually and by filtration. The fact that no solids remain is a clear indicator that all metal ions must have been released into solution. Therefore, assuming that the above error in recovery can be isolated and corrected, this procedure should be a viable technique for trace metal detection for natural water sources.

## Experimental

**General Procedures** Water sources where taken either from the Columbia River (Richland, WA), well water located on the Hanford site, (Richland WA), Pacific Ocean, (Sequim, WA) or Nanopure (18.2 mΩ) water produced in-house where noted. All natural water sources were passed through a 0.45 μm filter before use and stored in the dark. BVA was used as received. Glassware and plastic bottles were rinsed with a 10-20% nitric acid (low metal ICP-MS grade) solution followed by copious rinses with Nanopure water. All SAMMS materials were weighed out on a bench top analytical balance and reported to the nearest tenths of a mg. Digital pipettes (manual and electronic) were used to deliver small volumes of solutions (less than 100 mL). Large volumes were measured on a bench top analytical balance to the nearest tenth of a gram with the assumption of density equal to 1 for all solutions. Natural water samples were passed through a 0.2 μm filter by vacuum and stored in the dark until used. Test samples were filtered with 0.2 μm syringe filters before ICP-MS analysis. Samples were diluted as needed to range between 50 to 100 ppb to best match metal calibration curves. ICP-MS was performed on a Agilent Technologies 7500ce with calibration standards checked periodically to eliminate drift. All experiments were performed in duplicate or triplicate and values averaged before plotting unless otherwise noted.

*Uptake Experiments* SAMMS materials (approximately 10 mg) was weighed into 20 mL scintillation vials and 5-10 μL of MeOH was added to wet the material. To this, 10 mL of test solution was added and the vials agitated for 2 hrs on a platform shaker set to 1 Hz. After which, a small aliquot was removed and passed through a 0.2 μm syringe filter and diluted with a 5% nitric acid solution for ICP-MS.

*Thiol SAMMS* Thiol SAMMS were made in-house as described by Feng *et al* by means of 3-mercaptopropyltrimethoxysilane.[9]

*GT73* Resin was purchased from Aldrich and used as received. Samples were kept sealed until used to prevent evaporation of as shipped swelling solvent.

*Kinetics Study* 10 mg Thiol SAMMS was placed in a 250 mL Erlenmeyer flask and wetted with 5-10 μL MeOH. To this, 100 mL of test solution was added and the timing experiment started. The flask was continuously agitated with a platform shaker set to 1 Hz. A small aliquot was removed at the designated time and passed through a 0.2 μm syringe filter followed by dilution with 5% $HNO_3$ solution for ICP-MS.

*Microwave Digest of SAMMS and DMSA NP Materials* Unless otherwise noted, all solutions were prepared using Nanopure water (18.2 MΩ-cm). Glassware, digestion vessels and hardware, as well as high-density polyethylene (HDPE) bottles, were initially washed with an aqueous 10-20% $HNO_3$ solution to remove trace metals followed by a rinse with Nanopure water prior to use. Digestion vessels and hardware were air dried overnight before use. Pipette tips, Falcon tubes and glass scintillation vials were used as received without acid wash.

Metal stock solutions containing approximately 500 parts per billion (ppb) of Cd, Hg, Pb and Ag were prepared in either filtered (0.45μm) Columbia River water (CRW) or Hanford ground water (HGW). Approximately 0.0500 g of Thiol-SAMMS material was weighed and transferred into screw top Falcon tubes along with 50 mL of either CRW or HGW metal stock solutions (in triplicate totaling six samples). The mixtures were shaken horizontally on a platform shaker for 2.5 hours at 1Hz and allowed to rest vertically for 30 minutes to help with settling of solids. Then, sample tubes were centrifuged for 30 minutes at 7000 RPMs.

After centrifugation, solutions were decanted off into new Falcon tubes for metal ion uptake quantification by ICP-MS. The resulting pellet was washed three times with 1 mL Nanopure water while being careful not to disturb the pellet. Nanopure water (1 mL) was added to each tube and placed on a vortex mixer to re-suspend the solids. Each tube was then charged with 10 mL of acid solution and quickly transferred to a Teflon microwave reaction vessel and individually heated per the EPA guidelines outlined in method 3052 in report # SW-846.

## Bridge to Chapter IV

Chapter IV investigates cationic functionalized mesoporous silica materials for the uptake of arsenate and chromate oxyanions. This chapter is a continuation into the research pertaining to SAMMS sorbent materials first introduced in Chapter III. Studies include the effect of pH-dependent capture of target anions. Natural water sources are also tested to investigate the effects water chemistry has on binding.

# CHAPTER IV

# METAL ANION CAPTURE THROUGH CATIONIC METAL CENTERS

## General Overview

Chapter IV includes data from research performed at Pacific Northwest National Laboratory in Richland, Washington as a continuation of ongoing work with sorbent technology under the guidance of Dr. R. Shane Addleman. This chapter contains unpublished work with the intention of combining this data with existing pertechnetate data from PNNL for publication in either *Analysis* or *Analytical Chemistry*. Coauthorship will include Wassana Yantasee who provided experimental oversight and assistance, Thanapan Sangvanich who performed mass spectrometry analysis, Glen E. Fryxell who provided experimental oversight, Matthew O'Hara who performed pertechnetate studies and Darren W. Johnson and R. Shane Addleman who provided intellectual contributions and editorial input.

## Introduction

Oxyanions such as chromate, arsenate and pertechnetate pose serious environmental hazards yet are challenging remediation targets due to their tetrahedral ionic structure, weak basisity and diffuse electron density.[1]

Flocculation,[2] coprecipitation[3] and reverse osmosis[4] are typical techniques employed to remove toxic oxyanions from drinking water sources, none of which are selective toward oxyanions over common anions found in water such as $Cl^{1-}$. However, large, specialized equipment, reagents or multiple treatments are needed to achieve efficient scrubbing and are not practical in rural communities with limited resources. A more practical remediation approach is the capture of targeted oxyanions with sorbent materials housed in filter devices affixed to well heads or point-of-use water supplies. Examples of sorbent materials capable of sequestering oxyanions include ionic exchange resins,[5] biosorbents,[6] inorganic layered double hydroxides (LDHs),[7,8] quaternary ammonium containing materials[9] and ethylenediamine (EDA) functionalized mesoporous silicas complexed with either $Cu^{2+}$ or $Fe^{3+}$. This section is a continuation of the original study of $Cu^{2+}$-EDA and $Fe^{3+}$-EDA functionalized mesoporous silica with non-native water sources spiked with chromate ($Cr^{6+}$), arsenate ($As^{5+}$) and pertechnetate ($Tc^{5+}$) oxyanions to simulate waste streams.[10,11] The relevance of this work pertains to the expansion of test matrices into native water sources versus sterile laboratory prepared water samples. In both studies, test matrices are spiked with known amounts of metal anion and in some experiments, the pH is adjusted using $HNO_3$. Results from this work are compared to a commercially available ion exchange resin and a quaternary ammonium salt SAMMS material to simulate the functionality found in most anion specific exchange resins.

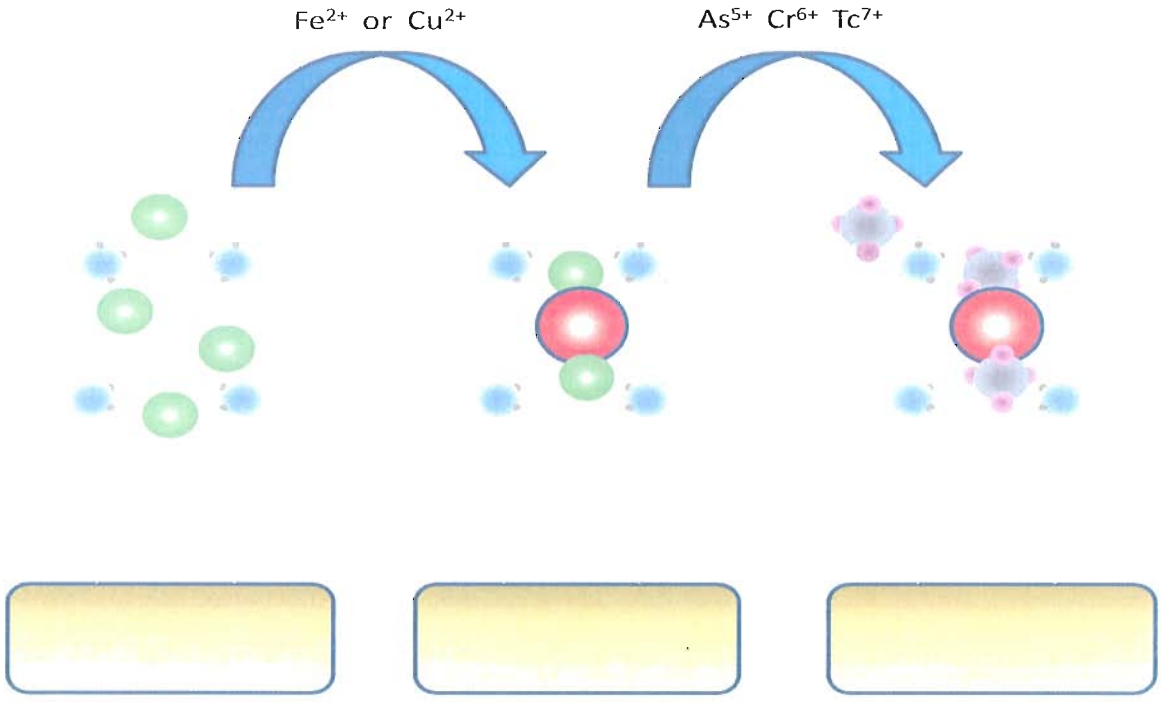


**Figure 1** Graphical depiction of ethylenediamine (EDA) functionalized mesoporous silica without Cu or Fe metal center (left) with Cu or Fe metal center (center) and with metal center and bound oxyanion (right). Note that $Fe^{2+}$ is used in solution but is quickly oxidized to $Fe^{3+}$ when bound as indicated by the appearance of a deep red color.

MCM-41 is reacted with 1-(2-aminoethyl)-3-aminopropyltrimethoxysilane to impart ethylenediamine (EDA) chelation functionality in a relatively dense monolayer after condensation of the silane monomers by azeotropic removal of water.[12,13] $Cu^{2+}$ or $Fe^{3+}$ is incorporated by simple mixing of the EDA-SAMMS material and the corresponding metal(II) acetate or chloride salt in water or isopropyl alcohol, respectively, for two hours at 25 °C.[1,10] Upon binding to the EDA ligand, iron undergoes oxidation from $Fe^{2+}$ to $Fe^{3+}$ as indicated by the formation of a deep red color. The result is a dense layer of cationic metal centers with a high affinity and specificity for chromate, arsenate and pertechnetate oxyanions over other anions typically present in surface waters (**Figure 1**).

## Results and Discussion

As discussed thoroughly in Chapter IV of this dissertation, pH has an overwhelming effect on metal ion binding and the efficiency of sorbent materials. To further study the pH-dependence of sorbents, water from the Columbia River (Richland, WA) was passed through a 0.2 μm filter followed by metal ion spiking and pH adjustment with $HNO_3$. River water was chosen over ion doped Nanopure water for the purpose of simulating real world applications by testing the effectiveness of the sorbent with competitive natural ions and buffering components. It is acknowledged that the filtering step does remove large particulates and bioorganisms which may affect the efficiency of the sorbent material but is necessary to prevent spoilage of the test sample over the period of the study. Due to the low concentration of metals, data is reported as the distribution coefficient ($K_d$) or the mass-weighted partition coefficient of the sorbent material and test solution unless otherwise stated.

The distribution coefficient can be determined by **Equation 1** as stated on page 65 in chapter III by knowing the initial and final concentration, $C_o$ and $C_f$, respectively, of the target ions which is determined by ICP-MS, the volume, $V$, in milliliters and the mass, $M$, in grams of the sorbent material. Capacity values which compare the amount of target ion to amount of sorbent material used would not be ideal for these experiments do to the potential of influencing the uptake equilibrium.

## pH Studies of $Cu^{2+}$- and $Fe^{3+}$-EDA SAMMS

The positive charge imparted on the Cu or Fe metal center when chelated to the surrounding amines provides for a high affinity of both $Cr^{6+}$ and $As^{5+}$ oxyanions from a pH range of 3 to 7 (**Figures 2** and **3**, respectively). Below pH 3, $Cu^{2+}$-EDA SAMMS quickly loses its ability to bind to $H_xAsO_4^{(x-3)}$ ion but only exhibits a modest loss in binding to $CrO_4^{2-}$ ion (**Figure 2**). $Fe^{3+}$-EDA SAMMS also suffers a decrease in binding affinity with $H_xAsO_4^{(x-3)}$ below pH 3 but to a much lesser extent than $Cu^{2+}$-EDA. However, $Fe^{3+}$-EDA SAMMS has an overall lower affinity for $HCrO_4^{1-}$ than $Cu^{2+}$-EDA. With the exception of a complete loss of binding to $H_xAsO_4^{(x-3)}$ at pH 1 for $Cu^{2+}$-EDA, both materials appear to maintain good uptake of the target ions over 7 pH units.

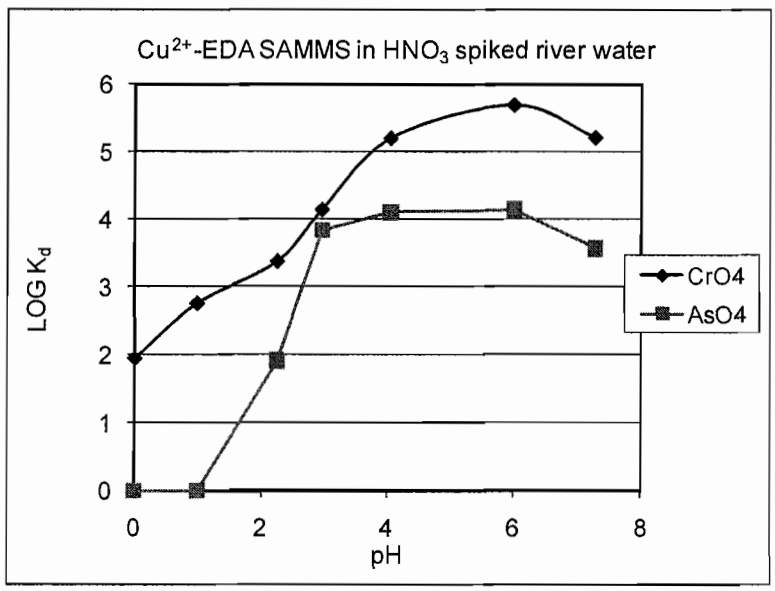


**Figure 2** pH-dependency of $Cu^{2+}$-EDA SAMMS material in $Cr^{6+}$ and $As^{5+}$ spiked Columbia River water. Low metal $HNO_3$ was used to adjust pH. Metal uptake was determined by ICP-MS.

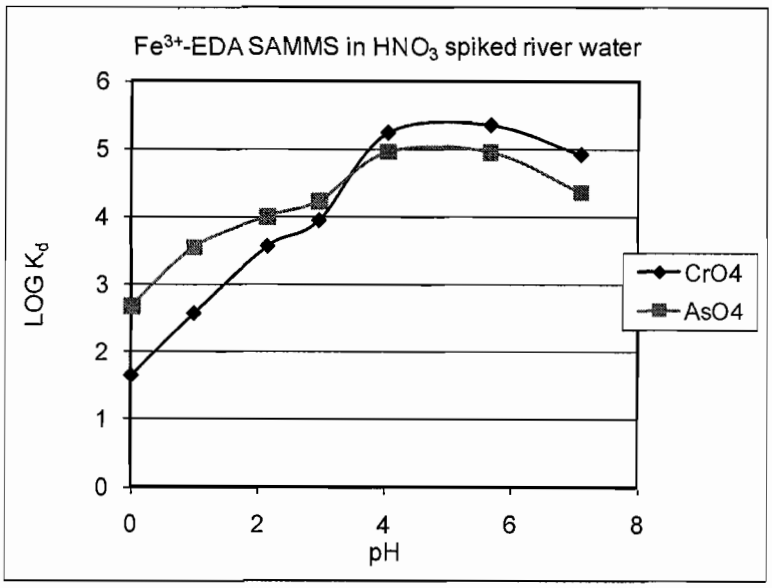


**Figure 3** pH dependency of $Fe^{3+}$-EDA SAMMS material in $Cr^{6+}$ and $As^{5+}$ spiked Columbia River water. Low metal $HNO_3$ was used to adjust pH. Metal uptake was determined by ICP-MS.

The observed decrease in binding can possibly be attributed to at least two causes: 1) protonation of the ethylenediamine nitrogen atoms, or, 2) change in speciation of the target oxyanions. To address the observed trends of both $M^{x+}$-EDA SAMMS materials, it is important to discuss each above scenario separately, starting with hypothesis 1 (amine protonation). Yoshitake and coworkers have demonstrated that soaking $Fe^{3+}$-EDA SAMMS in 1M HCl after metal uptake for 10 hours at room temperature results in almost complete desorption of both the captured oxyanions and the iron metal center due to protonation of the diamine nitrogen atoms.[1] Some $Fe^{3+}$ and oxyanion did remain, however, so complete stripping was not achieved but the treatment did not degrade the covalently attached EDA monolayer. Test batches of acid stripped EDA SAMMS were capable of undergoing regeneration by the simple loading of $Fe^{3+}$ back onto the material. Considering the extreme conditions necessary to strip the metal ions from the EDA

SAMMS, it is reasonable to conclude that the amines are not undergoing protonation to any appreciable extent and therefore not releasing the bound $Fe^{3+}$ or $Cu^{2+}$ metal centers (**Table 1**). Even with $pK_a$s around 10.3 and 7.5 for *N-n*-propylethylenediamine (a similar compound to the attached monolayer of EDA SAMMS material),[14] as in the case of organothiols when bound to metals, the $pK_a$ can drop many orders in magnitude to resist proton addition when acting as a chelate ligand.[15]

| Table of Acid Dissociation Values | | |
|---|---|---|
| Arsenate | $H_2AsO_4^{1-}$ | 2.24 |
| | $HAsO_4^{2-}$ | 9.20 |
| | $AsO_4^{3-}$ | 20.7 |
| Chromate | $HCrO_4^{1-}$ | -0.86 |
| | $CrO_4^{2-}$ | 6.51 |
| *N-n*-propylethylenediamine | R-$NH_2^{1+}$-R' | 7.5 |
| | R''-$NH_3^{1+}$ | 10.3 |

**Table 1** Acid dissociation values for arsenate and chromate oxyanions and *N-n*-propylethylenediamine (a similar diamine to 1-(2-aminoethyl)-3-aminopropyltrimethoxysilane used in EDA SAMMS).

Additional evidence suggests that the nitrogen centers are not being protonated due to the lack of a conserved trend in decreasing $K_d$ between materials and oxyanions. There is no indication of clearly defined titration curve as a result of protonation of the amines as would be expected, however, one could argue that some protonation does occur resulting in the decrease in $K_d$ values around pH 3.5 for both materials and oxyanions.

The second argument is due to a change in speciation of the target oxyanion as the pH decreases. This hypothesis does appear to fit in the case of $Cu^{2+}$-EDA binding $H_xAsO_4^{(x-3)}$ ion. At around pH 2.2, arsenate undergoes a loss of a proton (or gain depending on the direction of the reaction) resulting in the following equilibrium expression (**Equation 1**):[15]

$$H_3AsO_4 \Longleftrightarrow H^+ + H_2AsO_4^-$$

**Equation 1** Equilibrium equation of arsenate speciation under acid conditions. The $pK_a$ for this process is 2.2 which is in good agreement with the observed trend in Figure 2 resulting in a total loss of arsenate uptake.

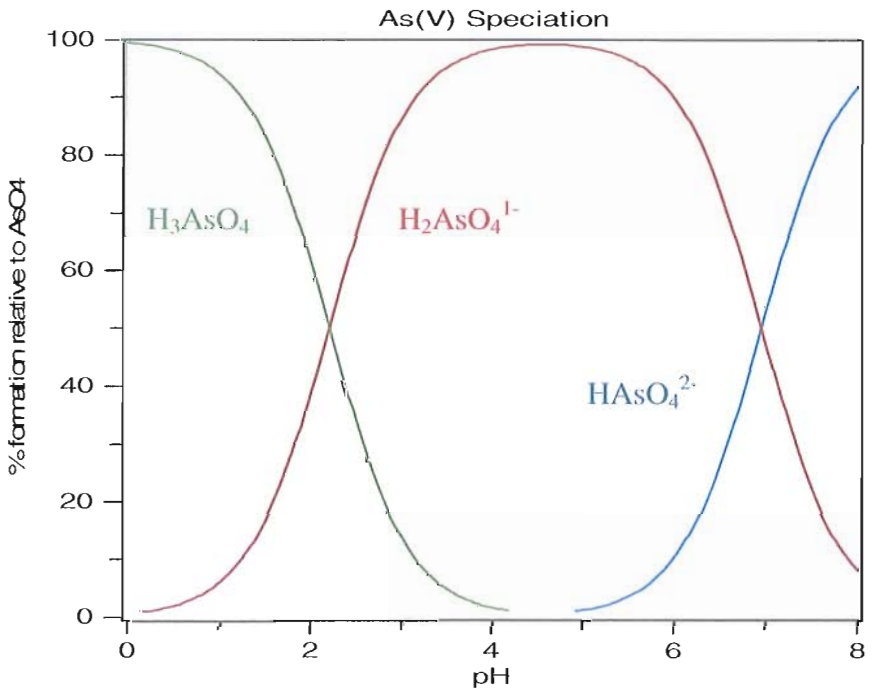


**Figure 4** Speciation diagram of $As^{5+}$ oxyanion from pH 0 to 8. Plot generated using HySS2006, part of the HyperQuad suite.

This is in good agreement with the observed data for $AsO_4$ binding with $Cu^{2+}$-EDA (**Figure 2**). The inflection point does appear to be close to pH 2.2 or equal to the $pK_{a1}$ of $H_3AsO_4$, a neutral species.[16] The formation of the neutral arsenate species below pH 2 results in the loss of any affinity toward the charged cationic $Cu^{2+}$ center **Figure 4**.

Albeit reasonable in explaining the trend for $Cu^{2+}$, it does not explain why $Fe^{3+}$-EDA SAMMS is unaffected by pH for $H_xAsO_4^{(x-3)}$ other than the drop in two log units typical of all EDA SAMMS tested. The observation with $Fe^{3+}$-EDA SAMMS can be explained by the formation of a tightly bound Fe(III) $H_2AsO_4^{1-}$ complex which alters the $pK_{a1}$ of the arsenate oxyanion.[17] The slight lowing of $pK_{a1}$ of the arsenate oxyanion allows for modest binding even at low pH. This complex does not form with copper therefore protonation of the oxyanion occurs as expected. However, further research into the mechanism for the observed behavior of cationic EDA SAMMS materials is needed to conclusively address the pH-dependence of this class of sorbents.

Chromium(VI) on the other hand does not experience any appreciable protonation between 0-6 and most likely remains unaffected by the drop in pH.[18,19] Above pH 6, $HCrO_4^{1-}$ loses a proton to become $CrO_4^{2-}$ which would still likely bind to the cationic metal center of EDA SAMMS. Below pH 6, $Cr_2O_7^{2-}$ forms which constitutes about 20% of the chromate species in solution and may attribute to reduced uptake at lower pH values. This is in good agreement with the observed data for both $Cu^{2+}$- and $Fe^{3+}$-EDA SAMMS which exhibit similar pH binding dependencies (**Figures 2** and **3**, respectively). There is clearly a reduction in binding as the pH decreases from 4 to 0, again requiring further investigation into the pH-dependant mechanism.

## Anion Uptake in Three Natural Water Types

To test the affects of water chemistry on binding of $Cr^{6+}$ and $As^{5+}$, three natural sources were investigated at near neutral (or as collected) pH. As described previously, water sources were passed through a 0.2 μm filter followed by the addition of chromate and arsenate ion. Sorbents were soaked for two hours and the amount of metal anion quantified (initial/final) by ICP-MS. All runs where in duplicate and reported as the average $K_d$ with the exception of the Bio-Rad resin and quaternary ammonium containing SAMMS data which were single runs and thus inherently contain some degree of error but are in agreement with past, in-house observations.

The inclusion of a quaternary ammonium-based resin from Bio-Rad as well as a *N*-propyl-*N*,*N*,*N*-trimethyl quaternary ammonium (Quat Salt) SAMMS in these studies provides a side-by-side comparison of the current technology for targeting these oxyanions. In the first graph (**Figure 5**), log $K_d$ values of $Cr^{6+}$ is compared with all four materials in spiked Columbia River water, Hanford site well water and Pacific Ocean sea water at near neutral pH. As expected, all materials perform particularly well in fresh water sources but are greatly affected by the high ion concentration in sea water.

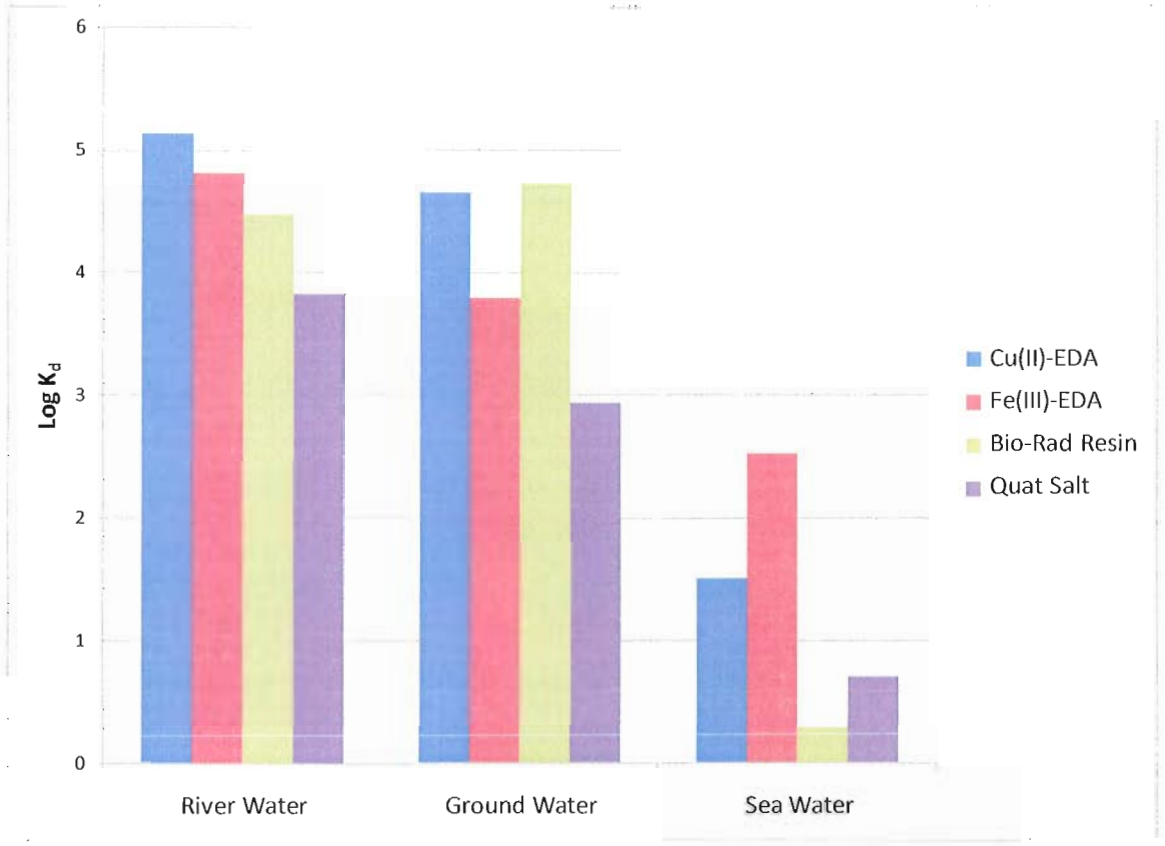


**Figure 5** Plot of log $K_d$ values for $Cr^{6+}$ oxyanion in neutral Columbia River Water (left), Hanford site ground water (center) and Pacific Ocean sea water (right). The high ion concentration of the sea water causes reduced binding of the oxyanion with all four test materials due to competing reactions.

Both EDA-based SAMMS perform about the same as the commercially available resin from Bio-Rad for arsenate ion in fresh water but suffer a similar reduction in binding in sea water (**Figure 6**). $Fe^{3+}$-EDA SAMMS again is the overall better performing material for both arsenate and chromate ion uptake from native water sources in each experiment.

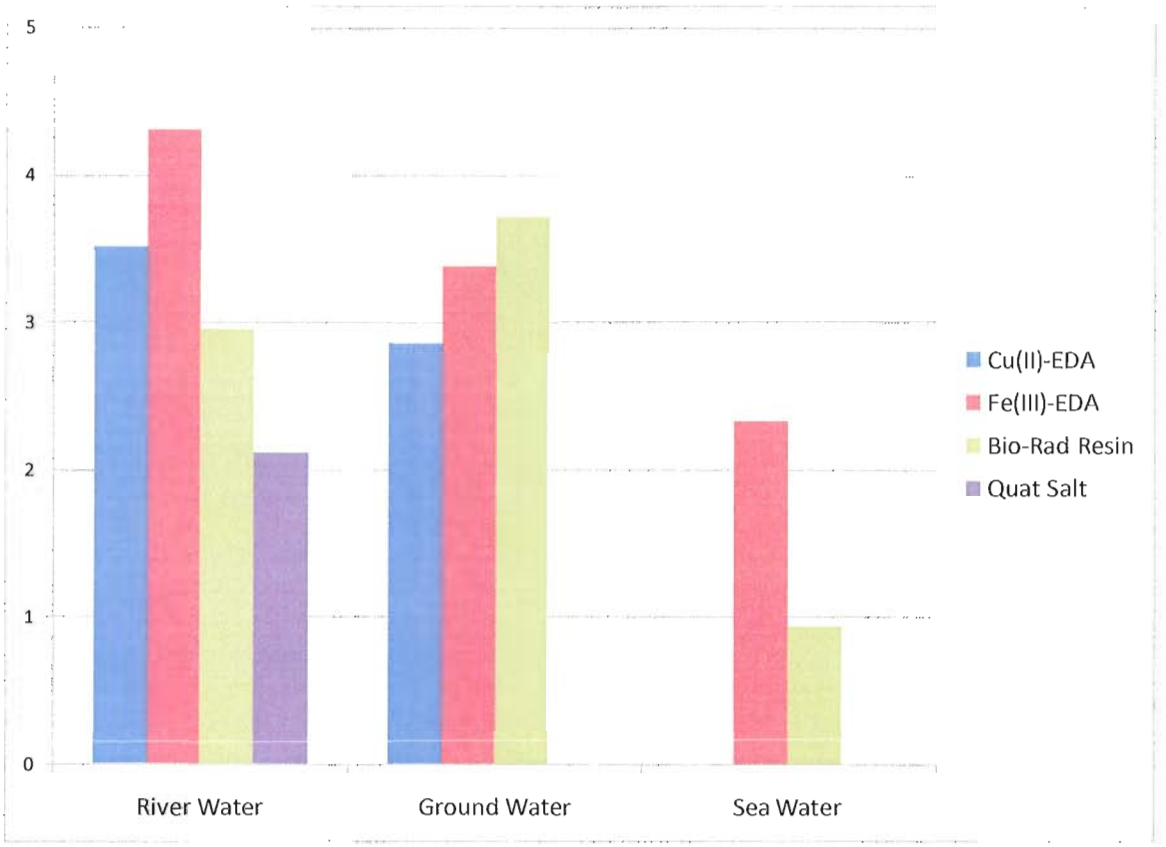


**Figure 6** Plot of Log $K_d$ values for $As^{5+}$ oxyanion in neutral Columbia River Water (left), Hanford site ground water (center) and Pacific Ocean sea water (right). The high ion concentration of the sea water causes reduced binding of the oxyanion with all four test materials due to completing reactions.

## Conclusion of Anion Binding

From the provided data, it is apparent that $Cu^{2+}$- and $Fe^{3+}$-EDA SAMMS are effective sorbents for arsenate and chromate oxyanions in natural water sources from neutral to highly acidic conditions. $Fe^{3+}$-EDA SAMMS is a better overall sorbent for both oxyanions at low to neutral pH although $Cu^{2+}$-EDA SAMMS exhibits a similar binding trend for $Cr^{6+}$ through this range. Water chemistry clearly affects metal binding in sea water greatly reducing the efficiency of both materials. Because of the complex makeup of the natural water sources, it is extremely difficult to claim conclusively which

species are present within each water source and how binding is affected by the presence of multiple ions. A number of organic acids present in natural water sources could be affecting binding through competitive binding routes. As a whole, $Cu^{2+}$- and $Fe^{3+}$-EDA SAMMS are easy to generate, perform equal to or better than commercially available resins and work over a wide pH range for the uptake of arsenate and chromate.

## Experimental

**General Procedures** Water samples were taken from the Columbia River (Richland, WA), a well water located on the Hanford site (Richland WA) the Pacific Ocean (Sequim, WA) and in-house Nanopure (18.2 mΩ) water sources where noted. Glassware and plastic bottles were rinsed with a 5% nitric acid (low metal ICP-MS grade) solution followed by copious rinses with Nanopure water. All SAMMS materials were weighed out on a bench top analytical balance and reported to the nearest tenths of a mg. Digital pipettes (manual and electronic) were used to deliver small volumes of solutions (less than 100 mL). Large volumes were measured on a bench top analytical balance to the nearest tenth of a gram with the assumed density equal to 1 for all solutions including sea water. Variation in the actual water sample densities results in a slightly higher or lower final metal concentration which is measured accurately by ICP-MS and therefore accounted for in each experiment. Natural water samples were passed through a 0.2 μm filter by vacuum and stored in the dark until used. Test samples were filtered with 0.2 μm syringe filters before ICP-MS analysis. Samples were diluted as needed to range between 50 to 100 ppb to best match metal calibration curves. ICP-MS

was performed on an Agilent Technologies 7500ce with calibration standards checked periodically to eliminate drift. All experiments were performed in duplicate or triplicate and values averaged before plotting unless otherwise noted. MCM-41 was generated in house with a pore size of approximately 35Å as determined by BET analysis and surface area of 761.1 $m^2/g$. Ethylenediamine SAMMS (EDA SAMMS) were made in house as detailed by Fryxell et al.[10]

*Quat Salt SAMMS* Combined 5.102 g MCM-41 with toluene (200 mL) in a 500 mL round bottom flask under nitrogen while stirring. Nanopure water (1.8 mL) was added and the solution stirred for approximately 4 hours. Added *N*-trimethoxysilylpropyl-*N,N,N*-trimethylammonium chloride (50% solution in MeOH, 5.053 g, 9.8 mmol) by syringe and heated to reflux. Continued stirring overnight for a total time of 16 hrs. Cooled slightly and affixed a Dean Stark trap between the flask and condenser, returned to reflux. Continued for two hours (until obvious signs of water collection in the trap) then cooled slightly. Added 100 mL of isopropyl alcohol (IPA), returned to reflux until ~4 mL total water was collected in the trap (approximately 1.5 hrs). Cooled to room temperature and added 200mL IPA while stirring. Vacuum filtered with a sintered glass Buchner funnel and washed with copious amounts of acetone, slurring each time to assure complete rinsing of SAMMS material. Dried in vacuum oven at 30 °C and -25 inches Hg overnight. Total mass gain 2.067 g for a loading of 1.621 molecules per $nm^2$ (target 1.5 molec./$nm^2$).

*$Cu^{2+}$-EDA SAMMS* Combined copper (II) acetate monohydrate (5.836 g, 29.2 mmol), and Nanopure water (250 mL) and stirred until dissolved. Added EDA-SAMMS (5.010 g, 761.1 $m^2/g$, 3.5 molec./$nm^2$) and swirled gently. Solution turned from dark blue to light blue while continuing to stir on a platform shaker at 1 Hz for 1 hr. The material was filtered then re-slurred with IPA. Dried in vacuum oven overnight at 30 °C and -25 in. Hg. Transferred to 500 mL round bottom flask and added toluene (200 mL) under $N_2$. Heated to reflux for 3.5 hrs then cooled slightly. Affixed a Dean Stark trap atop the flask and returned to reflux for 2 hrs. Cooled overnight and filtered the next morning. The solid was washed with 3 x 100 mL acetone, slurring each time. Dried in vacuum oven at 25°C over the weekend. Final weight 5.055g (0.22 mmols $Cu^{2+}$ addition).

*$Fe^{3+}$-EDA SAMMS* This material was prepared as described above using $FeCl_2$ as described by Yokoi and coworkers.[1]

## Bridge to Chapter V

Chapter V discusses a new class of sorbent material which utilizes weak intermolecular interactions to stabilize aryl ring containing ligands to an aryl monolayer on mesoporous silica. The use of benzyl and dibenzyl thiol ligands non-covalently bound to the silica substrate has proven to be quite effective in toxic metal ion capture. In many respects, this material performed as good as the covalently bound material previously studied in Chapter III. Studies include the effects of pH and water chemistry on binding cations in both $HNO_3$ spiked Nanopure and native water sources.

# CHAPTER V

## NEW FUNCTIONAL MATERIALS FOR HEAVY METAL SORPTION: "SUPRAMOLECULAR" ATTACHMENT OF THIOLS TO MESOPOROUS SILICA SUBSTRATES

Some of this work has been previously published and is reproduced with permission from: Carter, T.G.; Yantasee, W.; Sangvanich, T.; Fryxell, G.E.; Johnson, D.W.; Addleman, R.S. *Chem. Commun.* **2008**, *43*, 5583-5585.

### General Overview

Chapter V describes a research project conceived at the University of Oregon and reduced to practice at Pacific Northwest National Laboratory in Richland, Washington under the guidance of Dr. R. Shane Addleman. This chapter contains work published in *Chemical Communications* © by the Royal Chemical Society and coauthored with Wassana Yantasee who provided experimental oversight, Thanapan Sangvanich performed mass spectrometry analysis, Glen E. Fryxell provided experimental oversight, Darren W. Johnson and R. Shane Addleman provided intellectual contributions to the project and editorial input. Leaching data acquired by Sean A. Fontenot and Brian Theobald is included in the conclusion section. This work is ongoing at both the UO and PNNL by Sean A. Fontenot toward his dissertation.

## Introduction

Access to sustainable, clean drinking water is an increasing concern as the Earth's human population continues its steady growth.[1] Degrading water quality in both industrialized and non-industrialized nations has the potential to cause great economic strain on the world's governing bodies.[2] At the same time, this offers a challenge to chemists to discover new, functional, designer materials that have high loading capacities and selectivity for environmental contaminants.[3] Regenerable reusable functional materials have the added benefit of providing a sustainable approach to clean drinking water by reducing waste and increasing the lifetime of the product. Although water contamination from natural sources does occur, such as the devastating results of high arsenic levels in Bangladesh,[4] a significant level can be attributed to human activities. The need to develop inexpensive and efficient water purification media is a high priority.[a]

Current filter media typically consist of granular activated carbon (GAC) or a hybrid material that combines an inorganic oxide such as gamma alumina to achieve satisfactory water purification. This type of filter medium, although common and inexpensive, offers limited uptake potential. Additionally, spent media must be disposed of properly to prevent it from conceivably becoming a source of contamination due to leaching over time. An alternative to "one-shot" filters is the implementation of renewable media capable of many purification cycles before fouling. One such approach is described in this chapter utilizing the technique of non-covalent absorption of

[a] In February 2005, the National Academy of Engineering (NAE) announced a $1 million prize for practical technologies capable of sequestering arsenic from drinking water. Abul Hussam of George Mason University, Fairfax, VA SONO household filter system was the recipent of the prize in 2007.

organothiol ligands onto self-assembled monolayers on mesoporous supports (SAMMS™).

Both the Darren Johnson laboratory and Pacific Northwest National Laboratory have programs designed to understand how toxic metal ions, specifically main group and transition metal ions, interact with thiolate ligands by studying their binding preferences using a supramolecular approach or through monitoring hazardous ion uptake from contaminated waters using functionalized materials.[5-9] Functionalized mesoporous supports have been found to be excellent sorbent materials, capable of being chemically modified with reactive head groups for toxic metal, metalloid and oxyanion uptake as well as radioactive species.[10-12] One particular silica-based support, MCM-41, has garnered much attention due to its controllable honeycomb-like porosity, structural integrity, chemical resistivity and high surface area, approaching 1000 $m^2 g^{-1}$.[13,14] A variety of commercially available and synthetically accessible functionalized organosilanes can be affixed inside the pores of the silica support as self-assembled monolayers. The result is a dense population of chelating sites which can achieve exceptionally high uptake levels of target toxic ion species. Chapter IV and V describe in detail a number of covalently functionalized SAMMS materials for uptake of a variety of toxic metal cations and oxyanions, respectively, for use in natural aqueous media.

Thiol-SAMMS derived from covalent attachment of an alkylthiolsilane (tris(methoxy)mercaptopropylsilane, TMMPS, for example) have demonstrated excellent uptake levels of soft and moderately soft metal ions such as $Hg^{2+}$, $Pb^{2+}$, $Cd^{2+}$, and $Ag^{+}$(see chapter IV).[11] We have extended the breadth of thiol-SAMMS style sorbent

materials with this research to include noncovalently bound thiol and dithiol ligands attached by relatively weak, reversible π-stacking interactions. It was recognized that aryl monolayers (such as a phenyl-based system), in which the aromatic rings were rigidly held upright and perpendicular to the surface, were well suited, both sterically and electronically, to serve as hosts to other functionalized arenes. This approach was envisioned not only to be a very versatile and easy functionalization strategy, but also one that would readily provide for 'refreshable' functionalization. This chapter describes the functionalization of MCM-41 with phenyl monolayers at various densities to provide a hydrophobic scaffolding for noncovalently bound benzylmercaptan (BM), 1,3- and 1,4-bis(mercaptomethyl)benzenes (1,3- and 1,4-BMMB, respectively) for use in heavy metal cation uptake from native waters (**Figure 1**).

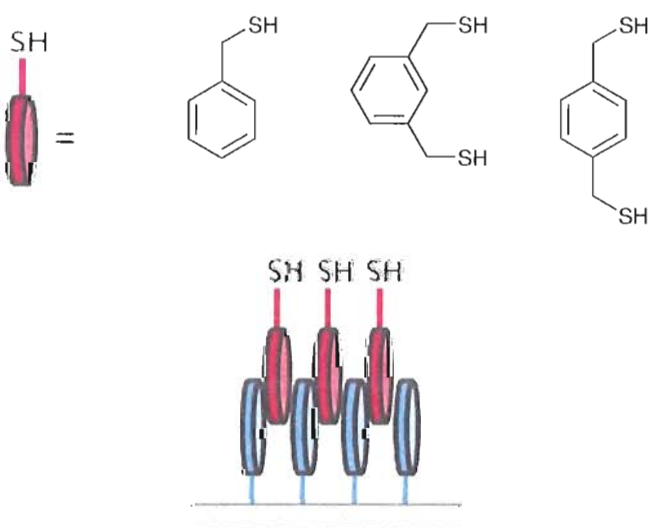


**Figure 1** Graphical representation of organothiol ligands benzylmercaptan (BM), 1,3-bis(mercaptomethyl)benzene (1,3-BMMB), 1,4-bis(mercaptomethyl)benzene (1,4-BMMB) (top). Graphical representation of functionalized mesoporous silica monolayer with π-π interactions between functionalized support and chemisorbed ligand (bottom). Shown is an idealized offset stacking but the actual arrangement may be in a herringbone-like manner as charecterized in other phenyl modified surface characterization data.

## Results and Discussion

Remarkably, 1,3- and 1,4-BMMB SAMMS exhibit comparable metal ion uptake levels to their covalently bound analogs. BMMB SAMMS were prepared by functionalizing MCM-41 at different loading levels by first hydrating the silica surface with a toluene/water mixture (equal to two monolayers of water based on total surface area) followed by addition of trichlorophenylsilane and an overnight stir at room temperature. This was achieved by first dispersing the MCM-41 in toluene by stirring. Water was added, resulting in flocculation of the silica immediately followed by dispersing over 2-3 hours of stirring. Trichlorophenylsilane was then added and stirred overnight. The resulting solution was translucent in appearance. Isopropyl alcohol (IPA) was added and the solid filtered, washed with IPA and vacuum dried in an oven at 40 °C. Phenyl coverage ranged from 0.01 molecules $nm^{-2}$ (sparsely covered surface) to 3.1 molecules $nm^{-2}$ (near maximum achievable loading accessible by this technique) by varying the trichlorophenylsilane and water concentrations.

## BMMB SAMMS Characterization

Transmission electron microscopy (TEM) of phenyl loaded MCM-41 shows an increase in electron density in the pore structure of 1,4-BMMB SAMMS with saturated $Pb^{2+}$ ion loading (**Figure 2**). The left hand image shows the honey comb hexagonal arrangement of the pores with thin $SiO_x$ walls circled in red. This structure is not visible in the $Pb^{2+}$ loaded material (right) presumably due to the high electron density of the lead versus the $SiO_x$ walls. Energy-dispersive X-ray spectroscopy (EDX) comparison of the

bright versus dark areas yields a high concentration of lead and sulfur in the bright areas and silica and oxygen in the dark regions. The lack of hexagonal porous structure could be due to the misalignment of the pores with the beam resulting in viewing down the length of the pore wall causing the effect of bright spots versus resolved pores. This is apparent in the non-lead containing TEM image as well. Nonetheless, the distance measured center to center between bright spots is in good agreement with the BET measurement of 40 Å pores.

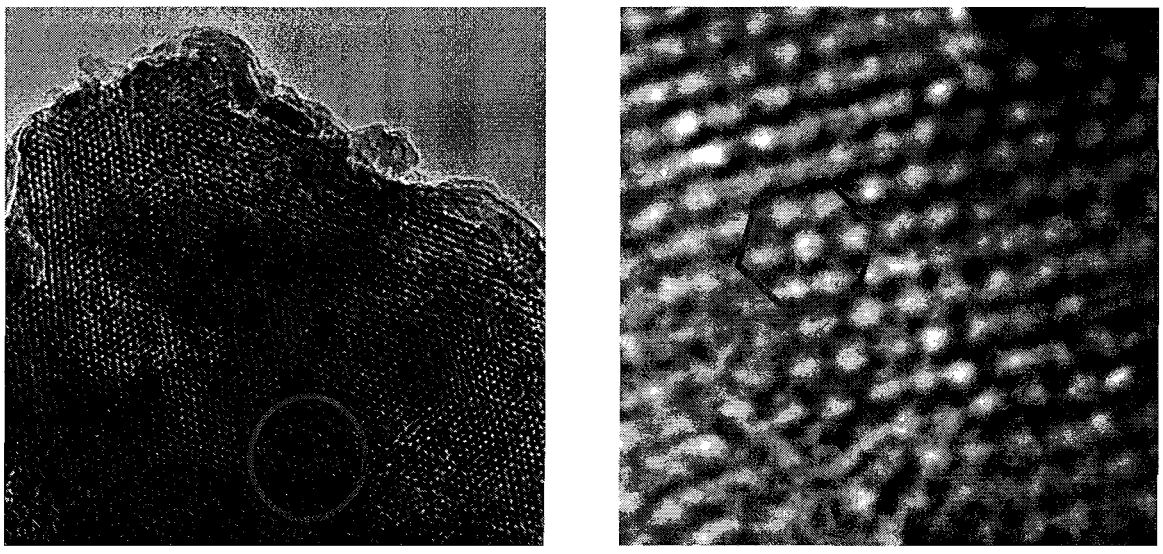

**Figure 2** TEM micrograph of 1,4-BMMB SAMMS without $Pb^{2+}$ (left) and with $Pb^{2+}$ right. Hexagonal arrangement indicated by red hexagon on right image.

Total phenyl loadings were determined by thermogravimetric analysis (TGA). TG analysis was collected on a TA Instruments 2950 coupled to an electron impact (EI) Balzers Thermostar mass spectrometer at a ramp rate of 2°C per minute up to 600 °C and capillary temperature of 100 °C to assure complete burn off of organics and provide clean

transition temperatures. A comparison of 1,4-BMMB physisorbed onto native MCM-41 versus the phenyl modified support (Phenyl-SAMMS) containing chemisorbed 1,4-BMMB revealed a significantly different burn off rate by TGA after the initial water desorption. Two different BMMB ligand loadings (equal to 2:1 or 1:1 phenyl moieties to BMMB molecules for the phenyl functionalized silica, low loading and high loading, respectively), were generated by adding Phenyl-SAMMS to a solution of BM, 1,3-BMMB or 1,4-BMMB dissolved in dichloromethane in a sealed vessel and placed on an orbital shaker and mixed overnight. After mixing, the vessel was uncapped and the solvent was evaporated followed by overnight vacuum drying at 40 °C. TGA of the native silica support shows a relatively rapid weight loss starting around 235 °C and ending near 255 °C (**Figure 3, dashed lines**).

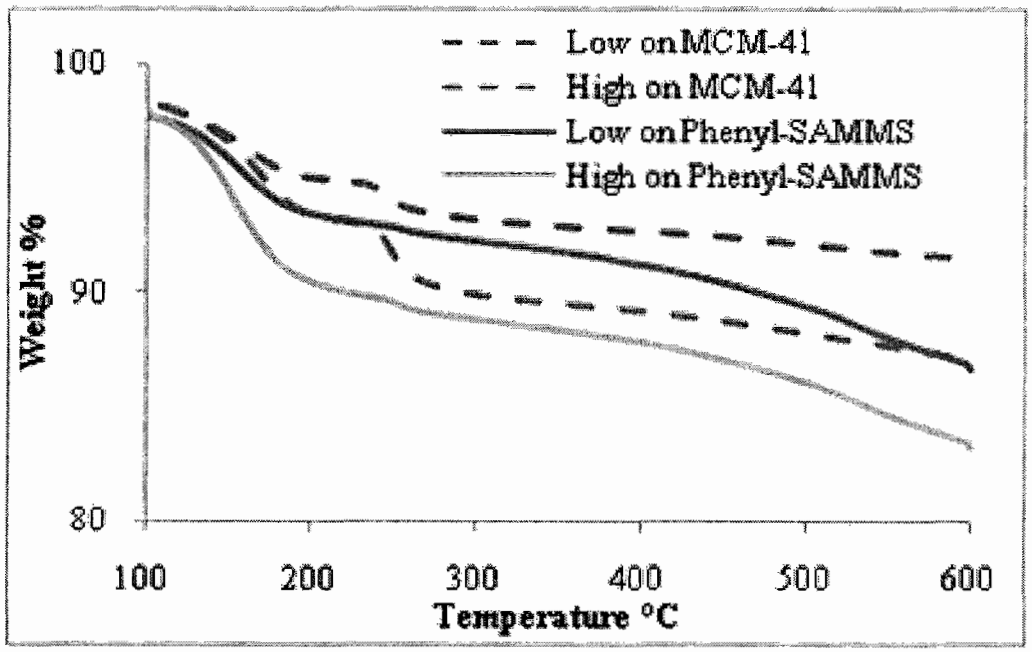


**Figure 3** TGA comparison of various chemisorbed loading densities of 1,4-BMMB on phenyl functionalized MCM-41 (solid lines) versus physisorbed 1,4-BMMB on native MCM-41 silica (dashed lines).

1,4-BMMB ligand desorption from the phenyl modified support occurs at a slightly elevated temperature compared to the non-phenyl monolayer stabilized silica and continues over roughly 200 °C to around 350 °C, verified by the continued detection of $SO^+$ (47.9 m/z) and $SO_2^+$ (63.8 m/z) by mass spectrometry. Degradation and oxidation of 1,4-BMMB occurred due to trace levels of oxygen contamination present in the TGA purge gas resulting in the observation of a large carbon dioxide peak and $SO_x$ peaks seen in **Figure 4**.

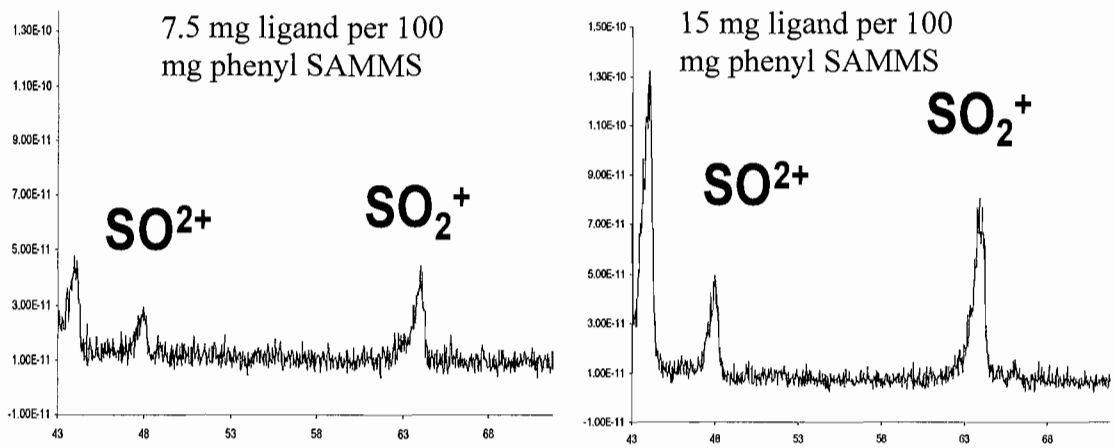


**Figure 4** EI mass spectra of evolved gasses during the burn off process. Collected between 200 and 300 °C.

The loss of the phenyl monolayer was observed above 350 °C and continued to 600 °C, also monitored by EI-MS with ions detected at 49.9, 50.8, 51.8 and 78.2 m/z which correspond to $C_6H_6^+$ fragmentation typical of this type of mass analyzer. The extended burn off range of 1,4-BMMB can be accounted for by an increase in stabilization of the chemisorbed arylthiol ligands afforded by the phenyl monolayer. Benzylmercaptan (BM) was also found to be stabilized by the phenyl monolayer as

indicated by TGA (data not shown) however, a strong, thiol odor emanated from this material making it unsuitable for use in filtration applications. Additionally, uptake levels for BM were less than those of 1,3- and 1,4-BMMB.

In addition to thermogravimetric analysis, Fourier Transform Infrared spectroscopy (FT-IR) and Powder X-ray Diffraction (PXRD) spectroscopy was used to qualitatively visualize loading of organic material onto the silica substrate. FT-IR provided useful analysis of the surface makeup by comparing relative intensities of prominent peaks between samples (**Figure 5**).

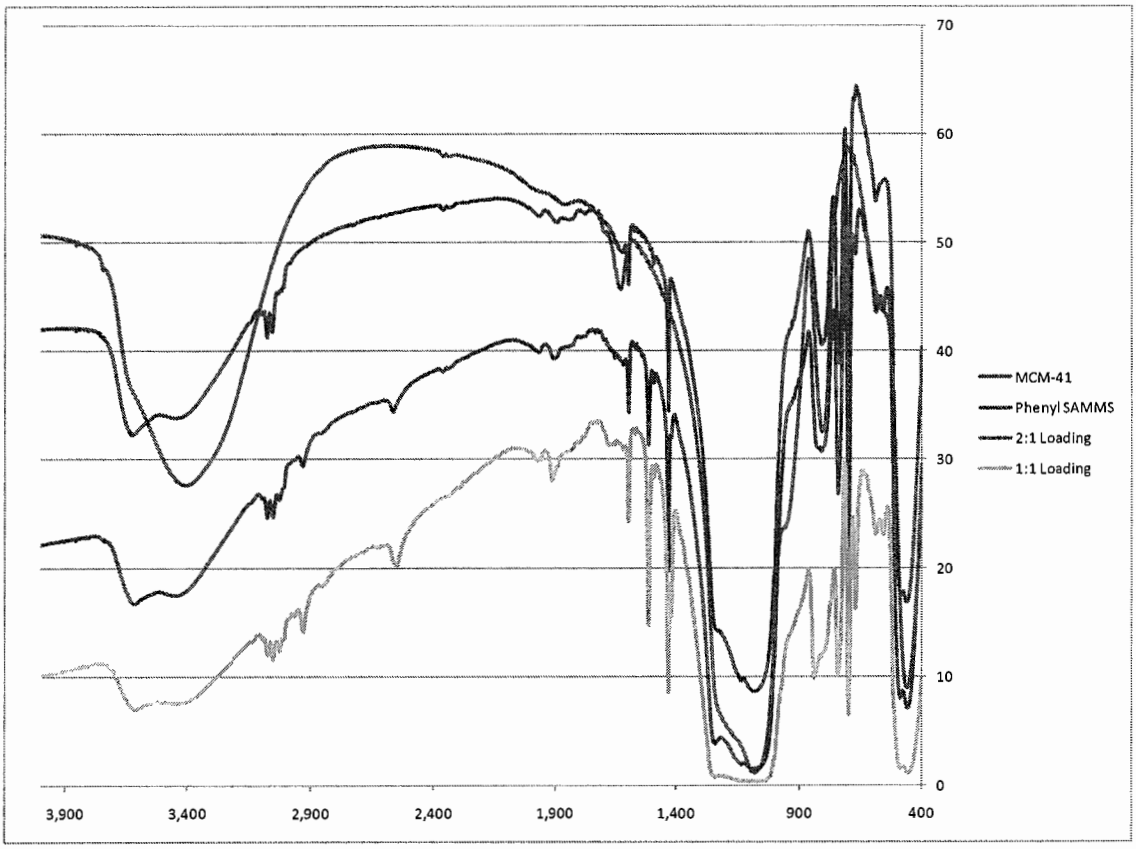


**Figure 5** FT-IR of native silica (blue trace), phenyl monolayer (red trace), 2:1 loading (purple trace) and 1:1 loading (green trace). Note the increase in C-H (aryl and alkyl) stretching as ligand loading increases as well as S-H stretching around 2545 wave numbers.

Changes in transmittance comparing to the native silica (MCM-41), phenyl monolayer a 2:1 loading and a 1:1 loading of phenyl base layer to 1,4-BMMB provides a qualitative spectroscopic handle for ligand loading. Thiol S-H and C-S stretching, 2545 and 669 $cm^{-1}$, respectively, was normalized to the aryl C-H (2926 and 698) and C=C (1595, 1512 and 1431 $cm^{-1}$) stretching to verify loading of both monolayer and adsorbed ligand.

Powder XRD revealed a dominant (100) peak at 2.11° but lacked higher angle peaks for all substrates. It has been reported by others in the field that a decrease in peak intensity is directly related to the extent of modification of the pore with organics. We observed a similar decrease in the (100) peak intensity consistent with the chemisorptions of 1,4-BMMB onto phenyl-SAMMS. [15]

## Solution Phase Uptake Studies

Initial metal uptake studies were carried out using well water from the Hanford site in Richland, Washington. Natural water sources such as that from a well provides a 'real world' test matrix containing typical ions and buffering agents. All aqueous solutions are from native sources from either a well located on the Hanford site, the Columbia River or the Pacific Ocean. Matrices were pretreated by passing through a 0.22μm filter followed by pH adjustments with $HNO_3$ and metal ion addition with target levels of 500 ppb per ion species in a typical experiment although some tests used 100 ppb ion concentration. Sorbent/matrix contact times were typically two hours with the sorbent material preconditioned with a few microliters of methanol to enable effective

surface wetting and facilitate metal ion uptake. This step is necessary due to the increased hydrophobicity imparted by the phenyl monolayer. Mass transfer of toxic ions from the aqueous test matrices to the functionalized sorbent material does not occur without the initial wetting—much like other neutral, organic modified silica sorbent materials.

Uptake values are reported as the distribution coefficient ($K_d$), which is the mass-weighted partition coefficient between the sorbent material and matrix. The distribution coefficient can be determined by **Equation 1** as stated on page 65 in chapter III by knowing the initial and final concentration, $C_o$ and $C_f$, respectively, of the target ions which is quantified by ICP-MS, the volume, $V$, in milliliters as measured accurately by volumetric pipettes and the mass, $M$, in grams of the sorbent material measured to the nearest $10^{th}$ of a milligram. Under trace level analysis such as this work, $K_d$ is a more relevant value to gauge ion capture rather than mg/g (amount of metal ion captured to grams of sorbent used), which is typically used under saturation conditions.

A plot of log $K_d$ values for Phenyl-SAMMS loaded at 3.1 molecules $nm^{-2}$ containing chemisorbed 1,4-BMMB loaded at either 2:1 (low) or 1:1 (high) (monolayer phenyl moiety to aryl dithiol ligand) shows similar uptake capacities with the covalently attached Thiol-SAMMS in Hanford well water matrix spiked with 500 ppb $Hg^{2+}$, $Pb^{2+}$, $Cd^{2+}$, and $Ag^{+}$ ions (**Figure 6**).

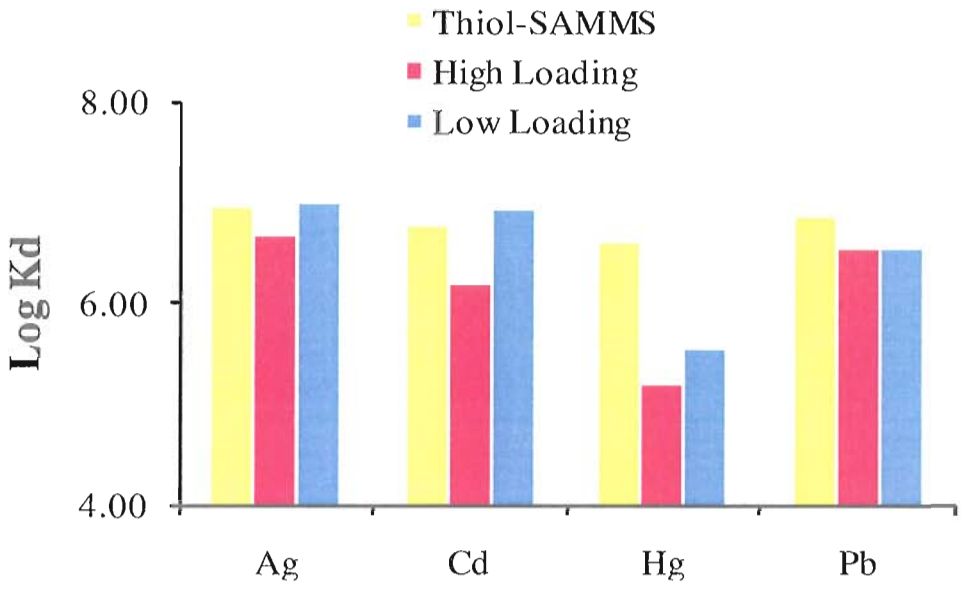


**Figure 6** Log $K_d$ values of Thiol-SAMMS, versus 1-4-BMMB at two different loading levels.

A slight preference for $Hg^{2+}$ with Thiol-SAMMS over the chemisorbed materials is observed possibly due to neighboring BMMB ligands binding with one $Hg^{2+}$ ion thus reducing the actual available binding sites for target ions.

Likewise, 1,3-BMMB and 1,4-BMMB exhibited similar uptake levels at near equivalent loadings (**Figure 7**). This is unexpected due to the assumed preferred orientation of the chelating thiol groups, with 1,3-BMMB positioned presumably with both chelating thiols above the plane of the monolayer whereas 1,4-BMMB could conceivably have one or both thiol group buried in the monolayer making it inaccessible to the metal ions. This argument assumes that the aromatic rings of the phenyl monolayer and BMMB are orientated in an edge-to-face herringbone-like manner.[16]

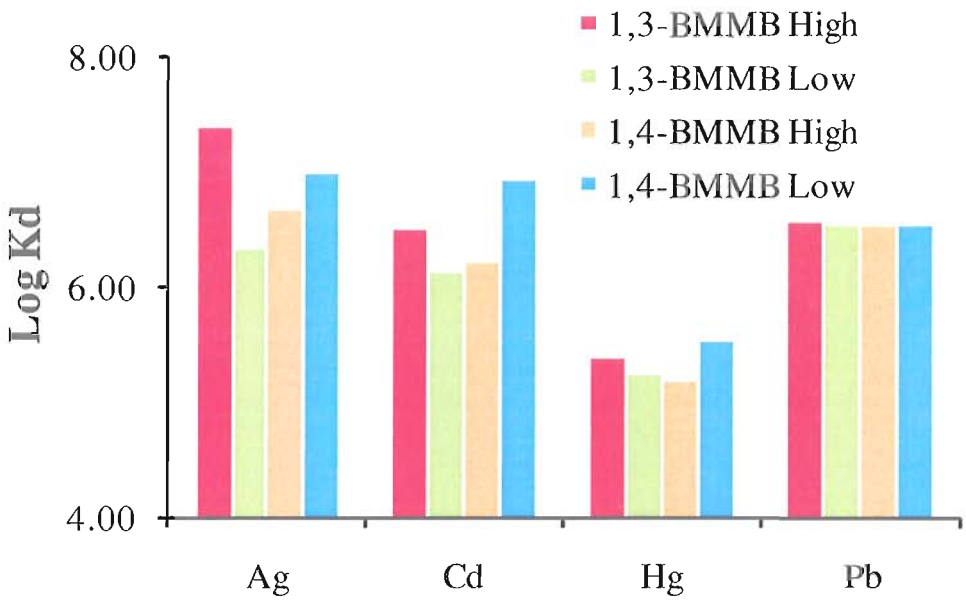


**Figure 7** Comparison of 1,3 and 1,4-BMMB at similar loading levels (bottom) in Hanford well water. All analyses performed in either duplicate or triplicate with variances greater than 10% discarded.

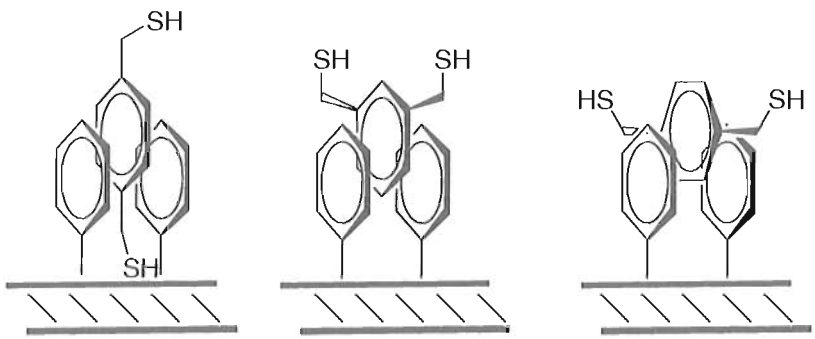


**Figure 8** Graphical representation of 1,3- and 1,4-BMMB ligands intercalated into phenyl monolayer with both thiols accessible (right and middle) 1,4-BMMB with one thiol buried in the monolayer.

However, this assumed packing appears not to be the case due to the similar uptake levels between Thiol-SAMMS, which has an overall higher surface ligand density (5 molecules $nm^{-2}$), versus the chemisorbed 1,3- and 1,4-BMMB, which have lower monolayer density

of 3.1 molecules $nm^{-2}$ but slightly higher chelation site density due to the difunctionality of the two arylthiol ligands (**Figure 8**).

A possible explanation of this observation is that the BMMB ligands are only partially intercalated into the phenyl monolayer in an offset stacking[17] resulting in sufficient accessibility by the metal ions to the bulk of the thiol head groups (**Figure 8**). One interesting observation is that as 1,4-BMMB loading increases, uptake decreases for $Hg^{2+}$, $Cd^{2+}$, and $Ag^{+}$ but not for $Pb^{2+}$. This may be due to the thiol sites becoming buried in the monolayer as loading densities increase. It has been shown that the densely packed thiol groups of Thiol-SAMMS material are shared by the same metal ion resulting in $ML_n$ species where $n > 1$ in previous studies.[9] This desire to maximize metal-thiol contacts may manipulate the weakly bound chemisorbed ligands to adopt a more ideal geometry for binding at the various loadings investigated. In either case, the metal affinity levels of the chemisorbed BMMB Phenyl-SAMMS is near equal to that of the covalently bound Thiol-SAMMS which has been shown to have affinity levels for heavy metal ions one to three orders of magnitude greater than commercially available thiol-based resins such as GT-73.[8]

The effects of density of the covalently bound phenyl layer were also probed by varying the loading from 0.01 phenyl molecules $nm^{-2}$ and as high as 3.1 molecules $nm^{-2}$ while maintaining 1,3- and 1,4-BMMB loadings levels equal to previous tests. Surprisingly, the sparsely populated Phenyl-SAMMS with chemisorbed BMMB performed equal to that of material of higher phenyl density for $Hg^{2+}$ ion uptake. The exact nature of the interaction between the covalently attached phenyl ring and that of

chemisorbed BMMB is not well understood at this time, but the bound phenyl ring appears to be capable of acting as a nucleation site resulting in BMMB anchoring to the surface to provide an area rich in chelation sites capable of metal ion uptake—a feature lacking with the native silica and phenyl modified support. There is however an apparent reduction in stabilization of the BMMB active layer by the low phenyl base layer loading as evident in leaching studies (vide infra).

## pH-Dependent Uptake Studies

The pH-dependent metal binding trend first described in Chapter IV of this dissertation is conserved for chemisorbed 1,3- and 1,4-BMMB SAMMS material. Experiments were carried out using metal ion spiked Columbia river water ($Co^{2+}$, $Cu^{2+}$, $As^{5+}$, $Ag^{1+}$, $Cd^{2+}$, $Hg^{2+}$, $Tl^{1+}$, $Pb^{2+}$ at roughly 100ppb initial concentration) with a L/S ratio of 5000 and pH ranging from 0-8 in 2 unit increments (measured both before and after the two hour soak to account for drift in pH). Experiments were performed in triplicate with average values plotted. To simplify the discussion, data will be limited to $Pb^{2+}$ and $Hg^{2+}$ and are plotted in **Figure 9** to demonstrate two typical pH-dependent binding extremes.

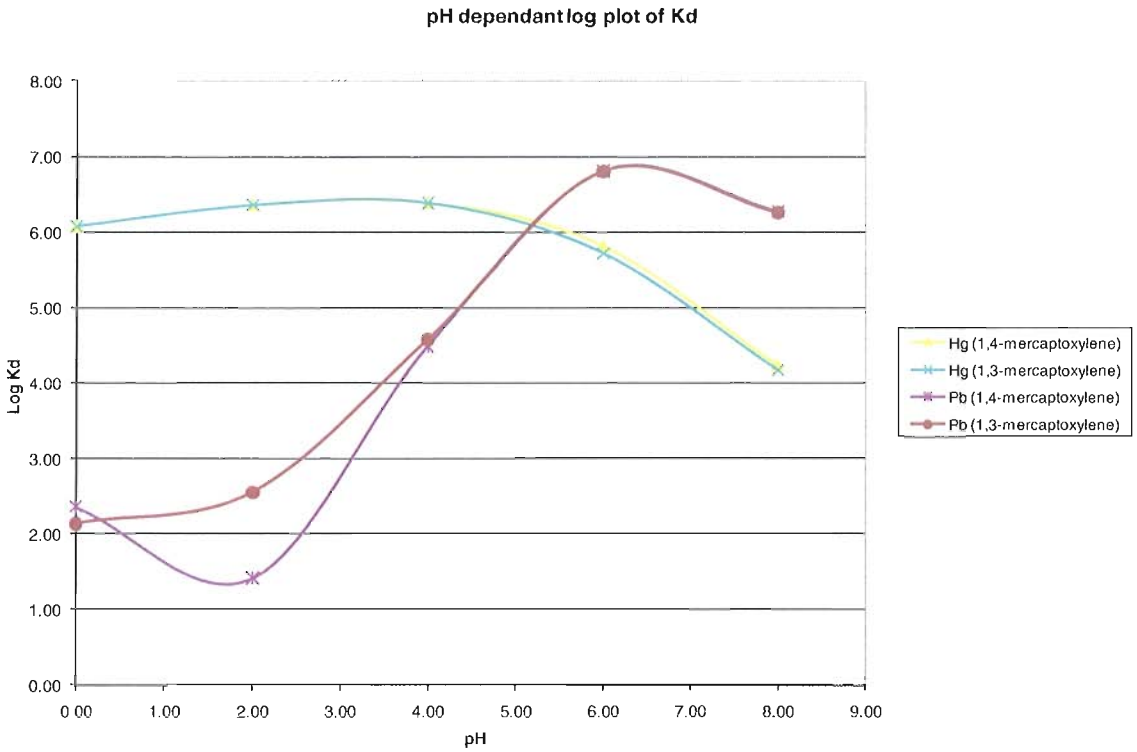


**Figure 9** pH-dependent log $K_d$ plot of $Hg^{2+}$ and $Pb^{2+}$ from a mixed metal ion spiked Columbia river water matrix.

From **Figure 9**, it is apparent that both 1,3- and 1,4-BMMB chemisorb SAMMS follow similar trends for $Hg^{2+}$ and $Pb^{2+}$ ion binding with Thiol SAMMS (see Chapter IV). The exact nature of the dip observed for lead at pH 2 is unknown but was verified in triplicate as well as $Pb^{2+}$ uptake experiments for benzoic acid-based and 1,3-BMMB chemisorbed ligands performed on different days (vide infra).

## Probing pKa Effects of Thiol Ligand

In an attempt to try to demonstrate the above observation of pH-dependent uptake of metal ions, an experiment was devised which used thiol-based ligands with different pKa values **Figure 10**.

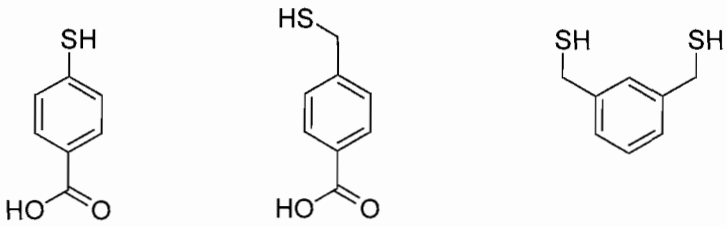


**Figure 10** Ligand selection with varying $pK_a$. From left, 4-mercaptobenzoic acid, 4-(mercaptomethyl) benzoic acid and 1,3-BMMB.

A rough estimate of the $pK_a$ values for 4-mercapto and 4-(mercaptomethyl) benzoic acid would lie around 10 and 15, respectively, based off of similar molecules in Bordwell's table measured in DMSO. It is reasonable to assume that these values will be closer to 6 or 7 for 4-mercapto and 10 to 12 for 4-(mercaptomethyl) benzoic acid in aqueous solutions.

**Figure 11** shows very little effect of metal uptake with varying pKa's of the thiol ligand. For all intents and purpose, these ligands behave similarly to each other within error and therefore no conclusions can be drawn from this data. Most likely, stronger electron donating and withdrawing groups will be necessary to properly verify the effect of pKa on metal binding with thiol ligands. It appears that the observed pH-dependent adsorption of metal ions can be primarily attributed to a metal ion's capacity to undergo

hydrolysis and secondly from an ion's water exchange rate or ease of forming a new, stable complex (see Chapter IV for a complete binding mechanism discussion).

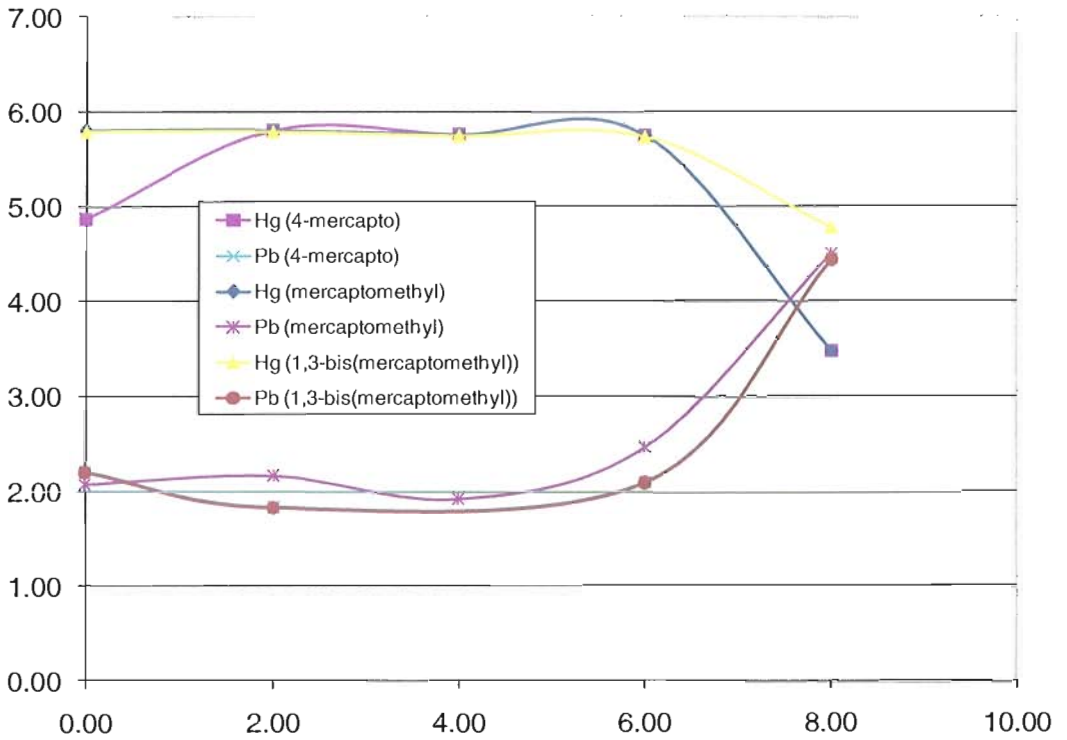


**Figure 11** pH-dependent comparison of thiol benzoic acids and 1,3-BMMB uptake for $Hg^{2+}$ and $Pb^{2+}$ over pH 0-8.

## Saturation Studies

This study was performed to determine the maximum uptake capacity of one metal ion ($Hg^{2+}$) which can be effectively absorbed by the chemisorbed sorbent material. Studies were carried out using pH-adjusted filtered Columbia River water doped with $Hg(NO_3)_2$ for a final concentration of 500 parts per million (500 mg/L or ppm) and a working pH of 2. Liquid to solid ratios of 5000 (L/S, 100 mL/0.020 g) were used to

assure a favored equilibrium to the metal bound versus unbound ligand. Sample aliquots were removed after two hours, during which samples were gently agitated on a table-top mixer. Samples were filtered as described above to remove suspended sorbent material and diluted to an appropriate concentration for ICP-MS (target concentration of 50 to 200ppb is ideal to fit the calibration curve for most experiments). Base layers consisting of 3.1, 1.6 and 0.01 phenyl molecules per nanometer of silica were used with corresponding BMMB ratios (i.e. 1:1 or 2:1 binding of base phenyl rings to BMMB active layer).

Under saturated conditions, 1,4-BMMB out performs 1,3-BMMB for every loading combination tested (**Figure 12**). This suggests that the thiol functional groups of 1,3-BMMB are in close proximity for one mercury ion to bind with two neighboring ligands thus effectively reducing the potential binding sites. This also suggest that the phenyl binding mechanism for both 1,3- and 1,4-BMMB are similar—with the BMMB phenyl rings intercalated into the phenyl monolayer in an offset stacking with both thiol functional groups available for binding. If this were not the case, and 1,4-BMMB had a buried thiol, a near equal or even slight preference for 1,3-BMMB would be observed. This is merely a hypothesis which requires advanced surface characterization techniques to elucidate absolute binding between the phenyl rings but many examples of solution data appear to support this binding motif.

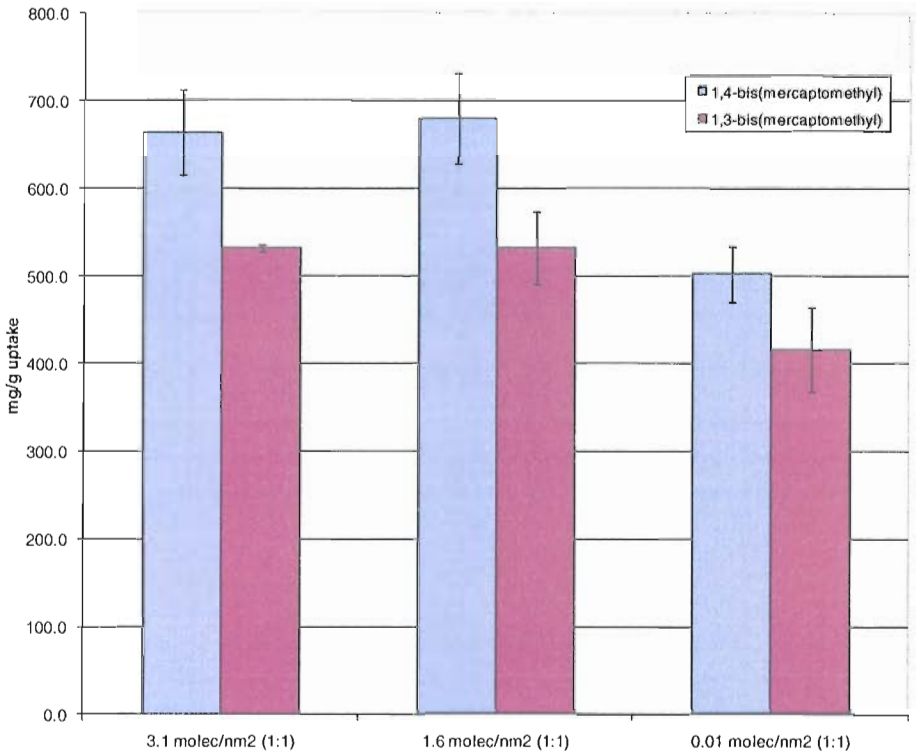


**Figure 12** Saturation studies of three 1,4-BMMB/Phenyl loadings with $Hg^{+2}$ doped Columbia river water. All samples run in triplicate.

In a similar experiment, low loaded phenyl SAMMS (1:2 BMMB active layer to phenyl base layer) was used under saturation conditions. This data supports the above hypothesis that one mercury ion is binding to two neighboring 1,3-BMMB ligands. As was assumed to be the case, the 1,3-BMMB ligands were more dispersed in the phenyl base layer in the lower loaded material thus distributing the thiol functional groups around the sorbent and preventing multiple ligand binding to one ion. This is apparent from **Figure 13** with the near similar uptake for both 1,3- and 1,4-BMMB, unlike the higher loaded material from **Figure 12**. At this lower loading, a slight improvement in the $Hg^{2+}$ uptake by 1,4-BMMB was also observed which would be expected as well.

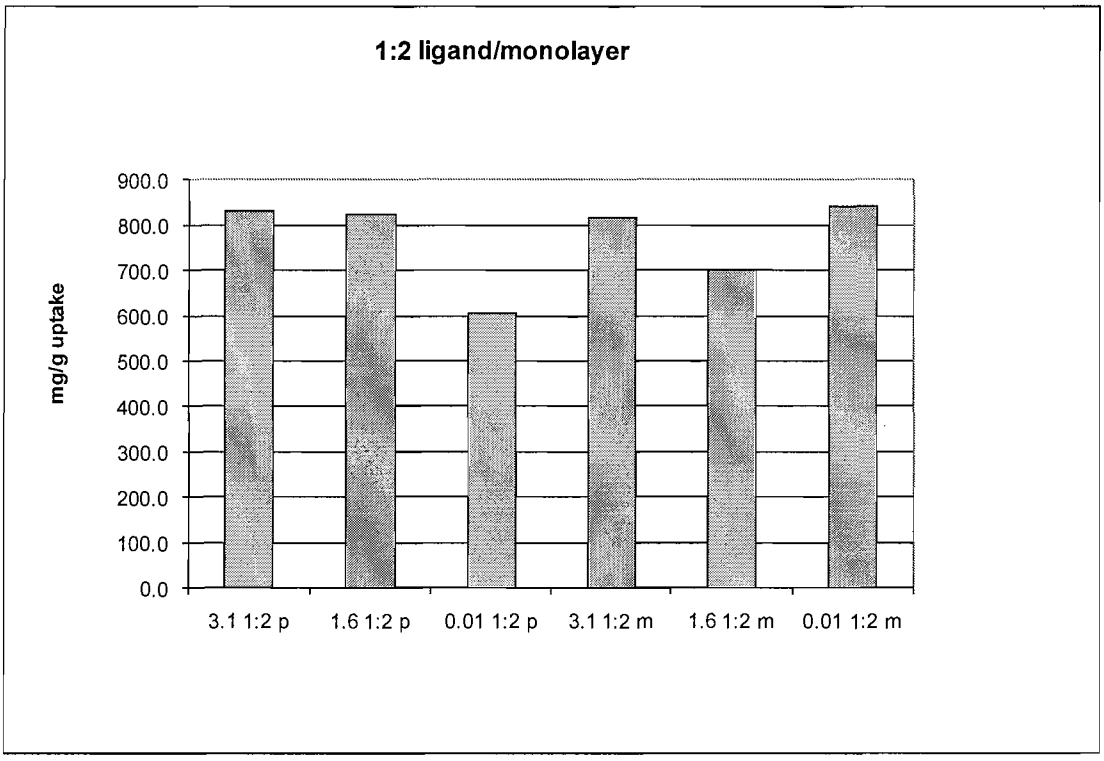


**Figure 13** Saturation data of low-loaded phenyl SAMMS with 1,4-(designated by p) and 1,3-BMMB (designated by m). In this experiment, the spacing of the thiol functional groups prohibits the shared binding of two ligands to one mercury ion.

## Binding Isotherm

An experiment was performed to test the sorbent capacity toward a single ion by varying the total concentration of the target while keeping all other parameters fixed.[18] This data is helpful when attempting to determine the amount of sorbent material necessary to achieve a desired binding density of toxic target ions. Due to the wide range of $Hg^{2+}$ concentrations for this experiment, a high L/S ratio (505000, 10mL/1.98E-05g) was necessary. In this study, the uptake capacity of 1:1 loaded 1,4-BMMB phenyl SAMMS was quantified with $Hg(NO_3)_2$ at pH 2 in spiked Columbia River water. $HNO_3$ was used to adjust the pH to an acceptable value.

At such a low sorbent concentration, it is possible to plot a binding or uptake isotherm from both experimental and calculated values. This is possible due to the increased target ion concentration driving the equilibrium to the right, forcing binding of the ion with the sorbent material. This experiment was not optimized due to the lack of allotted time while at PNNL but it does give a general idea about the materials uptake capacity (**Figure 14**). The actual data (blue diamonds) matches the predicted data (pink line) to a reasonable extent with the exception of actual uptake amount.

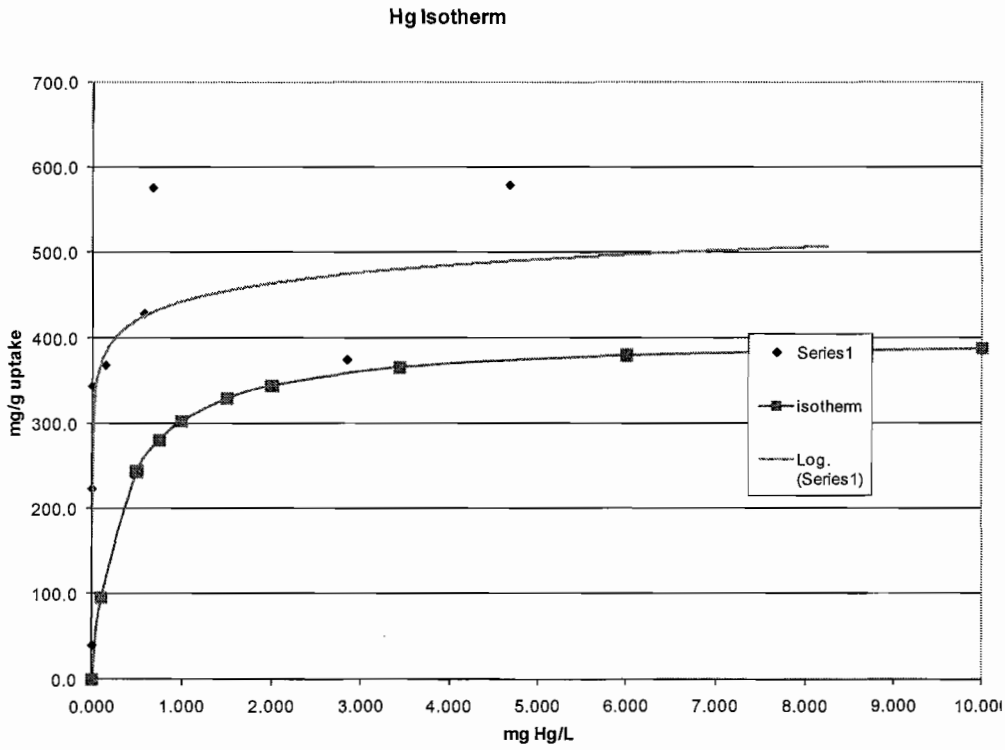


**Figure 14** Binding uptake isotherm for 1:1 loaded 1,4-BMMB phenyl SAMMS with Hg2+ ion. Red curve is calculated binding, blue line is log plot and blue diamonds are actual data. This experiment was not run in duplicate.

Despite the obvious erroneous data points due to single pass testing, this data is in good agreement with data obtained for thiol SAMMS as well as data in **Figure 12** for 1:1 loaded 1,4-BMMB SAMMS at 1.6 molecules/nm$^2$. The predicted binding (pink line, **Figure 14**) was found by using the Langmuir isotherm equation (**Equation 1**):

$$\frac{C}{Q} = \frac{1}{K} + \frac{C}{b}$$

**Equation 1** Langmuir isotherm equation.

where $C$ is the equilibrium concentration of mercury (mg/L), $Q$ is the mercury equilibrium loading on SAMMS (mg/g), $K$ is the Langmuir adsorption constant (g/L), and b is the maximum bound ion to the 1,4-BMMB SAMMS material. A plot of $Q_n$ over $C_n$ where $n$ is a value for each solution yields the theoretical plot (pink, **Figure 14**).

## Lead Contaminant Leaching Studies

From the data above, it is apparent that thiol-based sorbent materials have a high affinity for soft metal ions such as lead, mercury, cadmium and silver. Unfortunately, this can result in batch contamination if trace metals, specifically $Pb^{2+}$, are present on glassware, solvents or plastic labware. After a number of skewed data sets, it was determined by ICP-MS that four batches of BMMB (both 1,3- and 1,4-) where contaminated with lead at some point in the experiment, either during the synthesis of the material or during testing. The base MCM-41 and phenyl ligands were used in numerous experiments with no apparent sign of $Pb^{2+}$ contamination. To quantify the $Pb^{2+}$

contamination, a competitive binding experiment was devised using $Hg^{2+}$ to displace the $Pb^{2+}$ ions. This was carried out at pH 2, a range known to inhibit $Pb^{2+}$ binding to thiol-based ligands. Samples were prepared as described above with L/S ratio of 5000 and an initial $Hg^{2+}$ concentration of 4500 ppb to assure preferred binding. The result is a lead contamination range of around 1 mg/g (lead to sorbent) to nearly 8 mg/g (**Figure 15**).

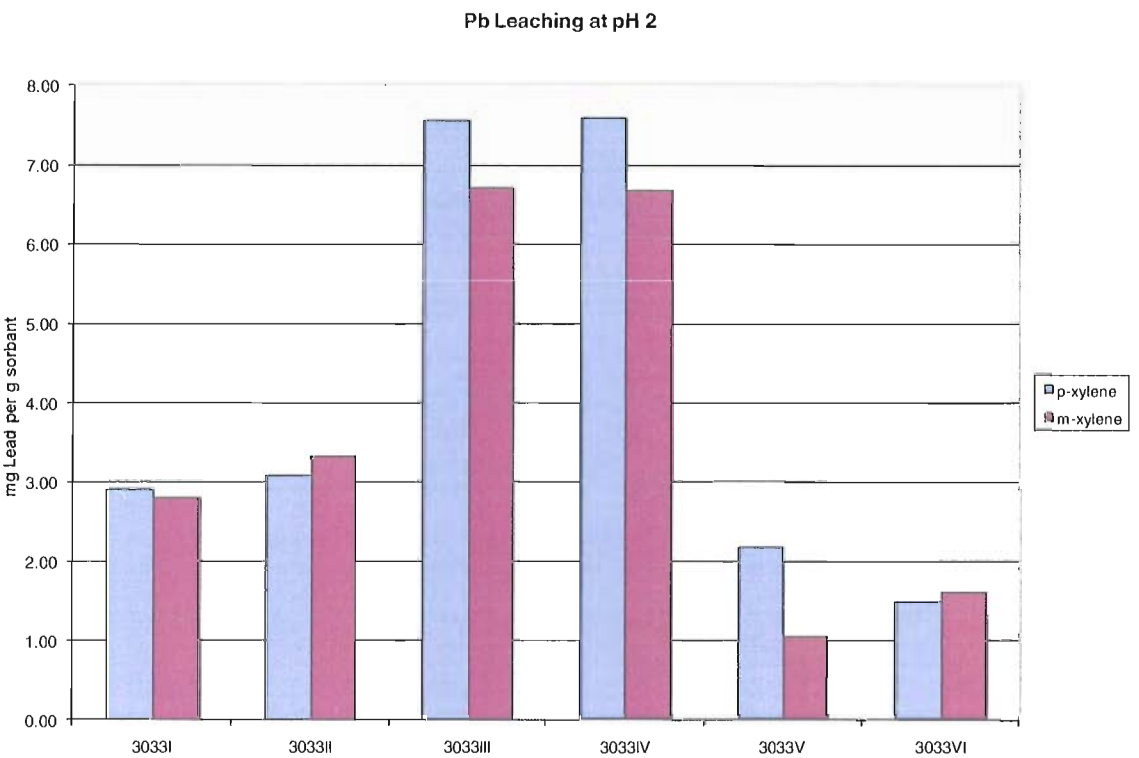


**Figure 15** Quantification of $Pb^{2+}$ contamination by means of competitive binding by $Hg^{2+}$. Blue bars are 1,4-BMMB and red are 1,3-BMMB. All tests performed at pH 2 to help with lead displacement. All data collected in duplicate and averaged.

From this data, it appears that lead contamination occurred fairly consistently between batches of 1,3- and 1,4-BMMB suggesting that contamination occurred during the addition of the active layer. This is a reasonable assumption due to the experimental

technique where batches of 1,3- and 1,4-BMMB are prepared together, using various phenyl base layers. Although this material could not be used for multiple ion uptake studies nor those specific to lead, this material showed no inhibition to $Hg^{2+}$ binding at low pH when compared to other BMMB-based sorbents.

## Conclusion

A new and versatile material utilizing weak interactions to reversibly bind aromatic molecules containing reactive head groups capable of selective capture of toxic metal ions from aqueous matrices at levels equal to covalently bound analogs has been described herein. Ultimately, this study will demonstrate the feasibility of loading this material with toxic ions, rinsing the bound material off the phenyl base support and reloading with more thiol-containing active layer to produce a 'regenerable' green material.

Initial studies indicate that the Hg-thiol complexes can be rinsed from the support with organic solvents regenerating pristine Phenyl-SAMMS as qualitatively measured by ICP-MS. 1,4-BMMB SAMMS (10mg) was placed in filter cartridges typically used in solid support flow-through synthesis containing sub-micron polypropylene filter disks. The samples were wetted first with methanol followed by exposure to $Hg^{2+}$ ion in filtered Columbia River water. Nanopure water was used to rinse the samples followed by a small methanol rinse and vacuum oven drying at 40°C overnight. Samples where then rinsed with approximately 1mL of the following: methanol, isopropanol, chloroform, hexanes, pentane and toluene. The effluent was evaporated and the residue was dissolved

in pH 2 Nanopure water. ICP-MS analysis of the acidified solution showed that chloroform and hexanes both contained reasonable levels of mercury with hexanes having a greater detectable amount.

It is important to understand that this experiment was merely qualitatively performed to demonstrate proof of concept and will be further studied by Sean Fontenot in the upcoming months. However, the ability to refresh or replace the surfaces of highly engineered sorbent support structures, such as mesoporous silica, could significantly increase the range of viable applications for these materials.

This material, although effective in toxic metal ion uptake, does suffer from ligand leaching and requires modification of either the base or active layers to address this problem. Studies by Sean Fontenot of the Johnson Laboratory have shown a direct correlation between base layer loading and percentage of active layer leaching (**Figure 16**). In his study, MCM-41 was functionalized with the phenyl base layer ranging from 2.4 to 0.06 molecules per $nm^2$. As expected, leaching of the active layer occurred at a much higher percentage with the sparsely populated surface, presumably due to a lack of stabilization of the active layer with $\pi$-contacts with the base layer.

From this data, MCM-41 populated with a phenyl base layer of 1.3 molecules per $nm^2$ performed the best due to its high active layer uptake and low leaching levels. Sean is currently working on modifying the base layer to include perfluorobenzene, naphthalene and cyclohexane. To be of any utility as a sorbent material, leaching of the captured ions must be addressed.

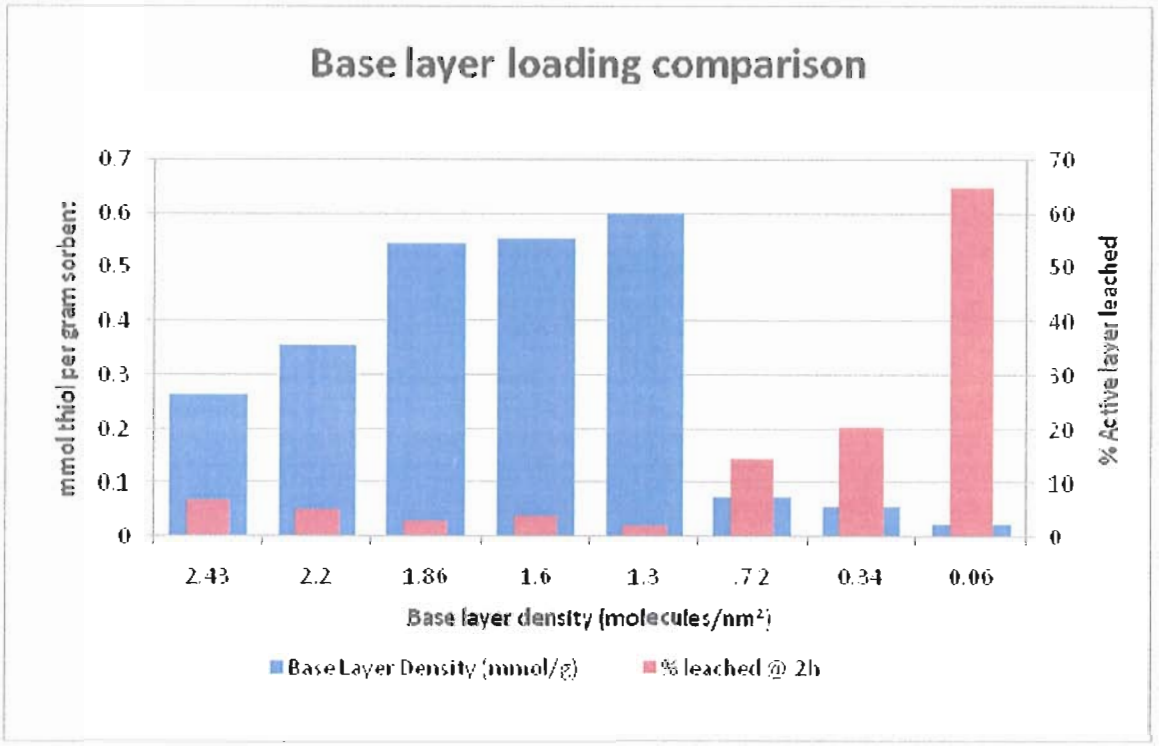


**Figure 16** Leaching studies of active thiol layer compared to phenyl base layer density. Blue bars indicate actual active layer loading in mmol (left axis) while red bars indicate percentage of active layer leaching (right axis). Data collected from Ellman's test and quantified by UV-Vis.

## Experimental

**General Procedures** Water sources where taken either from the Columbia River (Richland, WA), well water located on the Hanford site, (Richland WA) or Nanopure (18.2 mΩ) water produced in-house where noted. All natural water sources were passed through a 0.45 μm filter before use and stored in the dark. Glassware and plastic bottles were rinsed with a 10-20% nitric acid (low metal ICP-MS grade) solution followed by copious rinses with Nanopure water. All SAMMS materials were weighed out on a bench top analytical balance and reported to the nearest tenths of a mg. Digital pipettes (manual and electronic) were used to deliver small volumes of solutions (less than 100

mL). Large volumes were measured on a bench top analytical balance to the nearest tenth of a gram with the assumption of density equal to 1 for all solutions. Natural water samples were passed through a 0.2 μm filter by vacuum and stored in the dark until used. Test samples were filtered with 0.2 μm syringe filters before ICP-MS analysis. Samples were diluted as needed to range between 50 to 100 ppb to best match metal calibration curves. ICP-MS was performed on a Agilent Technologies 7500ce with calibration standards checked periodically to eliminate drift. All experiments were performed in duplicate or triplicate and values averaged before plotting unless otherwise noted. TGA was performed at the University of Oregon on a TA 2950 model starting at ambient temperature and ramping at 2°C a minute to 600°C under $N_2$ purge gas environment set to 90% balance, 10% furnace. A Balzers Thermostar residual gas analyzer (Electron Impact Mass Spectrometer) was hooked directly to the exit port of the TA 2950 furnace via stainless steel sheath to limit capillary damage. Scans were set in analog mode to targeted specific masses and ran the entire length of the TGA experiment.

*Phenyl SAMMS* MCM-41 (1.101g, 761.1 $m^2/g$) was combined with toluene (100 mL) in a 250 mL round bottom flask and stirred under $N_2$. To this 0.3757 mL Nanopure water was added (approximately 3 monolayers worth based off of surface area) and stirred for 4 hours or until the silica material re-dispersed in the toluene. 1.472 g ( 6.96 mmol, 1.2 mL) phenyl-trichlorosilane was added by syringe and the mixture stirred overnight (16 hours). Isopropyl alcohol (IPA, 100) mL was added to quench unreacted silane and stirred for 1 hour. The solution was filtered with a fine meshed sintered filter and rinsed with copious amounts of IPA then Acetone followed by drying in a vacuum

oven (-25 inches of Hg) at 40°C over night. Loading was determined gravimetrically using an analytical balance. Phenyl loading was adjusted as needed by altering the amount of silane.

*1,3-bis(mercaptomethyl) benzene (1,3-BMMB)* Reprehensive experimental procedure applicable to 1,4-BMMB as well. 1,3-bis(chloromethyl) benzene (3.014g, 17.2 mmol) was dissolved in 70 mL of reagent grade acetone in a 250 mL round bottom flask while stirring. To this, thiourea (2.889g, 37.9 mmol) was added and the mixture heated to reflux under $N_2$ for 3 hr. The mixture was allowed to cool. The white solid was filtered and rinsed with acetone followed by vacuum drying over night (3.77g, 67%). The thiouronium salt was placed back into a dry 250mL flask and to this, 50 mL of degassed 2M NaOH was added under a $N_2$ atmosphere. The solution was heated to reflux for 1.5 hr and allowed to cool. Degassed 2M HCl was added to adjust the pH to ~2 followed by the addition of dichloromethane. The organic layer was separated from the aqueous and washed 2 x 50 mL Nanopure water and dried over $Na_2SO_4$ for 15 minutes followed by filtration and evaporation *in vacuo* to produce a smelly clear liquid (1.694 g, 86%).

*BMMB SAMMS* Typical loading scheme for 1,3- and 1,4-BMMB SAMMS involves dissolving the appropriate amount of ligand calculated from phenyl base layer coverage and target loading (1:1 or 2:1 base layer to active layer) 0.2 mL dichloromethane or chloroform in a 20 mL scintillation vial. To this, Phenyl SAMMS is added and the vial capped and mixed gently overnight on a platform shaker set to 1Hz. The cap is removed and the solvent is allowed to evaporate over a 24hr period. After

which, the material is placed in a vacuum over overnight at ambient temperature and -25 in Hg. Total active layer uptake was determined by gravimetric analysis with an analytical balance or total ligand burn-off by TGA.

*Leaching tests* BMMB SAMMS material (10 mg) was first wet with MeOH then soaked in 0.1 M phosphate buffer (pH 8) for 2hrs while gently agitating at 1 Hz with a platform shaker. The solution is then filtered through a 0.2 μm syringe filter. To this, 100 to 200 μL of Ellman's reagent was added and the mixture shaken for 10-15 minutes. The solution was filtered with a 0.2 μm syringe filter and the absorbance was measured at 412 nm by an Agilent 8453 UV-Vis spectrometer.

# APPENDIX

## CRYSTALLOGRAPHIC DATA

*HI*: Monoclinic, *P*2(1)/*c*, $a$ = 8.1026(11), $b$ = 12.9398(17), $c$ = 11.2969(16) Å, $\beta$ = 91.735(3)°, $V$ = 1183.9(3) Å$^3$, $Z$ = 4, $D_c$ = 1.444 g cm$^{-3}$, $\mu$ = 0.265 mm$^{-1}$, $F$(000) = 536, $2\theta_{max}$ = 54.18° ($-10 \leq h \leq 10$, $-16 \leq k \leq 17$, $-14 \leq l \leq 14$). Final residuals (163 parameters) $R1$ = 0.0614 for 1323 reflections with $I > 2\sigma(I)$, and $R1$ = 0.1320, $wR2$ = 0.1827, GooF = 1.008 for all 2604 data. Residual electron density was 0.321 and –0.281 e.A$^{-3}$;

*[As$I_2$Cl]*: Triclinic, *P*-1, $a$ = 7.9782(7), $b$ = 18.8417(16), $c$ = 20.3116(17) Å, $\alpha$ = 97.856(2), $\beta$ = 97.098(2), $\gamma$ = 91.123(2) °, $V$ = 2999.4(4) Å$^3$, $Z$ = 4, $D_c$ = 1.644 g cm$^{-3}$, $\mu$ = 1.669 mm$^{-1}$, $F$(000) = 1496, $2\theta_{max}$ = 56.52° ($-10 \leq h \leq 10$, $-24 \leq k \leq 24$, $-26 \leq l \leq 26$). Final residuals (757 parameters) $R1$ = 0.0706 for 6238 reflections with $I > 2\sigma(I)$, and $R1$ = 0.1780, $wR2$ = 0.1428, GooF = 0.943 for all 13528 data. Residual electron density was 1.083 and –0.557 e.A$^{-3}$;

*[As**I**$_3$]*: Monoclinic, $P2(1)/n$, $a$ = 14.8242(19), $b$ = 10.6849(13), $c$ = 24.910(3) Å, $\beta$ = 103.239(4)°, $V$ = 3840.8(8) Å$^3$, $Z$ = 4, $D_c$ = 1.570 g cm$^{-3}$, $\mu$ = 1.115 mm$^{-1}$, $F(000)$ = 1856, $2\theta_{max}$ = 49.42° ($-17 \leq h \leq 17$, $-12 \leq k \leq 12$, $-29 \leq l \leq 29$). Final residuals (508 parameters) $R1$ = 0.0931 for 2108 reflections with $I > 2\sigma(I)$, and $R1$ = 0.2846, $wR2$ = 0.2456, GooF = 0.941 for all 6518 data. Residual electron density was 0.458 and –0.490 e.A$^{-3}$.

# BIBLIOGRAPHY

## Chapter I


(1) Desiraju, G. R. *Nature* **2001**, *412*, 397-400.

(2) Spessard, G. O.; Miessler, G. L. *Organometallic Chemistry*; Prentice-Hall Inc.: Upper Saddle River, 2000.

(3) Piguet, C.; Edder, C.; Rigault, S.; Bernardinelli, G.; Bunzli, J. G.; Hopfgartner, G. *J. Chem. Soc., Dalton Trans.* **2000**, 3999-4006.

(4) Holliday, B. J.; Mirkin, C. A. *Angew. Chem.* **2001**, *40*, 2022-2043.

(5) Orr, G. W.; Barbour, L. J.; Atwood, J. L. *Science* **1999**, *285*, 1049-1052.

(6) Sun, X.; Johnson, D. W.; Raymond, K. N.; Wong, E. H. *Inorg. Chem.* **2001**, *40*, 4504-4506.

(7) Garcia-Zarracino, R.; Höpfl, H. *J. Am. Chem. Soc.* **2005**, *127*, 3120-3130.

(8) Kieltyka, R.; Englebienne, P.; Fakhoury, J.; Autexier, C.; Moitessier, N.; Sleiman, H. F. *J. Am. Chem. Soc.* **2008**, *130*, 10040-10041.

(9) Lehn, J.-M. *Proc. Natl. Acad. Sci. U. S. A.* **2002**, *99*, 4763-4768.

(10) Vignon, S. A.; Jarrosson, T.; Iijima, T.; Tseng, H.-R.; Sanders, J. K. M.; Stoddart, J. F. *J. Am. Chem. Soc.* **2004**, *126*, 9884-9885.

(11) Caulder, D. L.; Raymond, K. N. *J. Chem. Soc., Dalton Trans.* **1999**, 1185-1200.

(12) Fiedler, D.; Leung, D. H.; Bergman, R. G.; Raymond, K. N. *Acc. Chem. Res.* **2005**, *38*, 349-358.

(13) Hamilton, T. K.; MacGillivray, L. R. *Cryst. Growth Des.* **2004**, *4*, 419-430.

(14) Truner, D. R.; Pastor, A.; Alajarin, M.; Steed, J. W. *Struct. Bonding* **2004**, *108*, 97-168.

(15) Hof, F.; Craig, S. L.; Nuckolls, C.; Rebek, J. *Angew. Chem. Int. Ed.* **2002**, *41*, 1488-1508.

(16) Radhakrishnan, U.; Stang, P. J. *J. Org. Chem.* **2003**, *68*, 9209-9213.

(17) Paver, M. A.; Joy, J. S.; Hursthouse, M. B. *Chem. Commun.* **2002**, 2150-2151.

(18) Garcia, A. M.; Romero-Salguero, F. J.; Bassani, D. M.; Lehn, J.-M.; Baum, G.; Fenske, D. *Chem. Eur. J.* **1999**, *5*, 1803-1808.

(19) Marcovich, D.; Duesler, E. N.; Tapscott, R. E.; Them, T. F. *Inorg. Chem.* **1982**, *21*, 3336-3341.

(20) Vickaryous, W. J.; Herges, R.; Johnson, D. W. *Angew. Chem., Int. Ed.* **2004**, *43*, 5831-5833.

(21) Vickaryous, W. J.; Rather Healey, E.; Berryman, O. B.; Johnson, D. W. *Inorg. Chem.* **2005**, *44*, 9247-9252.

(22) Kerr, P. G.; Leung, P. H.; Wild, S. B. *J. Am. Chem. Soc.* **1987**, *109*, 4321-4328.

(23) Shaikh, T. A.; Bakus, R. C.; Parkin, S.; Atwood, D. A. *J. Organomet. Chem.* **2006**, *691*, 1825-1833.

(24) Shaikh, T. A.; Parkin, S.; Atwood, D. A. *J. Organomet. Chem.* **2006**, *691*, 4167-4171.

(25) Cangelosi, V. M.; Carter, T. G.; Zakharov, L. N.; Johnson, D. W. *Chem. Commun.* **2009**, 5606-5608.

(26) Cangelosi, V. M.; Sather, A. C.; Zakharov, L. N.; Berryman, O. B.; Johnson, D. W. *Inorg. Chem.* **2007**, *46*, 9278-9284.

(27) Cangelosi, V. M.; Zakharov, L. N.; Fontenot, S. A.; Pitt, M. A.; Johnson, D. W. *Dalton Trans.* **2008**, 3447-3453.

(28) Alcock, N. W. In *Advances in Inorganic Chemistry and Radiochemistry*; Emeleus, H. J., Sharpe, A. G., Eds.; Academic Press, Inc.: New York, 1972; Vol. 15, p 1-58.

(29) Lindquist, N. R.; Carter, T. G.; Cangelosi, V. M.; Zakharov, L. N.; Johnson, D. W. Accepted, **2010**.

(30) Pitt, M. A.; Johnson, D. W. *Chem. Soc. Rev.* **2007**.

(31) Aposhian, H. V.; Aposhian, M. M. *Chem. Res. Toxicol.* **2005**, *18*, 1287-1295.

(32) Magalhaes, M. C. F. *Pure Appl. Chem.* **2002**, *74*, 1843-11850.

(33) Hindmarsh, J. T.; Abernathy, C. O.; Peters, G. R.; McCurdy, R. F. In *Heavy Metals in the Environment*; Sarkar, B., Ed.; Marcel Dekker, Inc.: New York, 2002, p 217-229.

(34) Bhattacharya, P.; Jacks, G.; Frisbie, S. H.; Smith, E.; Naidu, R.; Sarkar, B. *Arsenic in the Environment: A Global Perspective*; Marcel Dekker, Ink: New York, 2002.

(35) Roy, P.; Saha, A. *Curr. Sci.* **2002**, *82*, 38-45.

(36) Hossain, M. F. *Agriculture Ecosystems & Environment* **2006**, *113*, 1-16.

(37) Mandal, B. K.; Suzuki, K. T. *Talanta* **2002**, *58*, 201-235.

(38) Frisbie, S. H.; Ortega, R.; Manynard, D. M.; Sarkar, B. *Environ. Health Perspect.* **2002**, *110*, 1147-1153.

(39) Hinkle, S. R.; Polette, D. J. *Arsenic in Ground Water of the Willamette Basin, Oregon*, USGS, 1999.

(40) Solis, A. R.; Mukopadhyay, R.; Rosen, B. P.; Stemmler, T. L. *Inorg. Chem.* **2004**, *43*, 2954-2959.

(41) Cullen, W. R.; Reimer, K. J. *Chem. Rev.* **1989**, *89*, 713-764.

(42) Silver, S.; Phung, L. T. *Appl. Environ. Microbiol.* **2005**, *71*, 599-608.

(43) Adams, S. R.; Campbell, R. E.; Gross, L. A.; Martin, B. R.; Walkup, G. K.; Yao, Y.; Llopis, J.; Tsien, R. Y. *J. Am. Chem. Soc.* **2002**, *124*, 6063-6076.

(44) Cruse, B. W. T.; James, M. N. G. *Acta Crystallographica* **1972**, *B28*, 1325-1331.

(45) Farrer, B. T.; McClure, C. P.; Penner-Hahn, J. E.; Pecoraro, V. L. *Inorg. Chem.* **2000**, *39*, 5422-5423.

(46) Pappalardo, G. C.; Chakravorty, R.; Irgolic, K. J.; Meyers, E. A. *Acta Crystallogr., Sect. C: Cryst. Struct. Commun.* **1983**, *C39*, 1618-1620.

(47) Raston, C. L.; White, A. H. *Journal of the Chemical Society-Dalton Transactions* **1975**, 2425-2429.

(48) Garje, S. S.; Jain, V. K. *Coord. Chem. Rev.* **2003**, *236*, 35-56.

(49) Kuznik, N.; Wendt, O. F. *J. Chem. Soc., Dalton Trans.* **2002**, *15*, 3074-3078.

(50) Alcock, N. W. *Secondary Bonding to Nonmetallic Elements*; Academic Press, Inc.: New York, 1972; Vol. 15.

(51) Alcock, N. W. *Bonding and Structure: structural principles in inorganic and organic chemistry*; Ellis Horwood: New York, 1990.

(52) Alkorta, I.; Rozas, I.; Elguero, J. *J. Am. Chem. Soc.* **2002**, *124*, 8593-8598.

(53) Mascal, M.; Armstrong, A.; Bartberger, M. D. *J. Am. Chem. Soc.* **2002**, *124*, 6274-6276.

(54) Quiñonero, D.; Garau, C.; Rotger, C.; Frontera, A.; Ballester, P.; Costa, A.; Deyá, P. M. *Angew. Chem. Int. Ed.* **2002**, *41*, 3389-3392.

(55) Hof, F.; Rebek Jr., J. *Proc. Natl. Acad. Sci. U. S. A.* **2002**, *99*, 4775-4777.

(56) Tani, K.; Hanabusa, S.; Kato, S.; Mutoh, S.; Suzuki, S.; Ishida, M. *J. Chem. Soc., Dalton Trans.* **2001**, 518-527.

(57) Probst, T.; Steigelmann, O.; Riede, J.; Schmidbaur, H. *Chem. Ber.* **1991**, *124*, 1089-93.

(58) Ma, J. C.; Dougherty, D. A. *Chemical Reviews (Washington, D. C.)* **1997**, *97*, 1303-1324.

(59) Berryman, O. B.; Bryantsev, V. S.; Stay, D. P.; Johnson, D. W.; Hay, B. P. *J. Am. Chem. Soc.* **2007**, *129*, 48-58.

(60) Carmalt, C. J.; Norman, N. C. In *Chemistry of arsenic, antimony, and bismuth*; Norman, N. C., Ed.; Blackie Academic & Professional: London, 1998, p 1-38.

(61) Schmidbaur, H.; Nowak, R.; Steigelmann, O.; Muller, G. *Chem. Ber.* **1990**, *123*, 1221-1226.

(62) Camerman, A.; Trotter, J. *J. Chem. Soc.* **1965**, 730-8.

(63) Kersting, B.; Meyer, M.; Powers, R. E.; Raymond, K. N. *J. Am. Chem. Soc.* **1996**, *118*, 7221-7222.

(64) Pitt, M. A.; Cangelosi, V. M.; Fontenot, S. A.; Sather, A. C.; Zakharov, L. N.; Johnson, D. W. **In Prep.** .

(65) Bondi, A. *J. Phys. Chem.* **1964**, *68*, 441-451.

(66) Shannon, R. D. *Acta Crystallographica, Section A: Crystal Physics, Diffraction, Theoretical and General Crystallography* **1976**, *A32*, 751-67.

(67) Pauling, L. C. *The Nature of the Chemical Bond and the Structure of Molecules and Crystals. An Introduction to Modern Structural Chemistry. 3rd ed*, 1960.

(68) Vickaryous, W. J.; Zakharov, L. N.; Johnson, D. W. *Main Group Chem.* **2006**, *5*, 51-59.

(69) Johnson, D. W.; Pitt, M. A.; Harris, J. M.; USA: 2006; Vol. 11/350,202.

(70) Addleman, R. S.; Bayes, J. T.; Carter, T. G.; Fontenot, S. A.; Fryxell, G. E.; Johnson, D. W., **2009** U.S. Pat. Appl. # 61/120,321.

## Chapter II

(1) Carter, T. G.; Healey, E. R.; Pitt, M. A.; Johnson, D. W. *Inorg. Chem.* **2005**, *44*, 9634-9636.

(2) Vickaryous, W. J.; Herges, R.; Johnson, D. W. *Angew. Chem., Int. Ed. Engl.* **2004**, *43*, 5831-5833.

(3) Vickaryous, W. J.; Healey, E. R.; Berryman, O. B.; Johnson, D. W. *Inorg. Chem.* **2005**, *44*, 9247-9252.

(4) Cangelosi, V. M.; Zakharov, L. N.; Fontenot, S. A.; Pitt, M. A.; Johnson, D. W. *Dalton Trans.* **2008**, 3447-3453.

(5) Cangelosi, V. M.; Carter, T. G.; Zakharov, L. N.; Johnson, D. W. *Chem. Commun.* **2009**, 5606-5608.

(6) Cangelosi, V. M.; Sather, A. C.; Zakharov, L. N.; Berryman, O. B.; Johnson, D. W. *Inorg. Chem.* **2007**, *46*, 9278-9284.

(7) Carter, T. G.; Vickaryous, W. J.; Cangelosi, V. M.; Johnson, D. W. *Comments Inorg. Chem.* **2007**, *28*, 97-122.

(8) Dhubhghaill, O. M. N.; Saddler, P. J. *Struct. Bonding (Berlin)* **1991**, *78*, 129.

(9) Farrer, B. T.; McClure, C. P.; Penner-Hahn, J. E.; Pecoraro, V. L. *Inorg. Chem.* **2000**, *39*, 5422-5423.

(10) Johnson, J. M.; Voegtlin, C. *J. Biol. Chem.* **1930**, *89*, 5422.

(11) Matzapetakis, M.; Farrer, B. T.; Weng, T. C.; Hemmingsen, L.; Penner-Hahn, J. E.; Pecoraro, V. L. *J. Am. Chem. Soc.* **2002**, *124*, 8042-8054.

(12) Allen, F. H.; Kennard, O. *Chem. Des. Autom. News* **1993**, *8*.

(13) Alcock, N. W. In *Advances in Inorganic Chemistry and Radiochemistry*; Emeleus, H. J., Sharpe, A. G., Eds.; Academic Press, Inc.: New York, 1972; Vol. 15, p 1-58.

(14) Alcock, N. W. *Bonding and Structure: structural principles in inorganic and organic chemistry*; Ellis Horwood: New York, 1990.

(15) Bondi, A. *J. Phys. Chem.* **1964**, *68*, 441-451.

(16) Srivastava, P. C. *Phosphorus, Sulfur Silicon Relat. Elem.* **2005**, *180*, 969-983.

(17) Hof, F.; Rebek, J., Jr. *Proceedings of the National Academy of Sciences of the United States of America* **2002**, *99*, 4775-4777.

(18) Lehn, J.-M. *Proc. Natl. Acad. Sci. U. S. A.* **2002**, *99*, 4763-4768.

(19) Tani, K.; Hanabusa, S.; Kato, S.; Mutoh, S.; Suzuki, S.; Ishida, M. *J. Chem. Soc., Dalton Trans.* **2001**, 518-527.

(20) Cozzolino, A. F.; Vargas-Baca, I.; Mansour, S.; Mahmoudkhani, A. H. *J. Am. Chem. Soc.* **2005**, *127*, 3184-3190.

(21) Minkin, V. I.; Minyaev, R. M.; Milov, A. A.; Gribanova, T. N. *Russ. Chem. Bull.* **2001**, *50*, 2028-2045.

(22) Jankowski, Z.; Stolarski, R. *Pol. J. Chem.* **1981**, *55*, 555-563.

(23) Vickaryous, W. J.; Herges, R.; Johnson, D. W. *Angewandte Chemie* **2004**, *43*, 5831-5833.

(24) Vickaryous, W. J.; Rather Healey, E.; Berryman, O. B.; Johnson, D. W. *Inorganic Chemistry* **2005**, *44*, 9247-9252.

(25) Schmidbaur, H.; Nowak, R.; Steigelmann, O.; Muller, G. *Chem. Ber.* **1990**, *123*, 1221-1226.

(26) Rao, C. N. R. *Ultra-violet and Visible Spectroscopy*; 3 ed.; Butterworth & Co. Ltd.: London, 1975.

(27) Perkampus, H. H. In *UV-Vis Spectroscopy and Its Applications*; Springer-Verlag: New York, 1992, p 149-158.

(28) Wurthner, F. *Chem. Commun.* **2004**, 1564-1579.

(29) Rademacher, A.; Markle, S.; Langhals, H. L. *Chem. Ber.* **1982**, *115*, 2927-2934.

(30) Pitt, M. A.; Zakharov, L. N.; Vanka, K.; Thompson, W. H.; Laird, B. B.; Johnson, D. W. *Chem. Commun.* **2008**, 3936-3938.

(31) Inamoto, K.; Arai, Y.; Hiroya, K.; Doi, T. *Chem. Commun. (Cambridge, U. K.)* **2008**, 5529-5531.

(32) Banks, C. K.; Morgan, J. F.; Clark, R. L.; Hatlelid, E. B.; Kahler, F. H.; paxton, H. W.; Cragoe, E. J.; Andres, R. J.; Elpern, B.; coles, R. F.; Lawhead, J.; Hamilton, C. S. *J. Am. Chem. Soc.* **1947**, *69*, 927-930.

(33) Van Der Kelen, G. P. *Bull. Soc. Chim Belg.* **1958**, *65*, 343-349.

(34) Dyke, W. J. C.; Jones, W. J. *J. Chem. Soc.* **1930**, 2426-2430.

(35) Quick, A. J.; Adams, R. *J. Am. Chem. Soc.* **1922**, *44*, 805-816.

(36) Claeys, E. G. *J. Organomet. Chem.* **1966**, *5*, 446-453.

(37) Cline, D. J.; Thorpe, C.; Schneider, J. P. *J. Am. Chem. Soc.* **2003**, *125*, 2923-2929.

## Chapter III


(1) Nordberg, G. F.; Sandström, B.; Becking, G.; Goyer, R. A. In *Heavy Metals in the Environment*; Sarkar, B., Ed.; Marcel Dekker, Inc: New York, 2002.

(2) Shannon, M. A.; Bohn, P. W.; Elimelech, M.; Georgiadis, J. G.; Marinas, B. J.; Mayes, A. M. *Nature* **2008**, *452*, 301-310.

(3) Briggs, D. *British Medical Bulletin* **2003**, *68*, 1-24.

(4) Järup, L. *Occupational and Environmental Medicine* **2003**, *60*, 461-462.

(5) Wildung, R. E.; Cataldo, D. A. *Environ. Health Perspect.* **1978**, *27*, 149-159.

(6) Järup, L. *British Medical Bulletin* **2003**, *68*, 167-182.

(7) Smith, A. H.; Lingas, E. O.; Rahman, M. *Bulletin of the World Health Organization* **2000**, *78*, 1093-1103.

(8) Dermont, G.; Bergeron, M.; Mercier, G.; Richer-Lafleche, M. *J. Hazard. Mater.* **2008**, *152*, 1-31.

(9) Feng, X.; Fryxell, G. E.; Wang, L.-Q.; Kim, A. Y.; Liu, J.; Kemner, K. M. *Science* **1997**, *276*, 923-926.

(10) Fryxell, G., E.; Wu, H.; Lin, Y.; Shaw, W. J.; Birnbaum, J. C.; Linehan, J. C.; Nie, Z.; Kemner, K.; Kelly, S. *J. Mater. Chem.* **2004**, *14*, 3356-3363.

(11) Fryxell, G. E.; Liu, J.; Hauser, T. A.; Nie, Z. M.; Ferris, K. F.; Mattigod, S.; Gong, M. L.; Hallen, R. T. *Chem. Mater.* **1999**, *11*, 2148-2154.

(12) Fryxell, G. E. *Inorg. Chem. Commun.* **2006**, *9*, 1141-1150.

(13) Beck, J. S.; Vartuli, J. C.; Roth, W. J.; Leonowicz, M. E.; Kresge, C. T.; Schmitt, K. D.; Chu, C. T.-W.; Olson, D. H.; Sheppard, E. W.; McCullen, S. B.; Higgins, J. B.; Schlenker, J. L. *J. Am. Chem. Soc.* **1992**, *114*, 10834-10842.

(14) Kresge, C. T.; Leonowicz, M. E.; Roth, W. J.; Vartuli, J. C.; Beck, J. S. *Nature* **1992**, *359*, 710-712.

(15) Han, A.; Qiao, Y. *J. Phys. D: Appl. Phys.* **2007**, *40*, 5743-5746.

(16) Monnier, A.; Schüth, F.; Huo, Q.; Kumar, D.; Margolese, D.; Maxwell, R. S.; Stucky, G. D.; Krishnamurty, M.; Petroff, P.; Firouzi, A.; Janicke, M.; Chmelka, B. F. *Science* **1993**, *261*, 1299-1303.

(17) Gao, W.; Reven, L. *Langmuir* **1995**, *11*, 1860-1863.

(18) Wasserman, S. R.; Whitesides, G. M.; Tidswell, I. M.; Ocko, B. M.; Pershan, P. S.; Axe, J. D. *J. Am. Chem. Soc.* **1989**, *111*, 5852-5861.

(19) Linehan, J. C.; Stiff, C. M.; Fryxell, G. E. *Inorg. Chem. Commun.* **2006**, *9*, 239-241.

(20) Mattigod, S. V.; Feng, X.; Fryxell, G., E. *Sep. Sci. Technol.* **1999**, *34*, 2329-2345.

(21) Lam, K. F.; Yeung, K. L.; McKay, G. *Langmuir* **2006**, *22*, 9632-9641.

(22) Deratani, A.; Sebille, B. *Anal. Chem.* **1981**, *53*, 1742-1746.

(23) Richens, D. T. *The Chemistry of Aqua Ions*; John Wiley & Sons Ltd: West Sussex, 1997.

(24) Leckie, J. O.; James, R. O. In *Aqueous-Environmental Chemistry of Metals*; Rubin, A. J., Ed.; Ann Arbor Science Publishers Inc.: Ann Arbor, 1974, p 1-76.

(25) Helm, L.; Merbach, A. E. *Coord. Chem. Rev.* **1999**, *187*, 151-181.

(26) Dean, J. A. *Lange's Handvook of Chemistry*; 15 ed.; McGraw-Hill, Inc: New York, 1999.

(27) Jacobson, A. R.; Klitzke, S.; McBride, M. B.; Baveye, P.; Steenhuis, T. S. *Water Air and Soil Pollution* **2005**, *160*, 41-54.

(28) Pearson, R. G. *J. Am. Chem. Soc* **1963**, *85*, 3533-3539.

(29) Yantasee, W.; Warner, C. L.; Sangvanich, T.; Addleman, R. S.; Carter, T. G.; Wiacek, R. J.; Fryxell, G. E.; Timchalk, C.; Warner, M. G. *Environ. Sci. Technol.* **2007**, *41*, 5114-5119.

(30) Yantasee, W.; Hongsirikarn, K.; Warner, C. L.; Choi, D.; Sangvanich, T.; Toloczko, M. B.; Warner, M. G.; Fryxell, G. E.; Addleman, R. S.; Timchalk, C. *Analyst* **2008**, *133*, 348-355.

(31) Koehler, F. M.; Rossier, M.; Waelle, M.; Athanassiou, E. K.; Limbach, L. K.; Grass, R. N.; Gunther, D.; Stark, W. J. *Chem. Commun.* **2009**, 4862-4864.

(32) Liu, J. F.; Zhao, Z. S.; Jiang, G. B. *Environmental Science & Technology* **2008**, *42*, 6949-6954.

(33) Hancock, R. D. *J. Chem. Educ.* **1992**, *69*, 615-621.

(34) Steed, J. W.; Atwood, J. L. *Supramolecular Chemistry*; 2 ed.; John Wiley and Sons, Ltd, 2009.

(35) Cohen, S. M.; Raymond, K. N. *Inorg. Chem.* **2000**, *39*, 3624-3631.

(36) Fryxell, G. E.; Lin, Y.; Fiskum, S.; Birnbaum, J. C.; Wu, H. *Environ. Sci. Technol.* **2005**, *39*, 1324-1331.

(37) Sun, S. H.; Zeng, H. *J. Am. Chem. Soc.* **2002**, *124*, 8204-8205.

## Chapter IV

(1) Yokoi, T.; Tatsumi, T.; Yoshitake, H. *J. Colloid Interface Sci.* **2004**, *274*, 451-457.

(2) De Carlo, E. H.; Thomas, D. M. *Environmental Science & Technology* **1985**, *19*, 538-544.

(3) Roundhill, D. M.; Koch, H. F. *Chem. Soc. Rev.* **2002**, *31*, 60-67.

(4) Fox, K. R.; Sorg, T. J. *Journal American Water Works Association* **1987**, *79*, 81-84.

(5) Helfferich, F. *Ion exchange*; Dover: Mineola, 1995.

(6) Wang, J. L.; Chen, C. *Biotechnol. Adv.* **2009**, *27*, 195-226.

(7) Oliver, S. R. J. *Chem. Soc. Rev.* **2009**, *38*, 1868-1881.

(8) Goh, K. H.; Lim, T. T.; Dong, Z. *Water Res.* **2008**, *42*, 1343-1368.

(9) Atia, A. A. *J. Hazard. Mater.* **2006**, *137*, 1049-1055.

(10) Fryxell, G. E.; Liu, J.; Hauser, T. A.; Nie, Z. M.; Ferris, K. F.; Mattigod, S.; Gong, M. L.; Hallen, R. T. *Chem. Mater.* **1999**, *11*, 2148-2154.

(11) Yoshitake, H.; Yokoi, T.; Tatsumi, T. *Chem. Mater.* **2003**, *15*, 1713-1721.

(12) Wasserman, S. R.; Whitesides, G. M.; Tidswell, I. M.; Ocko, B. M.; Pershan, P. S.; Axe, J. D. *J. Am. Chem. Soc.* **1989**, *111*, 5852-5861.

(13) Feng, X.; Fryxell, G. E.; Wang, L.-Q.; Kim, A. Y.; Liu, J.; Kemner, K. M. *Science* **1997**, *276*, 923-926.

(14) Sillén, L. G.; Martell, A. E.; Bjerrum, J. *Stability constants of metal-ion complexes*; Chemical Society: London, 1964.

(15) Richens, D. T. *The Chemistry of Aqua Ions*; John Wiley & Sons Ltd: West Sussex, 1997.

(16) Godfrey, S. M.; McAuliffe, C. A.; Mackie, A. G.; Pritchard, R. G. In *Chemistry of Arsenic, Antimony, and Bismuth*; Norman, N. C., Ed.; Blackie Academic & Professional: London, 1998, p 94.

(17) Raposo, J. C.; Olazábal, M. A.; Madariaga, J. M. *J. Solution Chem.* **2006**, *35*, 79-94.

(18) Richard, F.; Bourg, A. C. M. *Water Res.* **1991**, *25*, 807-816.

(19) Palmer, C. D.; Puls, R. W.; EPA, Ed.; Technology Innovation Office: Ada, 1994.

## Chapter V

(1) Shannon, M. A.; Bohn, P. W.; Elimelech, M.; Georgiadis, J. G.; Marinas, B. J.; Mayes, A. M. *Nature* **2008**, *452*, 301-310.

(2) Hightower, M.; Pierce, S. A. *Nature* **2008**, *452*, 285-286.

(3) Dermont, G.; Bergeron, M.; Mercier, G.; Richer-Lafleche, M. *J. Hazard. Mater.* **2008**, *152*, 1-31.

(4) Smith, A. H.; Lingas, E. O.; Rahman, M. *Bull. World Health Organ.* **2000**, *78*, 1093-1103.

(5) Pitt, M. A.; Johnson, D. W. *Chem. Soc. Rev.* **2007**, *36*, 1441-1453.

(6) Carter, T. G.; Vickaryous, W. J.; Cangelosi, V. M.; Johnson, D. W. *Comments Inorg. Chem.* **2007**, *28*, 97-122.

(7) Yantasee, W.; Hongsirikarn, K.; Warner, C. L.; Choi, D.; Sangvanich, T.; Toloczko, M. B.; Warner, M. G.; Fryxell, G. E.; Addleman, R. S.; Timchalk, C. *Analyst* **2008**, *133*, 348-355.

(8) Yantasee, W.; Warner, C. L.; Sangvanich, T.; Addleman, R. S.; Carter, T. G.; Wiacek, R. J.; Fryxell, G. E.; Timchalk, C.; Warner, M. G. *Environ. Sci. Technol.* **2007**, *41*, 5114-5119.

(9) Fryxell, G. E.; Mattigod, S. V.; Lin, Y. H.; Wu, H.; Fiskum, S.; Parker, K.; Zheng, F.; Yantasee, W.; Zemanian, T. S.; Addleman, R. S.; Liu, J.; Kemner, K.; Kelly, S.; Feng, X. D. *J. Mater. Chem.* **2007**, *17*, 2863-2874.

(10) Fryxell, G. E.; Liu, J.; Hauser, T. A.; Nie, Z.; Ferris, K. F.; Mattigod, S.; Gong, M.; Hallen, R. T. *Chem. Mater.* **1999**, *11*, 2148-2154.

(11) Feng, X.; Fryxell, G. E.; Wang, L.-Q.; Kim, A. Y.; Liu, J.; Kemner, K. M. *Science* **1997**, *276*, 923-926.

(12) Fryxell, G. E.; Lin, Y.; Fiskum, S.; Birnbaum, J. C.; Wu, H. *Environ. Sci. Technol.* **2005**, *39*, 1324-1331.

(13) Kresge, C. T.; Leonowicz, M. E.; Roth, W. J.; Vartuli, J. C.; Beck, J. S. *Nature* **1992**, *359*, 710-712.

(14) Beck, J. S.; Vartuli, J. C.; Roth, W. J.; Leonowicz, M. E.; Kresge, C. T.; Schmitt, K. D.; Chu, C. T.-W.; Olson, D. H.; Sheppard, E. W.; McCullen, S. B.; Higgins, J. B.; Schlenker, J. L. *J. Am. Chem. Soc* **1992**, *114*, 10834-10842.

(15) Yoshitake, H.; Yokoi, T.; Tatsumi, T. *Chem. Mater.* **2002**, *14*, 4603-4610.

(16) Chang, S.-C.; Chao, I.; Tao, Y.-T. *J. Am. Chem. Soc* **1994**, *116*, 6792-6805.

(17) Hunter, C. A.; Sanders, J. K. M. *J. Am. Chem. Soc* **1990**, *112*, 5525-5534.

(18) Feng, X.; Liu, J.; Fryxell, G. E.; Gong, M.; Wang, L.-Q.; Chen, X.; Kurath, D. E.; Ghormley, C. S.; Klasson, K. T.; Kemner, K. M. *Self-Assembled Mercaptan on Mesoporous Silica (SAMMS) Technology for Mercury Removal and Stabilization*, Pacific Northwest National Laboratory, 1997.